Robust Semi-active Control of Aircraft Landing Gear System Equipped with Magnetorheological Dampers

Ajinkya A. Gharapurkar

A thesis

in

The Department

of

Mechanical and Industrial Engineering

Presented in Partial Fulfillment of the Requirements
For the Degree of Master in Applied Sciences (Mechanical Engineering) at
Concordia University
Montreal, Quebec Canada

"March 2014"

CONCORDIA UNIVERSITY

School of Graduate Studies

This is to certify that the thesis prepared

By: **Ajinkya A. Gharapurkar**

Entitled: **Robust Semi-active Control of Aircraft Landing Gear System Equipped**

with Magnetorheological Dampers

and submitted in partial fulfillment of the requirements for the degree of

Master in Applied Sciences (Mechanical Engineering)

complies with the regulations of the University and meets the accepted standards with

respect to originality and quality.

Signed by the final examining committee:

Dr. I. Contreras
_____ Chair

Dr. S. Williamson
_____ Examiner

Dr. I. Stiharu
_____ Examiner

Dr. R. Bhat
_____ Supervisor

Dr. C. Asthana
_____ Co-Supervisor

Approved by Dr. S. Narayanswamy
_____

MAsc Program Director,

Department of Mechanical and Industrial Engineering

Dean Christopher Trueman
_____

Faculty of Engineering and Computer Science

Date _____

ABSTRACT

Robust Semi-active Control of Aircraft Landing Gear System Equipped with

Magnetorheological Dampers

Ajinkya A. Gharapurkar

Landing is the most critical operational phase of an aircraft since it directly affects the passenger safety and comfort. The factors such as the undesirable wind and ground effects, runway unevenness, excessive sink speeds and approach speeds and pilot errors can deteriorate the landing performance of an aircraft several times during its entire lifetime. When an aircraft lands, large amplitude vibrations get transmitted to the fuselage from the runway thereby causing safety and comfort problems and hence need to be suppressed quickly.

Landing gear is an essential assembly that prevents the aircraft fuselage from the ground loads. A shock absorber which is considered as the heart of the landing gear assembly plays an important role in this process by absorbing the vibrations during landing. The existing Oleo-pneumatic shock absorbers are the most efficient in absorbing the vibrations during each aircraft operation. However, they are unable to provide the continuously variable damping required during the landing phase which might reduce their efficiency. Moreover, to account for the uncertainties during landing, a damper capable of providing the variable damping effect can play a vital role in increasing the passenger safety.

A semi-active control system of a landing gear suspension can solve the problem of excessive vibrations effectively by providing a variable damping during each

operational phase. Magnetorheological (MR) dampers are one of the most efficient and attractive solutions that can provide the continuously variable damping required depending on a control command.

This thesis focuses on the concept of the semi-active aircraft suspension system using the MR damper with the implementation of robust control strategy. Initially, the dynamic behavior of the MR damper is studied using the parametric modeling approach. Spencer dynamic model is adopted for simulating the dynamic behavior of the MR damper. This is followed by the analysis of the energy dissipation patterns of the MR damper for different excitation inputs.

A semi-active suspension system is developed for a three degree-of-freedom (3 DOF) aircraft model considering a tri-cycle landing gear configuration. A switching technique is developed in the simulation of the landing procedure which enables the system to switch from the single degree of freedom to three degrees of freedom system in order to simulate the sequential touching of the two wheels of the main landing gears and the nose landing gear wheel with the ground. For developing the semi-active MR suspension system, two different controller approaches, namely, the Linear Quadratic Regulator (LQR) and the H_∞ control are adopted. The results of the designed controllers are compared for a particular landing scenario for studying the performance of the controllers in reducing the overshoot of the bounce response as well as the bounce rate response. The simulation results confirmed the improved performance of the robust controller compared to the optimal control strategy when the aircraft is subjected to the disturbances during landing. Finally, implementing the robust control approach, the

landing performance of an aircraft embedded with the semi-active suspension system is

simulated and analyzed for different sink velocities considering the disturbances.

ACKNOWLEDGEMENTS

TABLE OF CONTENTS

LIST OF FIGURES

LIST OF TABLES

NOMENCLATURE

a_c	Constant model parameter (sigmoid model)
$[A]$	System matrix
A_1	A constant for adjusting the slope of the hysteresis curve (Spencer model)
$[A_{LQR}]$	System matrix for new gain
$[B]$	Input matrix
b_1	Constant model parameter (sigmoid model)
c_0	Viscous damping coefficient at larger velocities (N-s/m)
c_1	Damping coefficient of the nose landing gear (N-s/m)
C_1	Plant output
c_2	Damping coefficient of the left main landing gear
C_2	Plant output
c_3	Damping coefficient of the right main landing gear (N-s/m)
C_{eq}	Equivalent viscous damping coefficient (N-s/m)
c_r	Dashpot representing roll off effect (Spencer model) (N-s/m)
$[C_v]$	Damping matrix
E_{MR}	Energy dissipated by MR damper over one cycle (J)
f	Actuator constant
F	Controllable force (N)
F_0	Constant parameter of the model

F_1	MR damper force for nose landing gear (N)
F_2	MR damper force for left main landing gear (N)
F_3	MR damper force for right main landing gear (N)
$F_D(t)$	Hysteresis force function (N)
F_I	Non-linear function of current
F_{max}	Maximum MR damper force (N)
F_{min}	Minimum MR damper force (N)
$F_{MR}(t)$	Total MR damper force (N)
F_T	Transition force (N)
$[G]$	Disturbance input matrix
h_l	Distance of the right main landing gear from center point (m)
h_r	Distance of the right main landing gear from center point (m)
I	Identity matrix
I_0	Arbitrary constant in non-linear current function
I_x	Mass moment of inertia in roll (kg-m^2)
I_y	Mass moment of inertia in pitch (kg-m^2)
J	Cost function
$[K]$	Stiffness matrix
k_0	Control stiffness at larger velocities (Spencer model) (N/m)
k_1	Stiffness of the nose landing gear (N/m)

k_2	Stiffness of the left main landing gear (N/m)
k_3	Stiffness of the right main landing gear (N/m)
k_a	Constant model parameter (sigmoid model)
k_b	Constant model parameter (sigmoid model)
k_c	Constant model parameter (sigmoid model)
K_{LQR}	Optimal gain of LQR
k_p	Linear rise coefficient
k_r	MR damper accumulator stiffness (N/m)
l_f	Distance of nose landing gear form C.G. (m)
l_r	Distance of main landing gears form C.G. (m)
m	Mass of aircraft fuselage (kg)
$[M_1]$	Matrix representing solution of Riccati equation for H$_\infty$ controller
n	A constant for adjusting the slope of the hysteresis curve
$[N_1]$	Matrix representing solution of Riccati equation for H$_\infty$ controller
ω	Frequency of excitation (rad/sec)
P	Auxiliary variable defined in Spencer model
q	Internal state to account for roll off effect in Spencer model
$[Q]$	Symmetric positive semi-definite matrix
$[R]$	Symmetric positive definite matrix

$[S]$	Matrix representing solution of Riccati equation
u	Vector representing MR Damper forces
v_h	Zero force-velocity intercept (Sigmoid model)
v_m	Peak velocity (m/s)
w	Disturbance vector
x	Piston displacement (m)
$\dot{x}$	Piston velocity (m/s)
$\ddot{x}$	Piston acceleration (m/s^2)
X	State vector
X_1	Amplitude of sinusoidal excitation (mm)
Y	Plant output
z	Displacement of aircraft in vertical direction (bounce) (m)
α	A constant for adjusting the slope of the hysteresis curve (Spencer model)
β	A constant for adjusting the slope of the hysteresis curve (Spencer model)
γ	A constant for adjusting the slope of the hysteresis curve (Spencer model)
ζ	Parameter representing controller state
η	Controller performance index
θ	Angle of roll (rad)
φ	Angle of pitch (rad)

Ψ Constant model parameter (sigmoid model)

CHAPTER 1

INTRODUCTION AND LITERATURE REVIEW

1.1 Introduction and Research Motivation

Aircraft structure is a complex assembly of a number of different components and sub-assemblies. During its lifetime, the aircraft is subjected to different operational phases such as landing, take off, cruising and taxiing. Amongst all, the landing of an aircraft is the most critical operation as far as the passenger safety and airworthiness is concerned [1], [2]. According to the aircraft accident investigation reports [3]-[5] the probability of an aircraft meeting with an accident is more during the landing phase as compared to the other phases. The statistical analysis of the aircraft accidents from 1959 to 2001, by Boeing, reveals that the percentage of accidents occurred during the landing phase is 45%, which clearly dominates the percentage of accidents occurred in any other operational phase [3]. Many fatal landing accidents have been reported previously, which involved large number of human casualties. The crash landing of the Iran Air operated Boeing 727 reveals that the percentage of passengers died because of the multiorgan crushing injury was more than 50%. Another accident caused due to the unsuccessful landing was reported in 2009 at Amsterdam. The percentage of survivals was only about 25.7% [6].

The above statistical data is a clear indication of the criticality of the landing phase and the hazards related to it. It is a well-known fact that the primary objective of an aircraft is to fly with the best achievable efficiency. However, the aircraft also spends considerable time on the ground during landing, take-off and taxiing phases. The airlines

specify the time spent by an aircraft on ground in terms of number of landings and take-offs. During its lifetime, the aircraft should be able to perform approximately, up to 90000 landings and take-offs [7]. Almost 50 % of the aircraft accidents take place during landing and take-off phases [2], [3], [7]. Therefore, it becomes necessary to take into consideration the safety factors involved during landing. The issue is directly related to the design of the landing gear. Even though the non-technical professionals consider the landing gear as no more than a set of wheels, it is the most critical and invaluable assembly for the aircraft designers because it directly relates to the passenger safety during various operational phases [1], [8], [9]. The function of the landing gear is not just to facilitate the aircraft for safe landing but also to sustain the aerodynamic forces during its retraction and extension. These conflicting requirements during the various phases pose limitations in its design and often make it a tedious process for the designers [9].

The landing gear plays an important role by acting as an intermediate element between the aircraft body and the runway [1]. During the touchdown, large magnitude vibrations are transmitted to the aircraft fuselage through the landing gear because of the harsh landing conditions [10]. The influence of the landing impact on the aircraft structure depends upon the various factors such as the approach speed, the sink speed and the environmental conditions. According to the standards set by the airworthiness authorities, the civil aircraft are designed to land with a sink velocity of 3.05 m/s whereas the standard sink velocity for the fighters, trainers and the deck landing aircraft are 3.66 m/s, 4.0 m/s and above 6.0 m/s respectively. The aircraft often experience hard landing conditions if the standard sink rates are exceeded during landing. The hard landing conditions are responsible for the transmission of the large magnitude vibrations which is

2

the primary reason for the passenger discomfort and sometimes, serious crash landing situations. Therefore, in order to soften the landing impact, the vertical kinetic energy must be absorbed and dissipated as quickly and effectively as possible which reduces the accelerations induced in the aircraft structure upon landing, thereby preventing structural damage. This important task is accomplished by the shock absorber, which is considered as the most prominent component of the landing gear assembly [1], [2], [9], [10], [11].

Consistent attempts have been made in the past to design efficient shock absorbers without compromising the weight of an aircraft. Since the World War II, many revolutionary shock absorber designs were implemented for the fighters as well as for the commercial aircraft. A good shock absorber should absorb most of the impact kinetic energy during landing and taxiing of an aircraft. Currently, Oleo-pneumatic shock absorbers are the most commonly used shock absorbers in aircraft landing gears because of their high efficiency and ability to absorb shocks and dissipate energy effectively. Due to the conflicting damping requirements during taxiing and landing phases, the performance efficiency of the aircraft with the passive Oleo dampers is often limited. The existing dampers are not capable of providing the variable damping depending upon the requirements during each operational phase. In order to improve the landing performance, a soft suspension would be desirable during compression, whereas a stiffer spring would be needed during extension. These variable damping and stiffness requirements cannot be achieved with the existing passive shock absorbers [12].

The conflicting damping requirements pose limitations on the performance efficiency of the passive shock absorbers. In order to fulfill the need of variable damping, various designs of the active and semi-active suspension systems have been proposed by

3

researchers in recent years [12]-[16]. Though, the concept of the active and semi-active suspension design is limited in aircraft applications, it has been used to some extent for developing the intelligent suspensions for road vehicles [15]. None of the aircraft in today's era is embedded with an active or semi-active landing gear. However, intensive research has been going on since past four decades in order to stimulate the idea of the controllable landing gears to make the aircraft ride safer and more comfortable for the passengers [12], [13]. The active and the semi-active suspension systems have an edge over the passive systems when it comes to ride comfort problem. However, the actual implementation of these systems is a difficult task because of their high cost, weight and design complexities [14].

In actual practice various actuation systems can be used for developing the active and the semi-active suspensions. The use of hydraulic actuators for developing the intelligent vehicle suspensions has been reported previously in the literature [17]. The other actuation strategies involve the use of Magnetorheological (MR) dampers [18], [19], [20]. The MR damper makes use of a smart fluid called Magnetorheological fluid which has a property of changing its viscosity upon the application of a magnetic field. This makes MR damper an effective controllable device for the intelligent suspension applications. The MR dampers are attractive because of their reliable operation irrespective of the changes in temperature and the condition of fluid. They offer wide temperature range from - 40° to +150° C. The range of obtainable dynamic yield stress of the MR fluid is 50-100 kpa for considerably low voltages which makes them the ideal actuators for the semi-active aircraft and vehicle suspension applications [21]-[24]. Also, in case of power failure the MR dampers can act as passive dampers, thereby not

restricting the ongoing operation. However, the utilization of the MR dampers is limited to some extent because of their inherent nonlinear hysteretic behaviour upon application of magnetic field which makes the design of the controllers a critical task [14], [18].

Despite the difficulties in the design process, numerous control concepts have been developed and utilized for realizing the semi-active systems especially for road vehicles [25], [26]. However, the implementation of such systems in aircraft is yet to be tried, even if there are number of semi-active concepts available for developing the controllable landing gear [12].

The primary focus of all the research and development programs is to develop new technologies which would take away the repetitive and routine tasks from human hands. In case of aircraft, the focus is to improve the ride quality, comfort and safety during their operational phases and to avoid as many accidents as possible. In recent years, a lot of research has been going on with the objective of improving the safety of aircraft, especially during landing. These studies involve the vibration analysis during landing impact which ensures the structural integrity. A two degrees of freedom (2 DOF) aircraft model is used initially by researchers for simulating the vibration response [27]-[29]. The advantage of this model is the simplicity and the ease with which a control strategy can be developed. This model takes into account only the vertical motion of an aircraft after landing. However, during landing, the aircraft also undergoes the pitch and roll motions which must be identified in the analysis from the stability point of view.

In this thesis, a semi-active Magnetorheological (MR) landing gear system has been developed using two different control approaches, namely, the H_∞ and the Linear

Quadratic Regulator (LQR) for a three degrees of freedom (3 DOF) aircraft model. The performance of both the controllers is compared for a particular landing situation in order to select the appropriate controller. After selecting the appropriate control strategy, the response of an aircraft with the passive shock absorber is compared with that with the semi-active shock absorber for different landing scenarios. The advantages of the semi-active landing gear over the passive landing gear are analyzed from the obtained simulation results.

1.2 Literature Review

The proposed study focuses on designing a semi-active suspension for the existing landing gears using the H$_\infty$ and LQR control approaches. Therefore, in order to thoroughly understand the proposed concept, it is necessary to review the existing technologies, their advantages and limitations, and also technologies in the development phase which would be of great importance in near future. A thorough review of the relevant literature has been done in the following sections.

1.2.1 Recent developments in landing gear technology

The landing gear is one of the most essential aircraft assemblies, as the safety of the aircraft on the ground entirely depends upon its effective functioning. The primary objective of a landing gear is to absorb the vertical and horizontal kinetic energy which ensures the stability and safety of the aircraft during the ground operations. Therefore, with the advent of modern aircraft, researchers felt the need for developing more efficient landing gears. The design process of the landing gears has evolved in the last century from simple skids to sophisticated wheeled landing gears embedded with efficient shock absorbers [9]. Soon after the invention of the first ever aircraft by Wright brothers in the

6

early nineteenth century, an idea of the wheeled landing gears was implemented efficiently [1]. Few years after the initial implementation, during the World War I, many fighter aircraft were equipped with the tail wheel configuration landing gear system. Since then there has been a tremendous growth in the field of landing gear design. Throughout the development phase, more attention was focused on the efficient design of the shock absorber, which is considered as the most important component of the entire landing gear assembly. The earlier aircraft were equipped with the rugged struts attached to the airframes, which displayed very poor damping performance. The need for the high efficiency shock absorbers was not intense until the heavy weight aircraft started making their appearance on the aviation world. With increasing aircraft weights and sink speeds, it became necessary for the landing gear designers to look for more efficient solutions for the energy absorption during landing which would protect the aircraft structures from the ground loads [1], [9].

Since the initialization of the first concept of the shock absorber design, lot of attempts have been made so far to make them as efficient as possible. Early aircraft used the simplest type of shock absorbers which consisted of bungee cord rings or bungee blocks fitted inside a tubular cross section. Though these shock struts were able to absorb part of the energy during the touchdown, they were not able to provide any damping because of which they became inefficient in restricting the recoil of an aircraft after the initial touchdown. This followed the shock absorber design with steel coil springs which could absorb the landing energy but were unable to provide effective damping. This design is still used for very lightweight aircraft. One of the most innovative shock strut designs was the torsion bar. This type of absorber was able to withstand torsional loads

during landing and absorb the energy at the time of touchdown. The drawback of all the three designs mentioned above is their inability to provide effective damping during landing because of which the aircraft equipped with these shock struts used to undergo bounce and sway motions during ground operations [1].

In order to address these challenges, a few new shock absorber designs were proposed which included pneumatic shock absorber, oil shock absorber and the combination of both, namely, the Oleo-pneumatic shock absorber. The efficiency of the air and oil shock absorbers was better compared to the previously used ones but their excessive weight posed some limitations on their applicability. Today, the Oleo-pneumatic shock absorbers are most widely used in all aircraft because of their high efficiency and small weight [1], [2], [10], [30]. The Oleo-pneumatic shock struts are able to absorb the energy very effectively during each operational phase. Also, the absorbed energy is dissipated with a controlled rate in order to prevent the sudden loading on the airframe. Therefore, it becomes necessary to understand the basic functioning of the Oleo-pneumatic dampers before implementing the new shock absorber design concepts for the existing aircraft structures.

1.2.1.1 Oleo-pneumatic struts: Heart of today's landing gear technology

The concept of oleo finds its roots back in 1905 when it was first implemented and patented as a recoil device for large cannons [30]. The struts are called Oleo-pneumatic because their principle of operation involves using the combination of compressible gas and incompressible fluid for providing the spring and the damping effects, respectively. It consists of two cylindrical chambers. The upper chamber is filled with gas charge while the lower one is filled with the kerosene based mineral oil. Because of the rapid

movement of the piston inside the cylinder, large amount of heat is generated which has to be dissipated effectively. Due to the high heat involved during this process, the gas charge to be filled in the upper chamber must be an inert gas which would prevent the explosion of the oil vapour in case of temperature rise beyond a certain level [31]. Therefore, for heavy aircraft it is mandatory for the shock absorber manufacturers to use the nitrogen or other inert gas as a gas charge.

The gas charge in the upper chamber supports the aircraft weight and the oil contained in the lower chamber provides the damping effect during the operation. At the time of touchdown, the strut operates by pushing the chamber of oil against the chamber of dry air or nitrogen. The dissipation of energy takes place when oil flows through one or more orifices. A landing aircraft inevitably rebounds after the initial impact. During this phase, the pressurized air forces the oil back to the lower chamber through the recoil orifices. The rate of flow of oil through the recoil orifices determines the extent of rebound. If oil flows too quickly through the orifice, aircraft rebounds upwards rapidly. On the other hand, if oil flow is too slow, the oscillations will not be damped out effectively during soft landing and taxiing phases [1], [2].

The spring force in an oleo strut is provided by the compression and expansion of gas and the damping force by the fluid passing through the orifice. The orifice area changes as the metering pin moves up and down through the orifice. By appropriately designing the metering pin, it is possible to achieve the required damping force [30], [31]. However, sometimes because of the conflicting damping requirements, the efficiency of Oleo dampers is reduced which necessitates the need for developing the controllable dampers which would be able to provide variable damping forces. Magnetorheological

dampers can provide a solution for improving the overall damper efficiency and performance of the system.
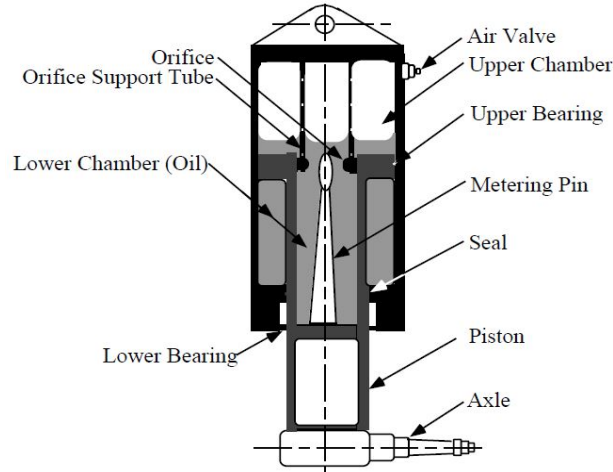
Figure 1.1 Oleo-pneumatic shock absorber [2]

1.2.2 Magnetorheological fluid dampers: Potential solution for future suspensions

Magnetorheological fluids belong to a class of smart materials because of their controllable inherent rheological characteristics [32], [33]. Jacob Rainbow [34] can be credited for the discovery and the development of MR fluid devices in early 1950s. The other type of controllable fluids, namely, Electrorheological (ER) fluids, was discovered and developed by Willis Winslow [35] in the same era. However, the research programs in the field of MR fluids were more extensive compared to those in the field of ER fluids. The controllable rheological properties of the MR fluids make them suitable in the application of shock and vibration control devices. The rheological properties of these fluids refer to the elasticity, plasticity and viscosity [36]. The application of the controlled magnetic field to these fluids increases their viscosity thereby improving the shock absorption. Conversely, when the magnetic field is removed, they come back to the

10

normal state. This basic property can be utilized in the semi-active vibration control approaches.

Magnetorheological fluid is basically, a composition made of the magnetizable particles dispersed randomly in liquid medium, called carrier oil, with a stabilizer [37]. The liquid medium is usually an organic or aqueous solution with insulation properties. Commonly used liquid media for preparing the MR fluid includes petroleum based oils, silicon oil, kerosene, mineral oils, synthetic hydrocarbon oils, polyester, polyether, water etc. The liquid medium used for a particular application must possess good temperature stability [38], [39]. The particles dispersed in carrier oil are iron based micron-sized particles having size in the range of 1-10 μm. These particles are magnetically soft which helps their smooth transition from polarized state to a normal state when the magnetic field is removed. The most commonly used magnetisable particles are carbonyl iron powder based, which is a product of decomposition of iron pentacarbonyl. However, the high density of iron powders (7.8 g/cm^3) compared to the carrier liquid poses some restriction on fluid re-dispersion as the particles settle down at the bottom. Research has been going on to reduce the size of these particles to a nano-scale in order to facilitate a smooth re-dispersion of a carrier fluid. The third element which completes the MR fluid composition is a stabilizer which serves the function of maintaining the agglomerative stability as well as the sedimental stability which prevent the particles from sticking together and settling down at the bottom with time. For a fluid immersed with coarse particles, silica gel is used as a stabilizer whereas the ionic surfactant such as oleic acid is used for the fluids immersed with finely dispersed particles [36]-[38].

11

Magnetorheological fluids possess a unique property of transforming from a free flowing state to a highly viscous semi-solid state when exposed to a magnetic field. In a typical MR damper device, when a current is passed through a coil placed adjacent to the fluid, the randomly dispersed iron particles in carrier oil acquire the dipole moment in alignment with the applied magnetic field. This process forms a chain of iron particles which is perpendicular to the direction of fluid flow thereby restricting it. In other words, velocity of fluid flow decreases. This effect continues as long as the magnetic field is maintained. Once the magnetic field is removed, iron particle chains are broken and the fluid comes back to its normal state. This phenomenon can be visualized from figure 1.2. This transformation takes place in milliseconds and is reversible, which allows the fluid to return back to its normal state when magnetic field is removed. This property can be utilized in MR fluid based devices to achieve variable damping, particularly in the shock and vibration attenuation applications [21]-[24]. In the absence of magnetic field, these fluids behave like Newtonian fluids having viscosity ranging from 0.1 to 1 Pa at room temperature. With the application of magnetic field of 150-200 kA/m, the dynamic yield strength of 50-100 kpa can be achieved which is significant in the applications where sudden impacts have to be attenuated quickly. The operating temperature range of these fluids span from - 40 to 150^0 C with minimal variation in yield strength. Generally, these fluids are not affected by the contaminants during the manufacturing process. Because of the dispersed iron particles, the density of these fluids ranges from 3-4 g/cm^3. The available devices which work on the MR effect typically requires 2-50 Watt power source [21]-[24], [38]-[40].
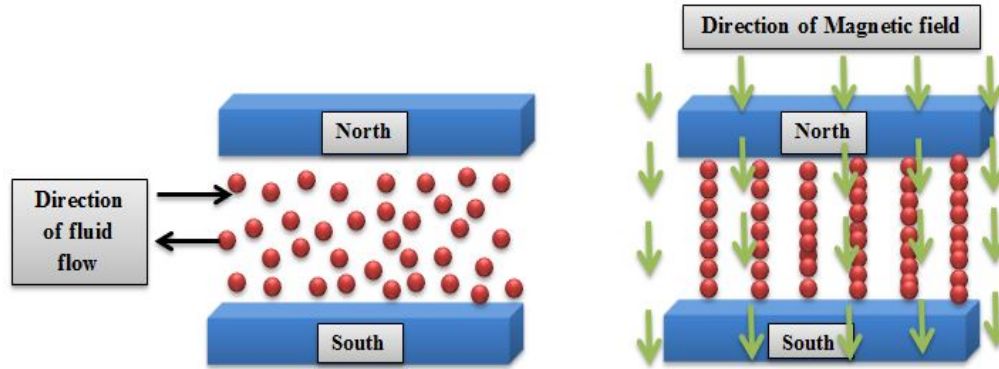
Figure 1.2 MR fluid behavior for applied magnetic field [16]

Based on their phenomenal controllable properties, MR fluids can be used in developing the innovative devices, particularly dampers. The focus of the research and development programs is to develop efficient MR fluid based dampers which would be able to achieve the goal of improving the safety in variety of applications like civil structures, road vehicles, railway vehicles as well as airplanes. The most effective application of MR fluids is in linear dampers to develop semi-active seat suspensions for heavy vehicles and struts for passenger cars. The linear MR dampers also find their application in protection of civil structures from seismic loads [41].
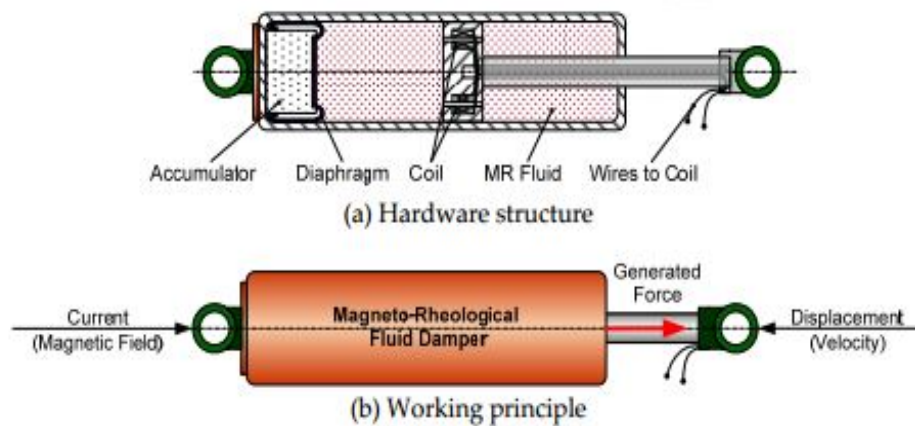
Figure 1.3 Configuration of Magnetorheological damper [42]

In recent years, researchers have developed new techniques for designing the suspension systems using Magnetorheological dampers for road vehicles to cope with the road irregularities and for improving the ride comfort. Wang et al [18], Kim and Jeon [43] and Lam and Liao [44] used the MR damper for designing a semi-active control system for a quarter car model and validated its applicability in improving the ride comfort. The implementation of semi-active MR damper concept for a full car model was also reported in literature [45] in which the primary objective was to improve the ride comfort when a car is subjected to road irregularities. Researchers have implemented the optimal control strategies for improving the performance of the semi-active MR suspensions to achieve the best ride quality [46]. A few studies validated the applicability of the MR damper for the seat suspensions where the aim was to supress the vibrations getting transferred to the human body through a seat [47].

Apart from vehicle engineering, MR dampers can also be utilized effectively for railway [48-51] and civil engineering applications. The purpose of using these dampers in railway applications is to attenuate the vibrations and improve the lateral ride quality. Liao and Wang [49]-[51] developed a secondary semi-active MR suspension system for railway vehicles to attenuate the vibrations getting transferred to the main body due to the bounce, pitch and roll motions. Intensive research has been going on in civil engineering field to develop the high capacity MR dampers for protecting the buildings and bridge structures against the wind and seismic loads [52], [53]. The concept of using the controllable dampers in aircraft landing gears has gained significant attention recently. Researchers have developed the aircraft models analogous to the vehicle models and designed the semi-active Magnetorheological landing gears for reducing the vibrations

getting transferred to the fuselage during landing and taxiing phases. A 2 DOF aircraft model representing the aircraft mass and wheel mass is the most commonly used model for the vibration analysis during landing phase, particularly. Because of the wide range of applications these dampers offer, they can be considered as the most effective solution for developing the intelligent damping systems for the future applications.

1.2.3 Semi-active suspension systems

The controllable properties of the Magnetorheological fluids can be used for developing the semi-active dampers which are capable of providing the variable damping without compromising efficiency. The intelligent damping concept has been widely used in vehicles, civil structures, railway vehicles, as well as in aerospace systems. The primary goal of implementing a semi-active suspension concept in vehicles and aircraft is to improve the passenger comfort and safety and to increase the stability whereas in the civil engineering field, this concept has been widely used for the protection of buildings and bridges against the wind and seismic loads.

The existing passive suspension systems are capable of dissipating energy effectively at a constant damping rate. Because of the unchangeable damping properties, variable damping forces cannot be generated which makes them unsuitable for the applications where the varying damping force is required depending on the operating conditions. In order to generate a force corresponding to the excitation input, the concept of the active and the semi-active suspensions was proposed in early 1950s. In active suspension systems, the force generating device used is the hydraulic actuator which requires a hydraulic power supply to operate. The actuator replaces the spring-damper configuration in the conventional passive dampers and generates the force relative to the

excitation inputs and operating conditions. However, the application of these systems is restricted because of the increased weight and cost involved. The large power requirement is also a limitation. The drawbacks of the passive and active suspensions can be overcome by the semi-active systems to achieve the effective vibration isolation. The semi-active systems are capable of providing the variable rate of energy dissipation according to operating conditions with the minimal power requirements. Moreover, the failure of the power in these systems does not lead to a complete failure of the operation since they can act as passive devices when the power is cut off. Because of their smaller weight, low power requirements and the ability to provide the variable energy dissipation rate, the semi-active suspensions can be considered to be the most effective solution for the aircraft and the vehicle suspensions [15].
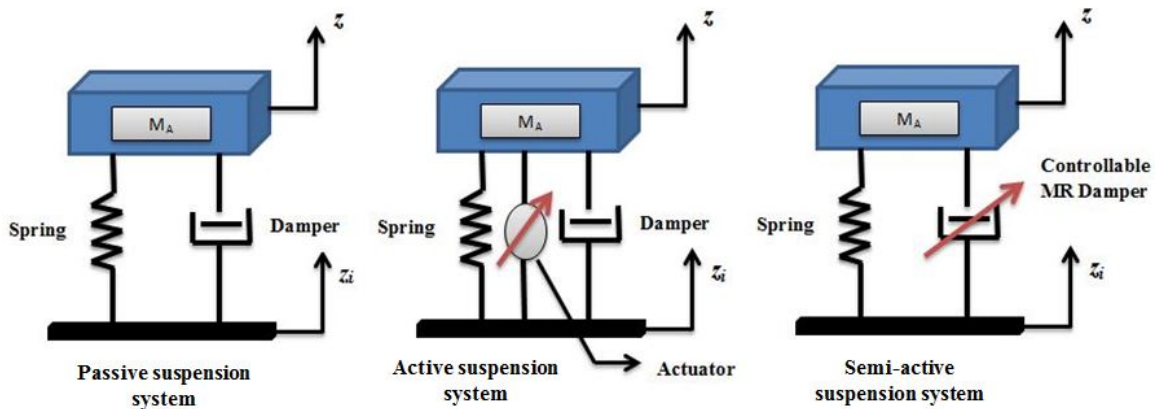
Figure 1.4 Configuration of passive, active and semi-active suspension systems [15]

The suitability of the semi-active systems for different applications was validated in the past using different approaches. Margolis [16] used a bond graph technique for comparing the semi-active systems with the passive and the active systems for the simple as well as the complex dynamic models and proved the applicability of the semi-active systems using optimal control strategies. Youn and Hac [54] used the concept of the

semi-active suspension for the 2 DOF vehicle model by implementing the optimal control strategies for the purpose of improving the ride comfort, road holding and the suspension rattle speed. Sims and Stanway [55] developed a semi-active suspension system for a quarter car model to prove the performance gains of the semi-active suspensions over the passive suspensions. A controllable viscous damper with a force feedback concept was developed for this study. To improve the performance of the semi-active vehicle suspensions, researchers have developed the robust control strategies such as H_∞ control in the recent past [17]. The application of the semi-active suspension systems in the aircraft landing gears is limited. No aircraft has been embedded with the semi-active struts so far. However, the research growth for developing the concept of the semi-active landing gears has been prolific [7], [12], [17], [28], [29], [56], [57]. Sivakumar and Haran [28] developed a semi-active landing gear for the 2 DOF aircraft model using the Proportional Integral Derivative (PID) controller to improve the ride comfort of the aircraft subjected to the runway excitations during landing, take-off and taxiing phases. Zapateiro et al [29] used the adaptive control approach for developing and comparing the performance of the active and the semi-active landing gears for the purpose of improving the passenger comfort during the aircraft ride. The concept of the adaptive aircraft shock absorbers was proposed by Mikulowski and Holnicki-Szulc [56] to cope with the variations in the landing conditions and to improve the impact absorption capacity. Kruger [57] designed a semi-active landing gear using three different control approaches and compared the simulated performance of the passive, active and the semi-active system for a multibody aircraft model of a transport aircraft. The criterion for comparing these systems was the vertical acceleration transmitted to the fuselage during landing. Su

et al [57] developed a predictive control algorithm for the nonlinear model to design a semi-active landing gear which could sustain the shocks during the landing and the taxiing phases and provide the adaptive damping for varying operating conditions. The reviewed literature is a clear indicator of the applicability of the semi-active systems in the aircraft landing gears as well as for other applications in near future.

1.2.4 Control strategies for the development of intelligent suspensions

The evolution of the development of the control approaches for building the most efficient semi-active suspensions for the vehicles [17], [19], [43], [55] and aircraft [12], [20] [28], [29], [56]-[60] has been remarkable so far. Lin et al [20] proposed a fuzzy PID controller for the landing gear system in order to reduce the accelerations transmitted to the fuselage during landing. A hybrid control algorithm combining the advantages of the PID and fuzzy control was developed and validated through a simulation approach. An active and a semi-active landing gear concept using a PID controller was used by Wang et al [27] and Sivakumar and Haran [28], respectively, to reduce the vertical motion of the aircraft body during landing and other phases. Considering the passenger comfort and aircraft fatigue life as the validation criterion, the applicability of the active landing gear concept was proved. Zapateiro et al [29] developed a concept of the adaptive backstepping control of the landing gear suspension using the robust H_∞ control approach for the purpose of improving the damping performance during different phases of the aircraft operation.

A few techniques to optimize the controllers for the landing gears were also reported, previously [56] by selecting the landing gear efficiency as an objective function. Kruger [57] used three different control approaches namely; a skyhook controller, a fuzzy

logic controller and a state feedback controller for developing the semi-active landing gear for the transport aircraft and designed a multi-objective optimization algorithm to optimize the control parameters of all the three controllers. A sliding model controller was utilized by Choi and Werely [59] to design the MR landing gear. Ghiringhelli [60] proved the applicability of the semi-active landing gears by optimally controlling the orifice area in the dampers to reduce the vertical impact on the aircraft during landing. Ghiringhelli and Gauldi [61] developed a multibody aircraft model through ADAMS simulation and validated the control approach for the landing gear drop test. The developed model is a good approximation of the real landing scenario. The primary goal of developing the semi-active landing gears using the optimal controllers is to provide safety and comfort to the passengers and reduce the fuselage vibrations during landing and taxiing.

1.3 Problem Definition

The aircraft, during its lifetime, is subjected to varying operating conditions in the air as well as on the ground. As landing is the most critical phase amongst all the operational phases, there is a need to design the most efficient landing gears. The shock absorber, which absorbs huge impact energy during the landing phase, is considered as the heart of the landing gear assembly and therefore, it becomes necessary to increase its performance efficiency and the life span. Though the existing shock absorbers are the most efficient till date, they are not able to meet the variable damping requirements to cope with the varying operating conditions. The problems such as bad weather conditions, runway unevenness and pilot inaccuracies might arise during the aircraft operation which could lead to accidents, sometimes. In such critical scenarios, it is necessary to have the most

19

efficient and the robust damping system which would prevent the aircraft from the potential accidents. The semi-active suspensions with the robust control strategies could prove to be a solid solution for preventing the potential aircraft accidents specifically, during landing.

1.4 Thesis Objectives

The literature review and the problem definition presented in the previous sections provide a strong basis for defining the objectives of this study. The specific objectives of this study are as follows:

- Study and analyze the force-velocity characteristics of the Magnetorheological damper to understand their dynamic behaviour for the sinusoidal excitations. Spencer model and sigmoid model are selected and a force velocity dynamic behavior is simulated using MATLAB based on the data available in the previous literature to validate their applicability.

- Analyze the energy dissipation characteristics of the MR dampers. Derive the equations for the energy dissipation of the MR damper in one cycle for a sinusoidal excitation and plot the graphs of the energy dissipated in one cycle against time. Plot the graphs of dissipated energy against the changing currents and frequencies.

- Develop a 3 DOF dynamic model of an aircraft embedded with a tricycle landing gear system and derive the equations of motion. A state-space approach is utilized for representing the system and developing the controller.

- Synthesize two different controllers, namely, a Linear Quadratic Regulator (LQR) and a robust H_∞ controller for developing the semi-active suspension system with MR damper as an actuator for the selected aircraft model.

- Validate the applicability and robustness of the designed semi-active suspension system by subjecting the aircraft to different landing scenarios considering runway roughness.

1.5 Thesis Organization

A thorough review of the relevant literature is presented in chapter 1 for developing a basic understanding of the concepts that will be implemented in the subsequent chapters. A problem definition and the thesis objectives are also presented in chapter 1.

Chapter 2 includes the study and analysis of the force-velocity characteristic of the MR damper in order to understand its dynamic behaviour. Various parametric and non-parametric models are reported for understanding the dynamic behaviour of the MR dampers. Finally, the two models, namely, Spencer model and Sigmoid model are selected and the response of the damper for the sinusoidal excitations is simulated based on the data already available in the literature.

Chapter 3 explains the basic concepts regarding the energy dissipation by the MR damper and its linearization. Spencer model which is used in chapter 2 for simulating the force-velocity characteristics is selected for analyzing the energy dissipation behaviour of the MR damper in one cycle for a sinusoidal input. The graph of the energy dissipated in one cycle is plotted against the time for a particular displacement and frequency input. As Spencer model is a current dependent model, the relationship of the dissipated energy

with increasing currents with a fixed value of the frequency and the displacement input is depicted graphically. Similarly, the relationship of the dissipated energy with changing frequencies is plotted for fixed current values.

In chapter 4, a 3 DOF dynamic model of an aircraft is developed and the equations of motion are derived. A state-space approach is followed for representing the system in order to synthesize two controllers for the developed system. The aircraft parameters are selected from the available literature.

Chapter 5 involves the simulation of the actual landing scenario for different sink velocities. The performance of the two controllers is compared for the purpose of selecting the appropriate control law. Finally, the response of an aircraft embedded with the developed semi-active system is plotted and compared with existing passive system. The applicability and the robustness of the controller are validated by subjecting the aircraft to the rough landing scenarios.

The important conclusions and the future recommendations are presented in chapter 6.

CHAPTER 2

DYNAMIC MODELING OF THE HYSTERETIC CHRACTERISTICS OF A MR FLUID DAMPER

2.1 Introduction

The Magnetorheological dampers are currently the focus of researchers and engineers [12] because of their potential to be used for the various engineering applications such as vehicle suspensions, aircraft landing gears, railway suspensions. A few civil engineering as well as biomechanical engineering [62], [63] applications have also been reported. The primary reason for the wide range of applications of the MR dampers is their controllable viscosity. The current levels required for achieving the required viscosity are also nominal. These dampers exhibit unique characteristics which enable their rapid transition from a low viscosity state to a high viscosity state according to the current variations. Their ability to provide a rapid interface between the mechanical systems and the electronic controls can be utilized for developing the semi-active systems [21].

In order to build the efficient MR fluid based dampers, it is imperative to understand their basic principle of operation. Moreover, these dampers exhibit a highly non-linear hysteretic behaviour which makes the process of the controller design critical. Therefore, it is necessary to understand the inherent hysteretic nature of these dampers to address the issue of the controller design. Various dynamic models have been proposed by the researchers, in the past, for accurately characterizing the behaviour of the MR dampers. In this section, the basic principle of the MR damper is presented first, followed by a critical review of the available dynamic models for characterizing the force-velocity

(f-v) hysteretic behaviour of these dampers. A simulation approach is adopted by taking into consideration two different dynamic models to plot and analyze the hysteretic behaviour of these dampers for a selected range of the sinusoidal excitations. As the data is taken from the previously available literature, the models are validated by comparing the simulation results of the f-v characteristics with the results available in the literature.

2.1.1 Operational features of the MR fluid based devices

The Magnetorheological fluid based devices are magnetic field dependent and are capable of producing high dynamic yield stress upon the application of a magnetic field. As mentioned in the literature, the achievable dynamic yield stress is about 100 kPa for typical MR fluid devices which makes them useful for the vibration mitigation applications. It is necessary to understand the behavior of the MR fluids under the influence of the magnetic field and analyze the stress development pattern.
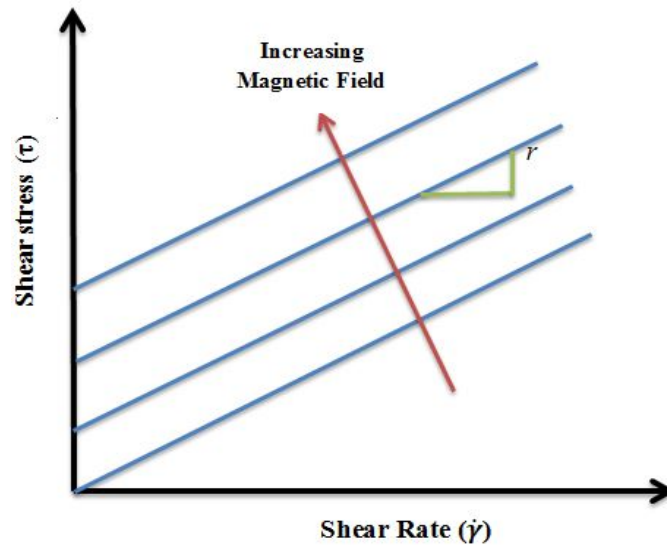
Figure 2.1 MR fluid behavior (non-Newtonian) in post-yield region [21]
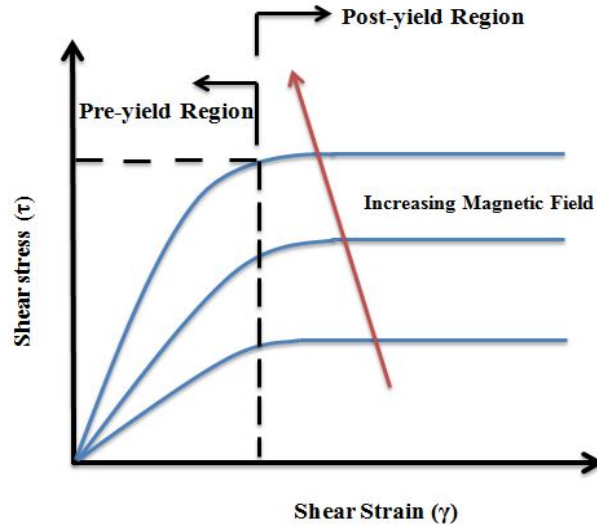
Figure 2.2 MR fluid behavior in pre-yield and post-yield regions [21]

The figures depict the dynamic behavior of the MR fluid under shear [21]. In the above figures, shear stress is plotted against the shear strain and shear rate to understand the behavior of the fluid in two distinct regions which are the pre-yield region and the post-yield region. The MR fluid exhibits different mechanical properties in these two regions. When the shear stress is below the yield stress, the fluid is said to be in the pre-yield region whereas it is said to be in the post-yield region when the shear stress exceeds the yield stress limit [64]. When the fluid is under the influence of a magnetic field, shear stress is developed which has two components; one of which is the viscous induced stress component and the other is the field dependent stress component. The field dependent stress component varies exponentially with the applied field. The MR fluid exhibits a linear viscoelastic behavior in the pre-yield region, a non-linear viscoelastic behavior in the yield region. Whenever, the shear stress exceeds the yield stress, the fluid enters the post-yield region showing a plastic behavior. It is important to understand the rheological properties of the fluid in these two regions to build MR fluid based devices [35].

As shown in the figure, the MR fluid devices can be operated in three different operational modes, namely, the flow mode, the direct shear mode and the squeeze flow mode or a combination of these three modes. The flow mode and the direct shear mode play a significant role in the development of all types of rotary and linear MR dampers whereas the squeeze film mode is used for developing the limited amplitude linear MR dampers [21], [65].
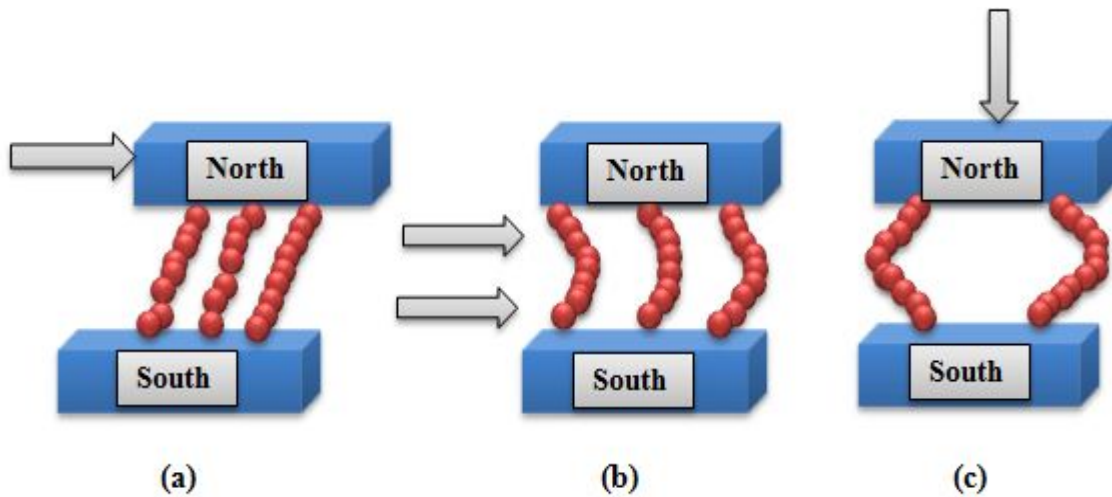
Figure 2.3 Operational modes of MR fluid (a) Shear mode (b) Flow mode (c) Squeeze mode [35]

The configuration of a typical linear MR damper is as shown in the figure 1.3. The damper operates in a mixed mode combining a flow mode and a direct shear mode. The cylinder consists of an upper chamber and a lower chamber, separated by a piston. There is an annular gap between the inside wall of the cylinder and the outside wall of the piston where MR fluid flows. The magnetic circuit is built along the piston and the cylinder which can generate a magnetic field for a particular time depending upon the current applied. When MR fluid flows through the activation regions, they are exposed to

the magnetic field to achieve the desirable viscous force. This way, by controlling the level of current at specific times, it is possible to magnetize the fluid and obtain high dynamic yield stresses according to the application requirements [66]. For the aircraft applications, these devices can prove their potential in mitigating the excessive vibrations at the time of landing, by generating the required viscous forces for nominal current levels.

2.2 Review of MR Damper Models

The non-linear hysteretic characteristics of the MR dampers refer to the force-velocity and force-displacement relations. The MR dampers exhibit inherent hysteretic behavior which has to be predicted accurately by using different modeling techniques in order to effectively implement these dampers for the variable damping applications. The force-velocity characteristic is a plot of variation of a damping force with the piston velocity which can be described in two distinct regions called the post-yield region and the pre-yield region. The shape of the hysteresis loop varies according to the variations in the parameters such as frequency, amplitude and current of the applied excitation signals. Many models have been developed so far, for accurately predicting the dynamic hysteretic behavior of the MR dampers for the purpose of developing effective control strategies [21]. The developed models must be applicable for a wide range of excitation conditions and should satisfy the validity criteria such as robustness, simplicity, accuracy and reversibility. Based on their properties, the MR damper models can be classified into two main categories; the dynamic models and the quasi-static models. The quasi-static models prove their ability in designing the MR damper but are not able to predict the non-linear hysteresis characteristics. The drawbacks of the quasi-static models can be

overcome by the dynamic models which can predict the non-linear hysteresis, making the process of the controller design less complicated.

The dynamic models can be further classified as the parametric dynamic models and the non-parametric dynamic models. The non-parametric modeling methods make use of the analytical approach for characterizing the behavior of the MR dampers. These models are applicable for the linear as well as non-linear systems because of their robustness [21]. Choi et al [67] proposed a polynomial model, which is a non-parametric model, to predict the MR damper hysteretic characteristics. In this model, the MR damper force is represented as a polynomial function in terms of piston velocity. However, the order of the polynomial was found out by trial and error method for accurately capturing the force-velocity hysteresis. Jin et al [68] proposed a black-box modeling technique for the MR dampers to cope with the structural control problems. The comparison between the non-linear black-box modeling and the semi-physical modeling is also reported in the literature [69]. The neural network model suggested by Wang and Liao [70] can be used for modeling and controlling the MR damper behavior as it is evident from the literature that the feed-forward neural networks can find an approximate solution for any continuous function. The other non-parametric models involve the fuzzy model, the Ridgnet model, the wavelet model and the multi-function model [21].

The parametric dynamic models represent the other class of the dynamic models. The parametric models represent a system as a collection of elements such as the springs and dampers and require a parameter identification procedure for modeling the dynamic behavior of the MR dampers. The complexity of the model can be judged depending upon the number of parameters to be identified. The parametric dynamic models fall into

various classes, namely, the Bouc-Wen hysteresis operator based dynamic models, the biviscous models, the sigmoid function based models, the Bingham model-based dynamic models, the viscoelastic plastic models, the hyperbolic tangent function models, the equivalent models and few others [21]. Werely et al [71] implemented four different parametric models for predicting the force-velocity hysteresis and the energy dissipation analysis of the MR dampers. These models involve the linearized equivalent viscous damping model, the non-linear Bingham plastic model, the non-linear biviscous model and the non-linear biviscous hysteretic model. The proposed Bingham plastic model assumes the material to be rigid in the pre-yield zone which starts flowing like a Newtonian fluid once the damper force exceeds the yield force. In the non-linear biviscous model proposed by Stanway [72], the material is assumed to be plastic in both pre-yield and the post-yield regions and the damping in the pre-yield condition is assumed to be significantly higher than that in the post-yield condition. The extension of the non-linear biviscous model is the non-linear biviscous hysteretic model, which is a four parameter model for accurately describing the hysteresis phenomenon in the pre-yield region. The sigmoid function based models [73]-[75] use the symmetric and asymmetric sigmoid functions for depicting the force-velocity relation. The Bouc-Wen hysteresis operator based dynamic models are the most widely used models for accurately identifying the hysteretic characteristics for control purpose. Spencer [76] proposed a novel model based on the Bouc-Wen hysteresis model which could accurately predict the inherent non-linear behavior of the MR dampers. The accuracy of the model was validated for a wide range of operating conditions. Further modifications in the Bouc-Wen model were suggested and implemented by Dominguez et al [77], [78] for

improving the ability of the model to predict the dynamic behavior. These models were used for developing the semi-active systems for structural control.

2.3 Modeling the Dynamic Behavior using Parametric Approach

A parametric modeling approach can be adopted for simulating the dynamic behavior of the MR damper when subjected to excitation forces. This approach not only provides the ease of simulation but is also useful in reducing the complexity in controller design. The MR damper force depends on the frequency and amplitude of the excitation signal to large extent. However, the dependency of the MR damper force on current cannot be neglected and has to be taken into consideration for accurately simulating the dynamic behavior for a particular excitation signal [21], [79], [80]. The variations in the current levels significantly affect the peak MR damper force, the post-yield saturation and the hysteresis force magnitude [79]. Most of the reported parametric models represent a relation between its inherent parameter and a current. Therefore, the total MR damper force can be represented as a combination of the hysteresis force function and a current function as follows:

$$F_{MR}(t) = F_D(x, \dot{x}, \ddot{x}) . F_I(I) \tag{2.1}$$

$$F_I(I) = 1 + \frac{k_c}{1 + e^{-a_c(i+I_0)}} - \frac{k_c}{1 + e^{-a_c I_0}} \tag{2.2}$$

Equation (2.1) represents the total MR damper force generated, F_{MR}, for a sinusoidal excitation. F_D is the hysteresis force which is a function of the piston displacement, velocity and acceleration as shown in equation (2.1). The expression for calculating F_D differs according to the model configuration. Equation (2.2) represents non-linear current function F_I which can be integrated with the hysteresis force to

calculate the total MR damper force, F_{MR}. Although, the method for calculating the hysteresis force differs for each model, the expression for the current function F_I, to be integrated, remains the same. Therefore, in order to understand the effects of applied current on the MR damper force, Spencer model and Sigmoid model are selected for simulating the force-velocity hysteretic behavior of the MR damper. The parameters of Spencer and Sigmoid model presented in [79] and [80] are selected for analyzing the hysteretic behavior. The simulation results are compared and validated with the results in [79]. In the following sections, the equations for Spencer model and Sigmoid model are expressed to predict the dynamic behavior of the MR dampers analytically. A simulation approach is adopted and the force-velocity behavior is plotted in MATLAB/SIMULINK for both the models.

2.3.1 Spencer model

Spencer model is an extension of the Bouc-Wen model with the addition of the spring and damper elements for improving the smoothness of the hysteretic characteristics. The dynamic equations of Spencer model for the damper force calculations can be derived from the model configuration as shown in figure 2.4. [76], [79], [81].
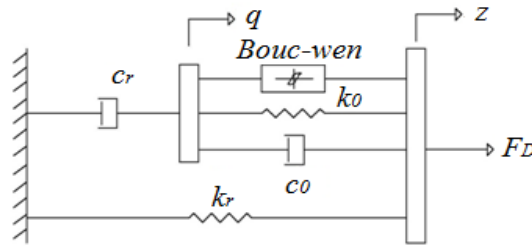
Figure 2.4 Spencer (extended Bouc-Wen) model for MR dampers [76]

The total MR damper force generated by the system is

$$F_D = \alpha p + c_0(\dot{z} - \dot{q}) + k_0(z - q) + k_r(z - z_i)$$

Adicionaria 4 componentes
no vetor de estados

(2.3)

where, k_r is the MR damper accumulator stiffness and z_i is the initial displacement associated with spring k_r and the control stiffness at larger velocities is represented by k_0. The relative displacement between the ends of the MR damper is given by z and q represents the internal state to account for the roll-off effect caused by the damping coefficient c_r. The restoring force F_D involves the non-dimensional auxiliary variable p which represents the hysteresis of the MR damper model.

$$\dot{p} = -\gamma p |p|^{n-1} |\dot{z} - \dot{q}| - \beta(\dot{z} - \dot{q})|p|^n + A_1(\dot{z} - \dot{q})$$

(2.4)

where, β and γ are the non-dimensional values to describe the hysteretic loop in the negative and positive slopes. Also, a is a non-dimensional value for defining the loop size with respect to the relative velocity of the two ends of MR damper. The transition of the MR fluid from elastic to plastic state should be smooth to eliminate the subjective feel of a damper. The smoothness of the transition between the two states is governed by a scalar n. The equation for q is presented as follows,

$$\dot{q} = \frac{1}{c_0 + c_r}\left(\alpha p + c_0 \dot{z} + k_0(z - q)\right)$$

(2.5)

The parameter related to the MR fluid yield stress is designated by α. The viscous damping coefficient at larger velocities is represented by c_0. The dashpot represented by c_r is included in the model to account for the roll-off effect, which is observed at low

velocities. In order to consider the effect of the magnetic field on the model parameters, Spencer [76] suggested a linear relationship between the applied voltage and the parameters α, c_0 and c_r. However, for the simulation purpose, the methodology suggested by Wang [15] and Ma [79], [80] is adopted in order to improve the model prediction abilities. Therefore, a modification in Spencer model can be done by considering the parameters α, c_0 and c_r as constants and integrating the non-linear current function shown in equation (2.2) with the hysteretic force function for predicting the hysteretic behavior accurately [15], [21], [79], [80].

$$F_{MR} = \left[\left(\alpha p + c_0(\dot{z} - \dot{q}) + k_0(z - q) + k_r(z - z_i) \right) \cdot \left(1 + \frac{k_c}{1 + e^{-a_c(i + I_0)}} - \frac{k_c}{1 + e^{-a_c I_0}} \right) \right] \qquad (2.6)$$

A álgebra não é tão complexa, mas achar os valores das constantes deve ser bem complexo

For the ease of simulation, a hysteretic force function, F_D, described in equation (2.3) is calculated separately and integrated with the non-linear current function. Equation (2.6) represents the total MR damper force for this model.

2.3.2 Sigmoid model

Sigmoid model is a parametric dynamic model which formulates the hysteretic force function using the symmetric sigmoid function. This function does not take into account the current dependency. To consider the effect of current on the MR damper hysteresis loop, a non-linear current function described in equation (2.2) can be integrated with the hysteretic force function. The hysteretic force function depends on the displacement, velocity and the acceleration of the input applied. This function can be described by the following equation [15], [21], [79], [80].

$$F_D = F_T \frac{1 - e^{-\mu(\dot{x} + v_h)}}{1 + e^{-\mu(\dot{x} + v_h)}}(1 + k_p |\dot{x}|)$$

(2.7)

In equation (2.7), the term F_T represent the transition force. The transition force represents the value of the force at a particular point at which the hysteresis loop enters the post-yield region. The governing equation for the transition force can be described as follows,

$$F_T = F_0(1 + e^{b_1 v_m})$$

(2.8)

Another term that is involved in the hysteretic force function equation is the zero force-velocity intercept, v_h. The shape of the hysteresis loop, especially its width varies according to the variations in v_h. The mathematical equation for calculating this term can be represented as shown below.

$$v_h = sign(\ddot{x})k_a v_m \left(1 + \frac{k_b}{1 + e^{-\psi(i + i_0)}} - \frac{k_b}{1 + e^{-\psi i_0}}\right)$$

(2.9)

It can be interpreted from the above equation that the input excitation conditions have a significant effect on v_h. On the other hand, the dependency of v_h on applied current is nominal. This indicates that for Sigmoid model, the current variations only have a slight effect on the width of the hysteresis loop.

In equation (2.7), k_p and μ are the linear rise coefficient and the hysteresis slope coefficient which can be formulated as,

$$k_p = k_m e^{-a_1 v_m}$$

(2.10)

$$\mu = \frac{a_0}{1 + k_0 v_m} \tag{2.11}$$

From the equations presented above, it can be observed that the terms defined above depend on the term designated as v_m which is the peak velocity. In actual practice, the values of v_m cannot be measured directly. However, it is necessary to measure this velocity in order to depict the force-velocity relationship accurately. The peak velocity v_m can be measured from the instantaneous displacement, velocity ad the acceleration of the applied input. The equation for measuring the peak velocity v_m can be represented as follows.

$$v_m = \sqrt{(\dot{x})^2 - (\ddot{x}x)} \tag{2.12}$$

Therefore, the total MR damper force including the non-linear current function can be represented as shown in equation (2.13). The constants defined in the above equations are F_0, i_0, a_0, a_1, b_1, k_0, k_a, k_b, k_m and Ψ.

$$F_{MR} = \left[\left(F_T \frac{1 - e^{-\mu(\dot{x}+v_h)}}{1 + e^{-\mu(\dot{x}+v_h)}} (1 + k_p |\dot{x}|) \right) \cdot \left(1 + \frac{k_c}{1 + e^{-a_c(i+I_0)}} - \frac{k_c}{1 + e^{-a_c I_0}} \right) \right] \tag{2.13}$$

To simulate the response of the MR damper using the above equations it is necessary to identify the constant parameters involved in these equations. Wang [15] and Ma [79], [80] presented a methodology for the parameter identification. The parameters identified in [79] can be used for the simulation in order to validate the developed model.

2.4 Simulation Results

Based on the hysteretic force equations and the current relationships, a hysteretic force-velocity behavior is plotted using Spencer model and Sigmoid model described in the sections (2.3.1) and (2.3.2).

In order to validate the accuracy of the developed Simulink model, the obtained force-velocity hysteresis curves are compared with the results in [79]. The accuracy of the Simulink model is necessary to validate since the built Simulink model will be used again for defining the actuation system for the semi-active aircraft landing gear which is the main objective of the study. According to the experimental analysis done in [15], [79], [80] the MR damper is excited by a sinusoidal signal with the amplitude of 6.25 mm. Three different frequency values are selected which are 1.5 Hz, 2.5 Hz and 5Hz. The applied current values are 0.00 A, 0.25 A, 0.50 A, 0.75 A, 1.00 A, 1.25 A and 1.50 A. Maintaining the amplitude constant, the hysteretic behavior of the MR damper for a particular frequency is depicted for seven different current levels. The simulation results for the hysteretic f-v characteristics for Spencer model and Sigmoid model can be observed from the following figures.

Figures (2.5)-(2.7) show the results of the force-velocity hysteresis for Spencer model whereas figures (2.8)-(2.10) depict the behavior for Sigmoid model.
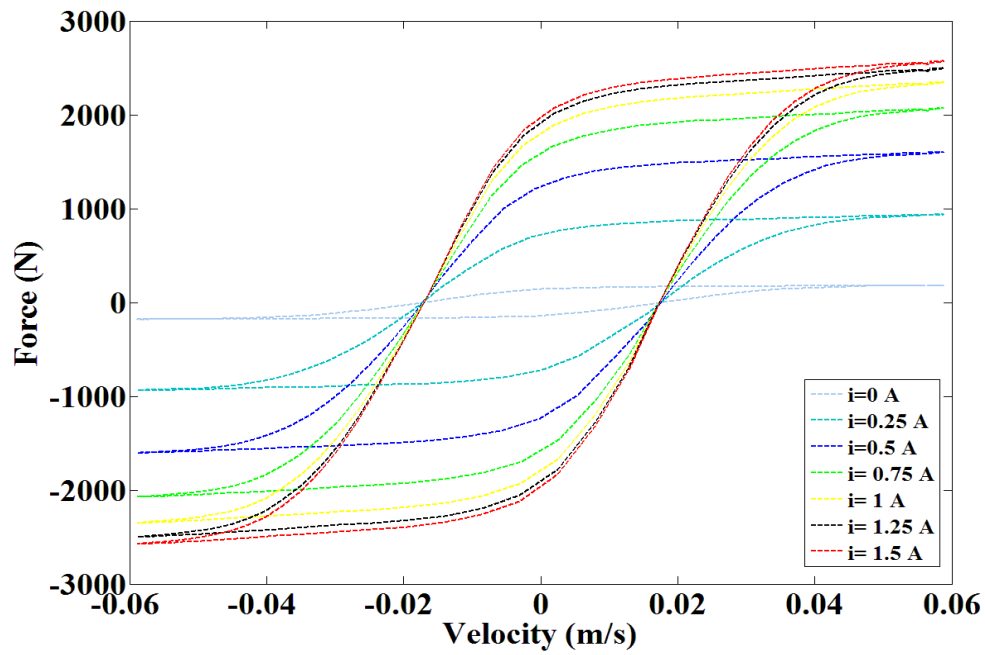
Figure 2.5 Simulation of hysteretic f-v characteristics of MR damper for frequency of 1.5 Hz using Spencer model
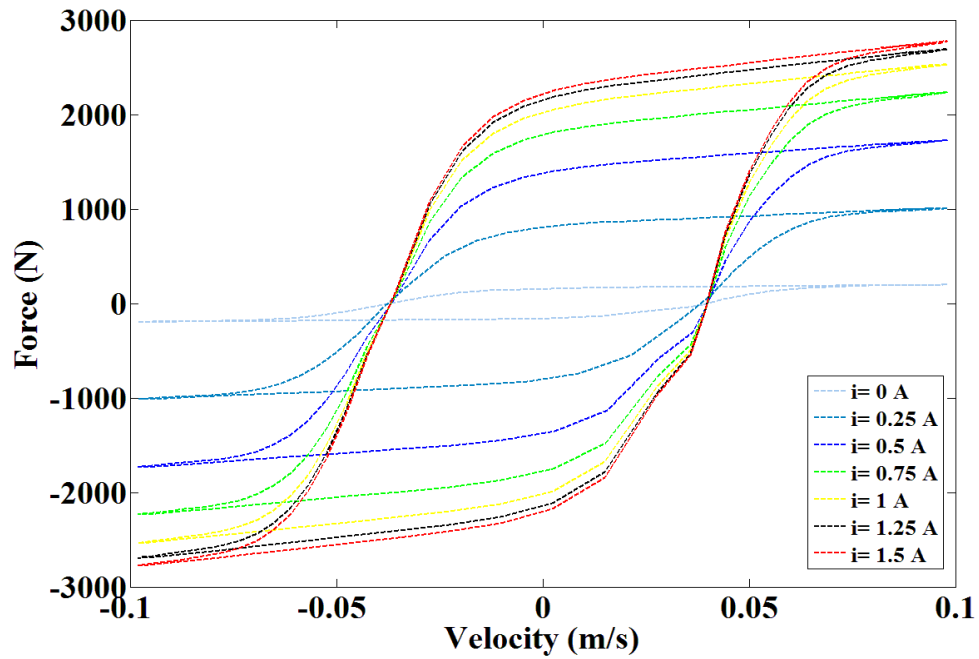
Figure 2.6 Simulation of hysteretic f-v characteristics of MR damper for frequency of 2.5 Hz using Spencer model
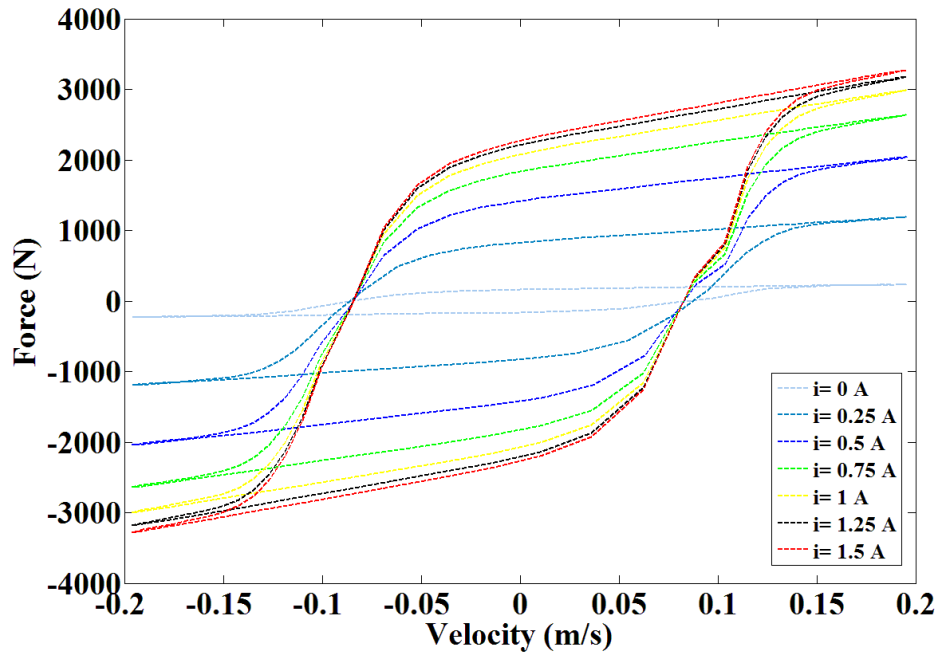
Figure 2.7 Simulation of hysteretic f-v characteristics of MR damper for frequency of 5.0 Hz using Spencer model
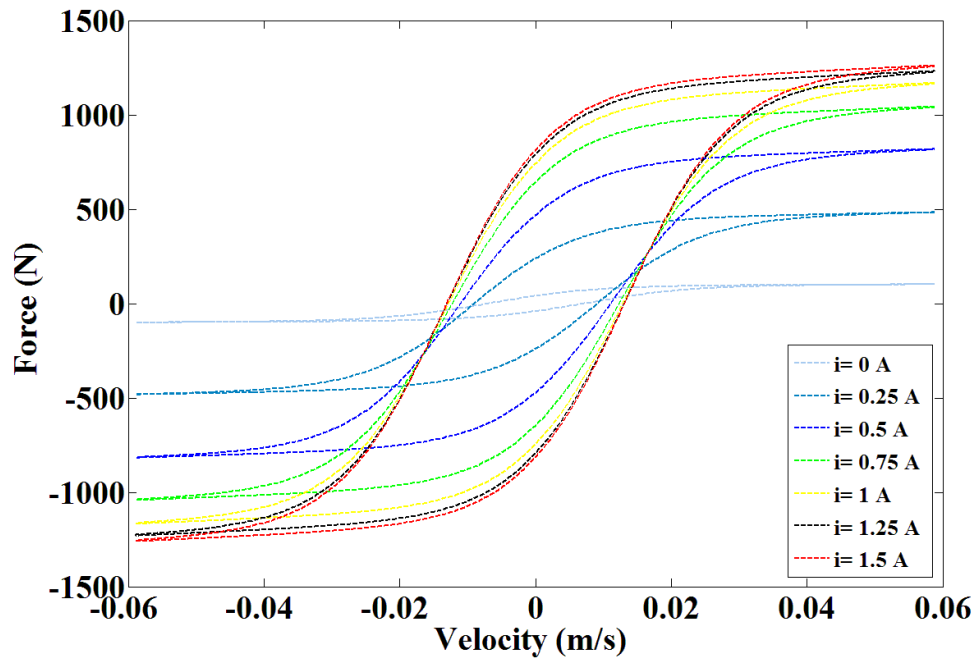
Figure 2.8 Simulation of hysteretic f-v characteristics of MR damper for frequency of 1.5 Hz using Sigmoid model
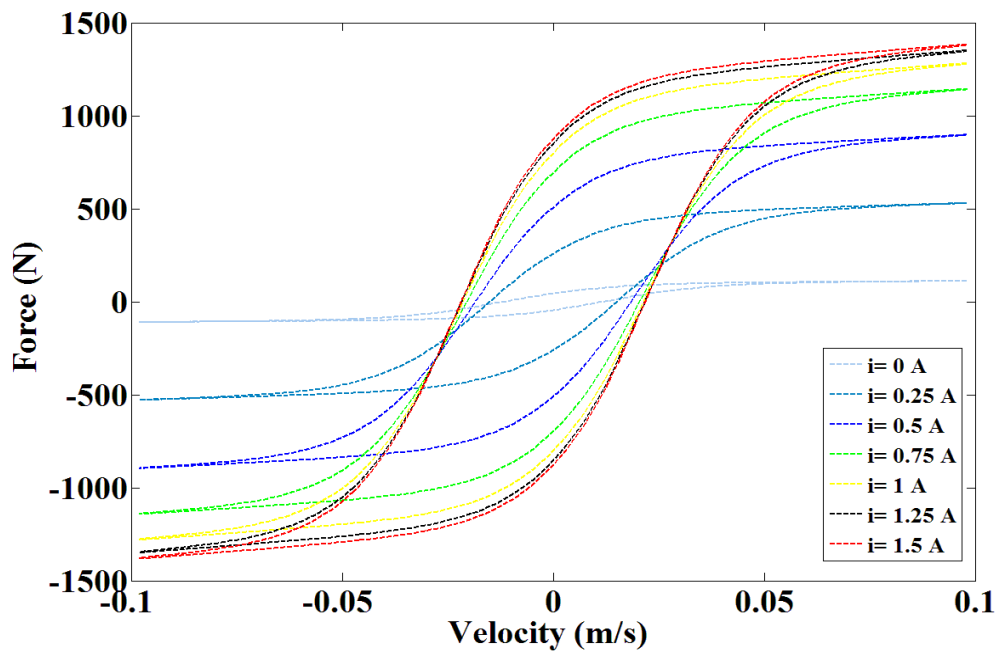
Figure 2.9 Simulation of hysteretic f-v characteristics of MR damper for frequency of 2.5 Hz using Sigmoid model
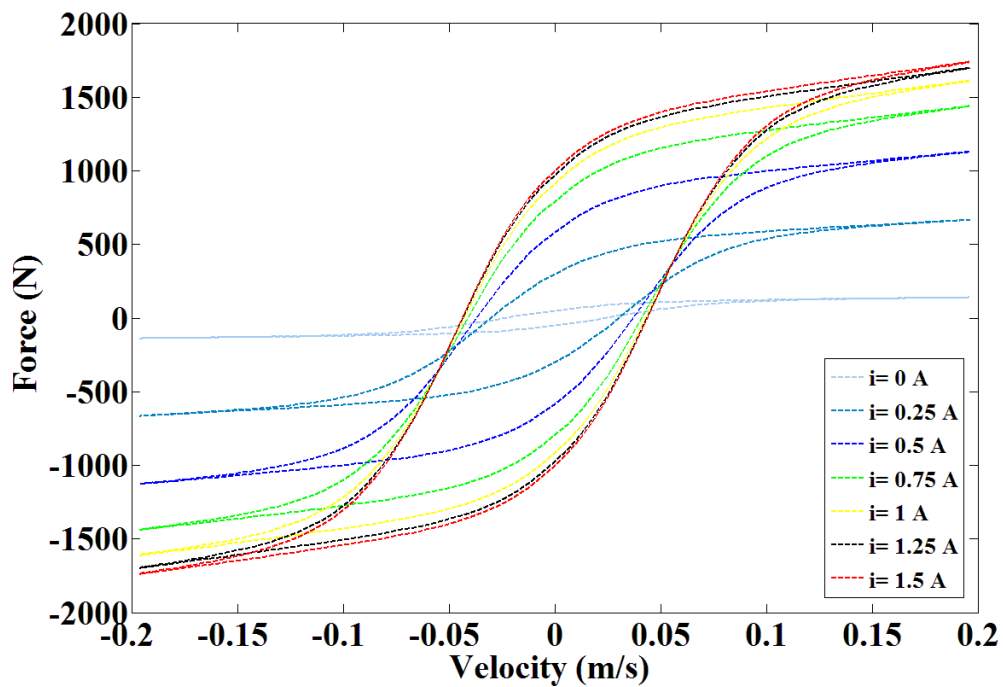
Figure 2.10 Simulation of hysteretic f-v characteristics of MR damper for frequency of 5.0 Hz using Sigmoid model

2.5 Discussions

The dynamic behavior of the MR damper can be analyzed from the simulation results of the hysteretic force-velocity characteristics. The important observations from the obtained results are summarized as follows:

- For both models, the MR damper behaves as a linear viscous damper when there is no current applied in a circuit. The force varies approximately linearly with the velocity, which is depicted as the light grey curve in the figures. It can be interpreted that the MR damper behaves as a passive device whenever there is no current in the circuit.

- For small increments in current levels, the magnitude of the MR damper force increases significantly. The path of the hysteresis loop follows a counter-clockwise direction when plotted against time. Motion to the right corresponds to positive acceleration and vice versa. The mean curve of the hysteresis loop approximately corresponds to the viscous damping coefficient of the MR fluid. In the pre-yield region, a strong hysteresis can be observed. The force velocity relationship is linear for larger positive velocities in the post-yield region.

- The variations in the frequency values of the applied signal have a significant effect on the magnitude of the force as well as on the hysteresis loop. The force increases with the frequency. Moreover, at higher frequencies, the width of the hysteresis loop increases in size, especially in case of Spencer model.

- The upper curve in the hysteresis loop depicts the relationship of the MR damper force with the decreasing velocities whereas the lower curve represents the force with the increasing velocities. The force velocity relationship is linear for the

larger positive velocities. However, when the velocity decreases and before the loop enters the negative region, the force velocity relation drops off suddenly but smoothly. This rapid drop is due to bleed or blow-by of fluid between the piston and the cylinder. This non-linear effect is called the roll-off effect and it allows a smooth transition between the two operating regions of the MR dampers thereby avoiding a sudden shock like feeling. A simulation approach using Spencer model can satisfactorily consider this effect thereby proving its advantages over sigmoid as well as the other existing models, particularly for the suspension applications.

2.6 Summary

In this chapter, the literature regarding the basic principle of operation of the Magnetorheological dampers, their characteristics and the dynamic modeling strategies for describing those characteristics is thoroughly reviewed. A simulation approach was adopted in order to gain in-depth understanding of the force-velocity hysteretic characteristics of the Magnetorheological damper using two parametric dynamic models, namely, Spencer model and Sigmoid model. Both the models were built using MATLAB/SIMULINK. To validate the accuracy of the models, the results of the hysteretic force-velocity characteristics are plotted and checked with the results in the literature. Once the simulation results matched with the results in the available literature, the two models were compared in order to select the best out of two for further applications in the remaining part of the study. From the observations, it can be interpreted that the Spencer model is easy to build and is robust and accurate. Moreover, it also takes into consideration the roll-off in the lower velocity region of the hysteresis loop which plays a significant role in building MR damper actuating systems for the

semi-active suspensions. Therefore, Spencer model is used for the further analysis in the next chapter for studying the phenomenon of the energy dissipation by the MR damper through the simulation approach.

CHAPTER 3

ANALYSIS OF THE ENERGY DISSIPATION BY THE

MAGNETORHOLOGICAL DAMPER

3.1 Introduction

A thorough review of the literature suggests that the Magnetorheological dampers are capable of effectively controlling the vibration. They have a wide range of applications almost in every stream of engineering. However, achieving the effective vibration attenuation using the controllable MR dampers is a critical task because of their inherent non-linearity. The MR dampers exhibit a highly non-linear hysteretic behavior upon the application of the external signal which is evident from the force-velocity hysteresis results obtained through simulation in chapter 2. As mentioned in the literature, this inherent non-linearity poses some limitations in the controller design thereby making the task of semi-active suspension design more critical.

Since the primary objective of this study is to build an effective semi-active suspension system for the aircraft landing gears for vibration suppression during landing, it is necessary to understand completely, the non-linear characteristics of the MR dampers to facilitate the task of controller design. The force-velocity hysteretic characteristic gives an understanding of the dynamic behavior of the MR damper to some extent. However, it is also necessary to analyze the pattern of the energy dissipation by the MR damper over a cycle. The analysis of the energy dissipation can provide better understanding of the damping characteristics and also can facilitate the process of linearizing the MR damper for finding the equivalent viscous damping coefficient for the given operating conditions to simplify the non-linearity problem.

In this chapter, an analysis of the energy dissipation behavior of the MR damper is carried out. Again, Spencer model, which was used in the previous chapter, is used for depicting the force-displacement characteristics of the MR damper which are useful for calculating the energy dissipation by the damper over one cycle. The excitation conditions are same as those in chapter 2. The energy dissipation behaviour is analyzed for three different frequencies and seven different current levels. An equivalent viscous damping coefficient is calculated for each operating condition in order to linearize the MR damper. Finally, the graphs of the energy dissipated versus the current and the frequency are plotted. Similarly, the graphs can be plotted for the calculated equivalent viscous damping coefficients.

3.2 Linearization of the Magnetorheological Damper

The Magnetorheological damper can be linearized using the concept of equivalent viscous damping [71]. In normal practice, the equivalent damping coefficient (C_{eq}) is calculated for approximating the performance of the non-linear MR damper by a conventional viscous damper. The equivalent viscous damping coefficient provides the same damping effect as that of the MR damper [82]-[85]. Linearization would facilitate the understanding of the damping characteristics of the MR dampers.

In order to calculate the equivalent viscous damping coefficient, C_{eq}, it is necessary to calculate the amount of energy dissipated by the MR damper in one cycle for a given input signal. Moreover, since the dynamic behaviour of the MR damper is analyzed using the current dependent Spencer model, the effect of the current on the dissipated energy has to be taken into consideration. The rate of energy dissipation is the

important factor in determining the effectiveness of the damper for vibration mitigation applications.

The energy dissipated by the MR damper over a cycle for a particular sinusoidal input signal can be calculated from the force-displacement (f-d) characteristic which is a plot of the MR damper force versus the displacement. The f-d characteristics can be plotted similar to the force-velocity characteristics. The force-displacement characteristic takes a clockwise path, opposite to that of the force-velocity characteristic and is approximately elliptical in shape as shown in figure 3.1 [83].
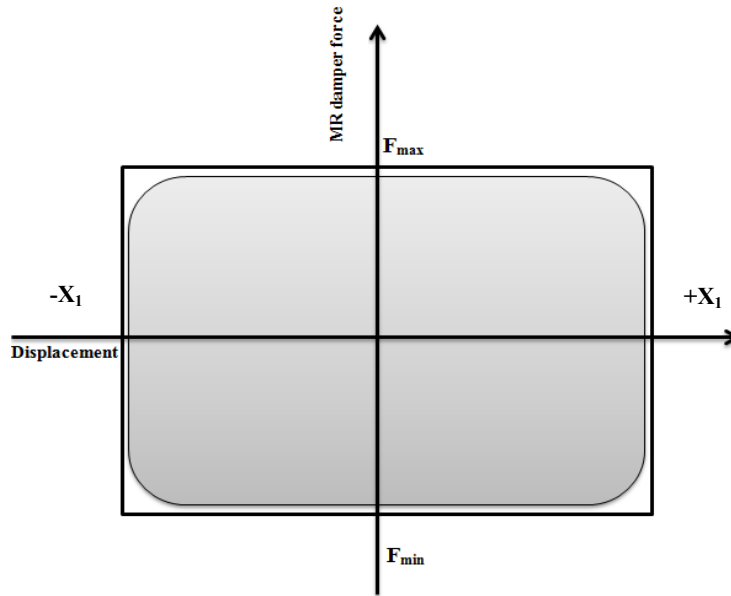
Figure 3.1 Schematic of energy dissipated by MR damper in one cycle [83]

As shown in figure 3.1, the energy dissipated by the MR damper in one cycle can be calculated by finding the area under the elliptical force-displacement loop for a particular sinusoidal input signal and a current. Ideally, the grey area in the diagram represents the energy dissipated in a cycle for a particular input. However, for the initial approximation, the energy dissipated can also be calculated by considering the ellipse as

a rectangle and finding out the peak values of the force and the displacement. Accordingly, the energy dissipated can be calculated with reference to figure 3.1 as follows.

$$E_{MR} = 2 \cdot (F_{max} - F_{min}) \cdot X_1 \qquad (3.1)$$

The above equation calculates the approximate value of the dissipated energy by considering the rectangular area as shown in figure 3.1. However, in order to accurately calculate the amount of energy dissipated by the MR damper in one cycle, it is necessary to find the area under the elliptical loop.

For a sinusoidal excitation signal, $x(t) = X_1 * sin \omega t$, where X_1 is the amplitude and ω is the frequency, the energy dissipated by the MR damper over one complete hysteretic cycle is represented by the grey area in figure 3.1 and is given by equation 3.2. [82]-[85].

$$E_{MR} = \oint F_{MR} dx = \int_0^{2\pi/\omega} F_{MR} \dot{x} dt \qquad (3.2)$$

Once the energy dissipated by the MR damper over a cycle is calculated using the above integral equation, the equivalent viscous damping coefficient can be calculated for each excitation input which would be useful for comparing the performance of the non-linear MR damper with its equivalent viscous damper. Following equations can be used for calculating the equivalent viscous damping coefficient. The C_{eq}, also exhibits a relationship with the applied current which will be analyzed in the results section.

$$F_{MR} = C_{eq} \dot{x}(t) \qquad (3.3)$$

$$E_{MR} = \int_{0}^{2\pi/\omega} C_{eq}(\dot{x})^2 \, dt \tag{3.4}$$

$$E_{MR} = \int_{0}^{2\pi/\omega} C_{eq}(X_1 \omega \cos \omega t)^2 \, dt \tag{3.5}$$

$$E_{MR} = C_{eq} \pi \omega X_1^2 \tag{3.6}$$

$$C_{eq} = \frac{E_{MR}}{\pi \omega X_1^2} \tag{3.7}$$
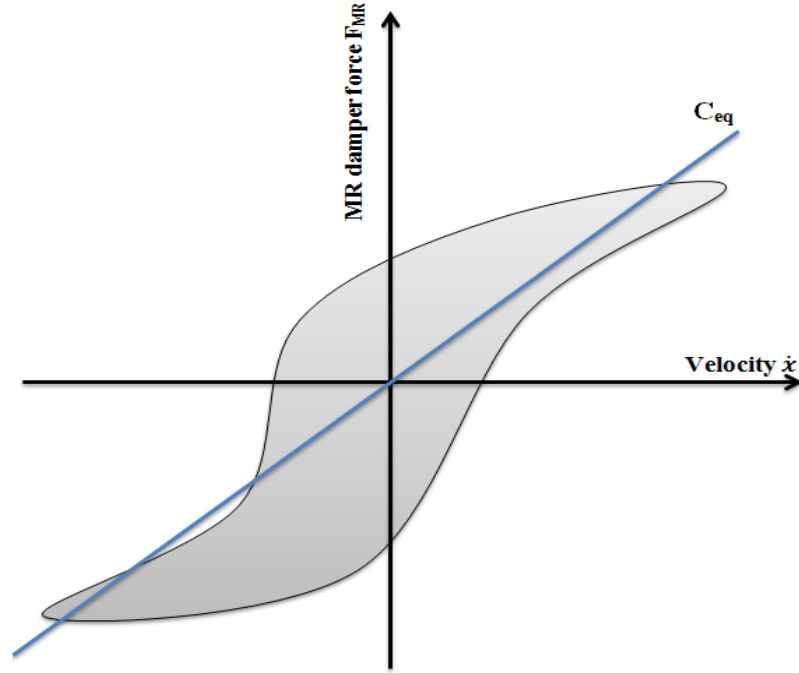
Figure 3.2 Schematic representing equivalent viscous damping [71]

3.3 Analysis of the Energy Dissipation by the MR Damper using Spencer model

For characterizing the non-linear hysteretic force-velocity behavior of the MR damper, Spencer model was used previously using the parameters available in the literature. For the energy dissipation analysis, it is necessary to characterize the force-displacement

47

hysteretic behaviour of the damper. The force-displacement characteristic of the MR damper can be depicted using the Spencer dynamic model which was used previously. The MR damper is excited by a sinusoidal input signal with the amplitude of 6.25 mm. Three different frequency values are selected which are 1.5 Hz, 2.5 Hz and 5Hz. The applied current values are 0 A, 0.25 A, 0.5 A, 0.75 A, 1 A, 1.25 A and 1.5 A. Maintaining the amplitude constant, the hysteretic force-displacement behavior of the MR damper for a particular frequency is depicted for seven different current levels. The simulated results for the force–displacement characteristics are as shown in figs. 3.3-3.5.

3.3.1 Simulation results for the force-displacement characteristics
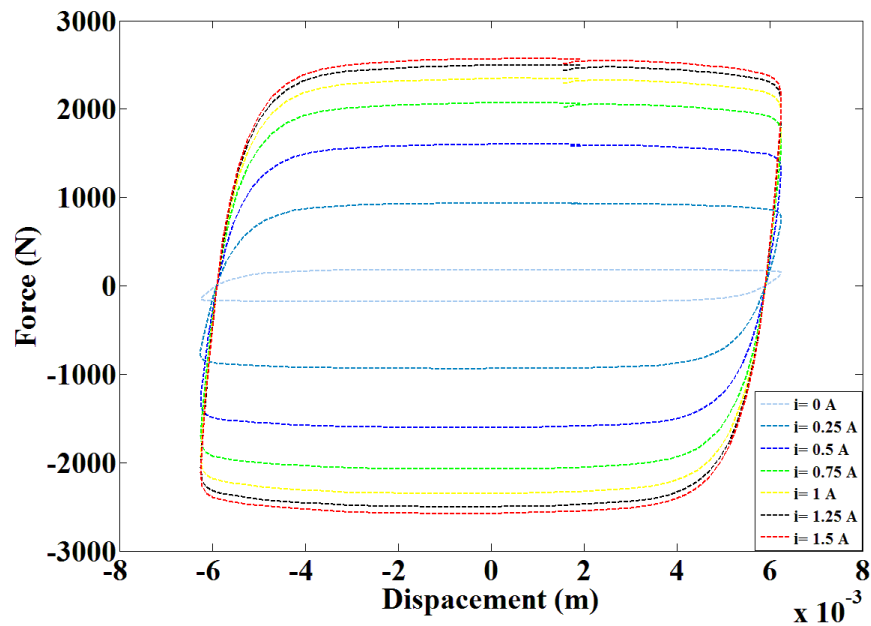
Figure 3.3 Simulation of hysteretic f-d characteristics of MR damper for frequency of 1.5 Hz using Spencer model
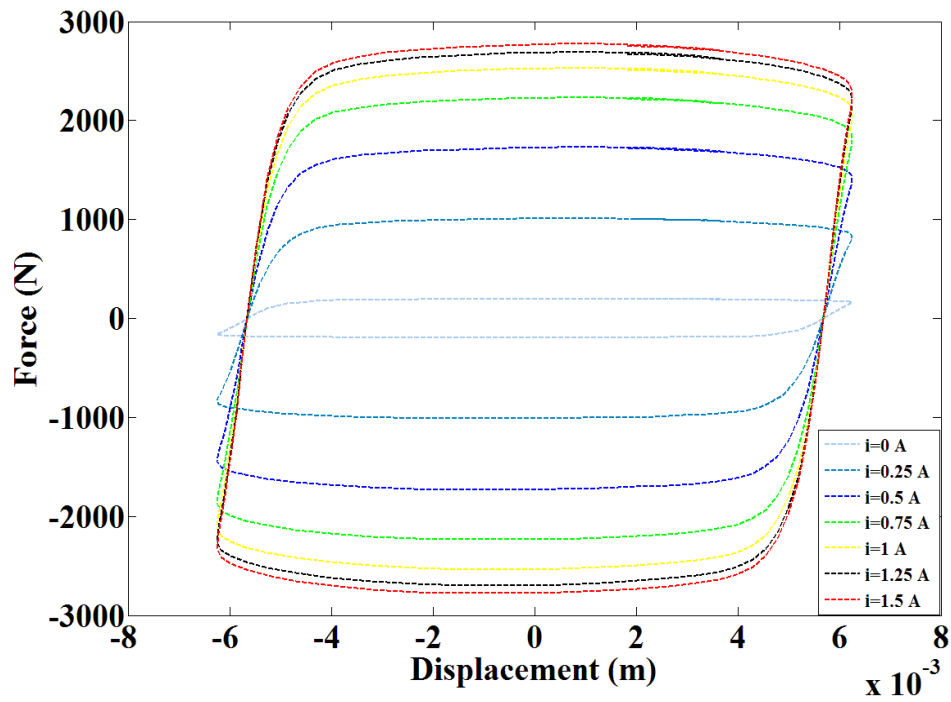
Figure 3.4 Simulation of hysteretic f-d characteristics of MR damper for frequency of 2.5 Hz using Spencer model
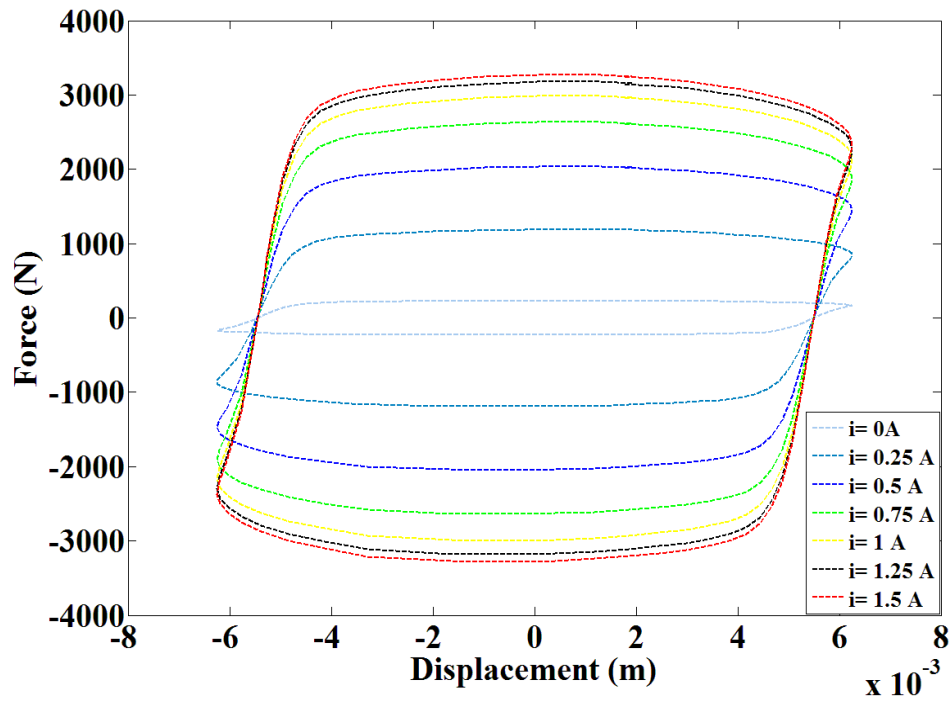
Figure 3.5 Simulation of hysteretic f-d characteristics of MR damper for frequency of 5.0 Hz using Spencer model

It can be observed from the force-displacement curves that the area of the ellipse increases with increase in current. The energy dissipated can be calculated for each current level simply by calculating the area under the elliptical curve. The frequency variations largely affect the MR damper force.

3.3.2 Simulation results for energy dissipation

Based on the force-displacement characteristics, the energy dissipated by the MR damper can be calculated by using equation (3.2) and integrating it in SIMULINK with the developed Spencer model. Figs. 3.6-3.8 depict the results for the dissipated energy against time for three different frequencies. The effect of increasing current levels can also be observed from the obtained results.
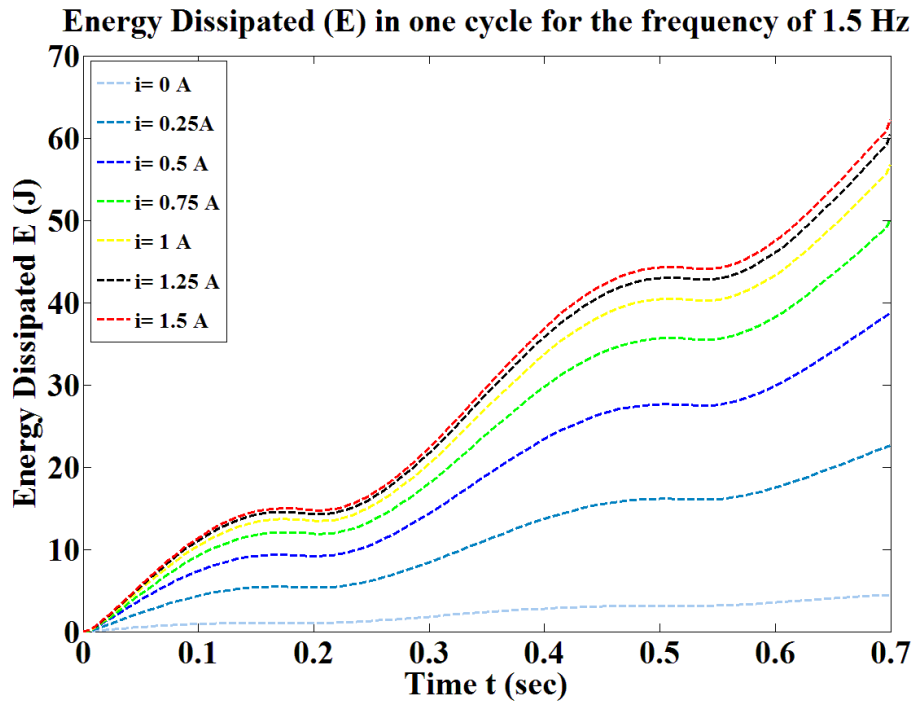
Figure 3.6 Energy dissipated by MR damper over one cycle for frequency of 1.5 Hz for increasing current levels

Energy Dissipated (E) in one cycle for the frequency of 2.5 Hz
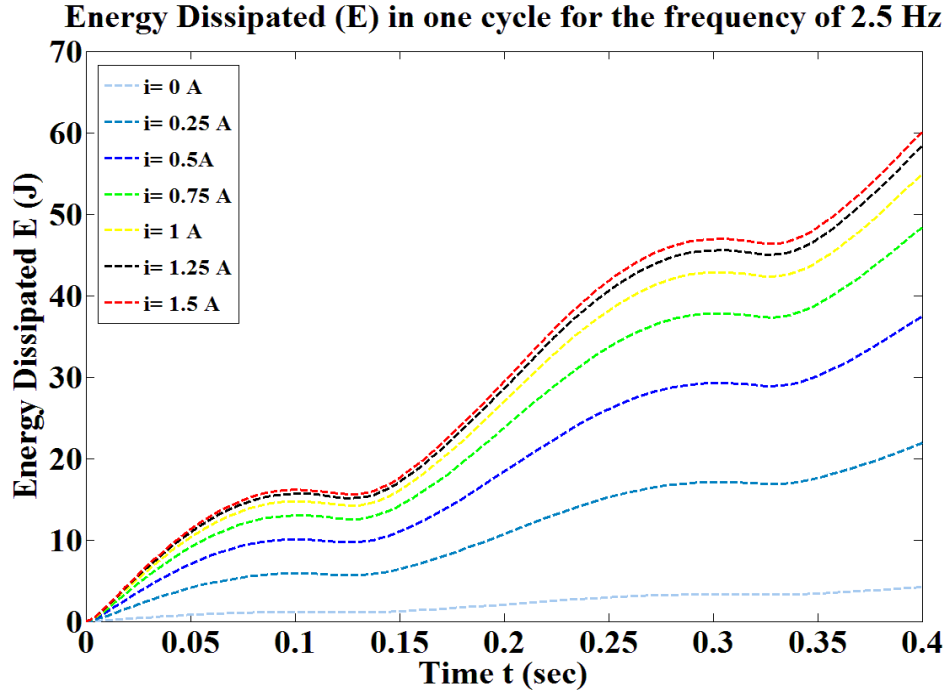
Figure 3.7 Energy dissipated by MR damper over one cycle for frequency of 2.5 Hz for increasing current levels

Energy Dissipated (E) in one cycle for the frequency of 5 Hz
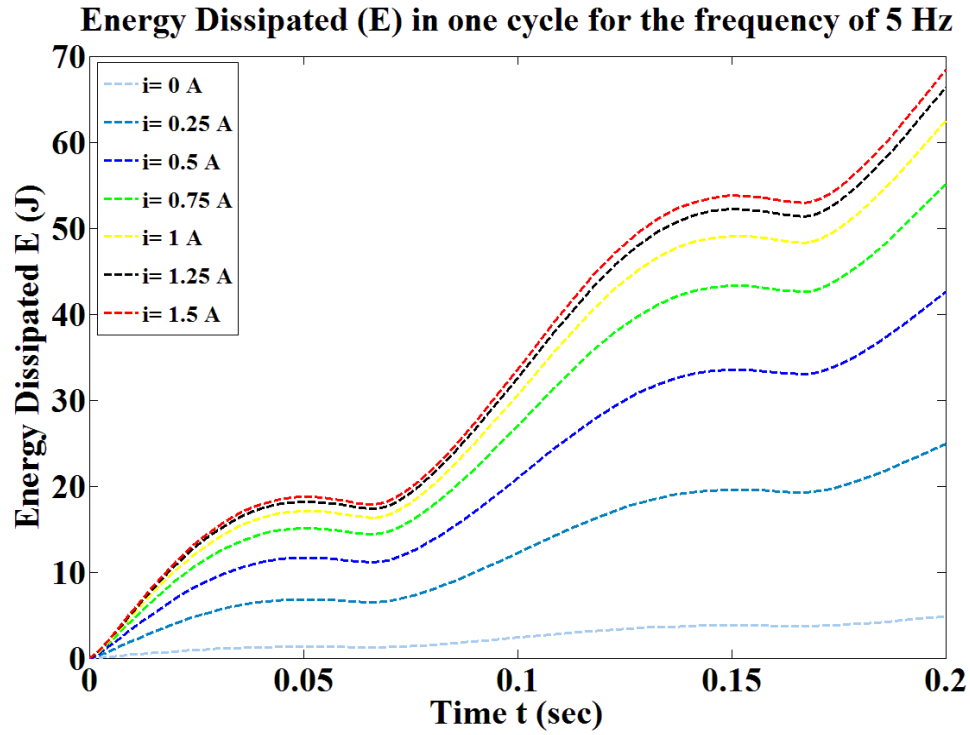
Figure 3.8 Energy dissipated by MR damper over one cycle for frequency of 5.0 Hz for increasing current levels

The effect of the variations in the frequency and the current levels on the energy dissipation behavior can be observed from figs. 3.6-3.8. The exact numerical values of the dissipated energy at the end of one cycle for each operating frequency and current are extracted from the MATLAB workspace and summarized in the following tables.

Table 3.1 Dissipated energy for input frequency of 1.5 Hz for increasing current levels

No.	Current I (Amp.)	Energy Dissipated E (J)
1	0	3.9739
2	0.25	20.4856
3	0.5	35.0747
4	0.75	45.3059
5	1	51.3764
6	1.25	54.6267
7	1.5	56.2719

Table 3.2 Dissipated energy for input frequency of 2.5 Hz for increasing current levels

No.	Current I (Amp.)	Energy Dissipated E (J)
1	0	4.2471
2	0.25	21.8857
3	0.5	37.4788
4	0.75	48.4149
5	1	54.9031
6	1.25	58.3772
7	1.5	60.1355

Table 3.3 Dissipated energy for input frequency of 5.0 Hz for increasing current levels

No.	Current I (Amp.)	Energy Dissipated E (J)
1	0	4.8338
2	0.25	24.9276
3	0.5	42.6509
4	0.75	55.0935
5	1	62.4760
6	1.25	66.4289
7	1.5	68.4297

Tables 3.1-3.3 summarize the numerical analysis of the dissipated energy with increasing levels of the current and the frequency. It can be interpreted that the amount of energy

dissipated per cycle increases with the frequency and current. As the frequency increases from 1.5 Hz to 5 Hz, the amount of energy dissipated per cycle increases. Moreover, for each frequency, the energy dissipation rate can be improved by applying a very nominal current. It can be observed from the numerical data that for a small increase in current, there is a significant increase in the dissipated energy.
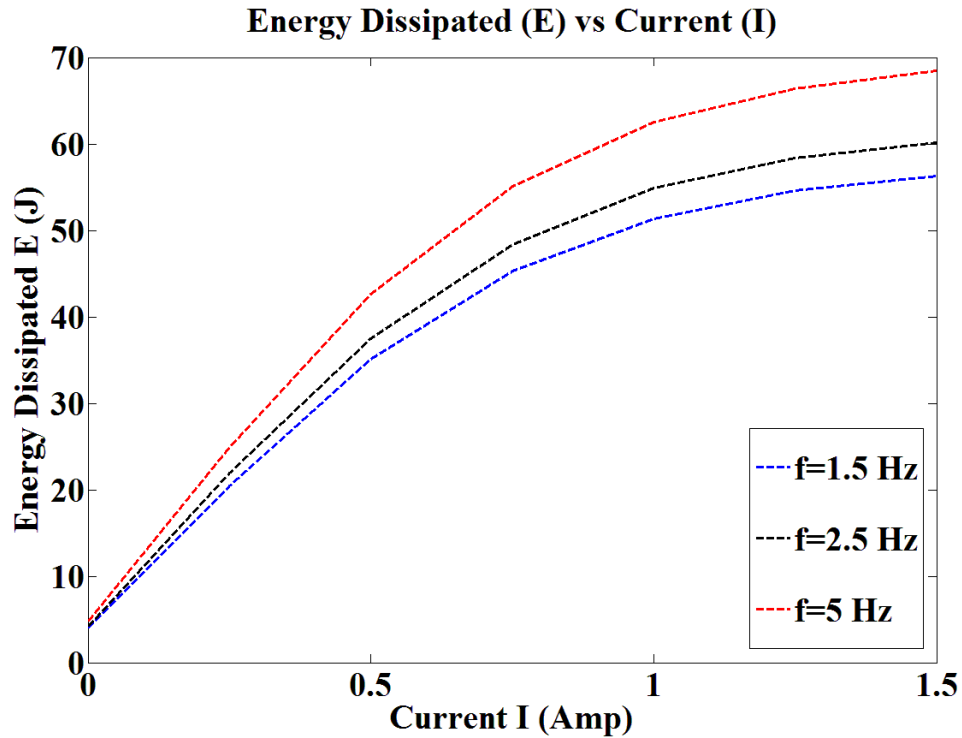
Figure 3.9 A graph of energy dissipated versus current

For currents less than 1 A, the increase in the dissipated energy levels is significant. However, for the current values greater than 1 A, the dissipated energy levels increase slowly towards the end of the cycle. Similar pattern can be observed for all three input frequencies.
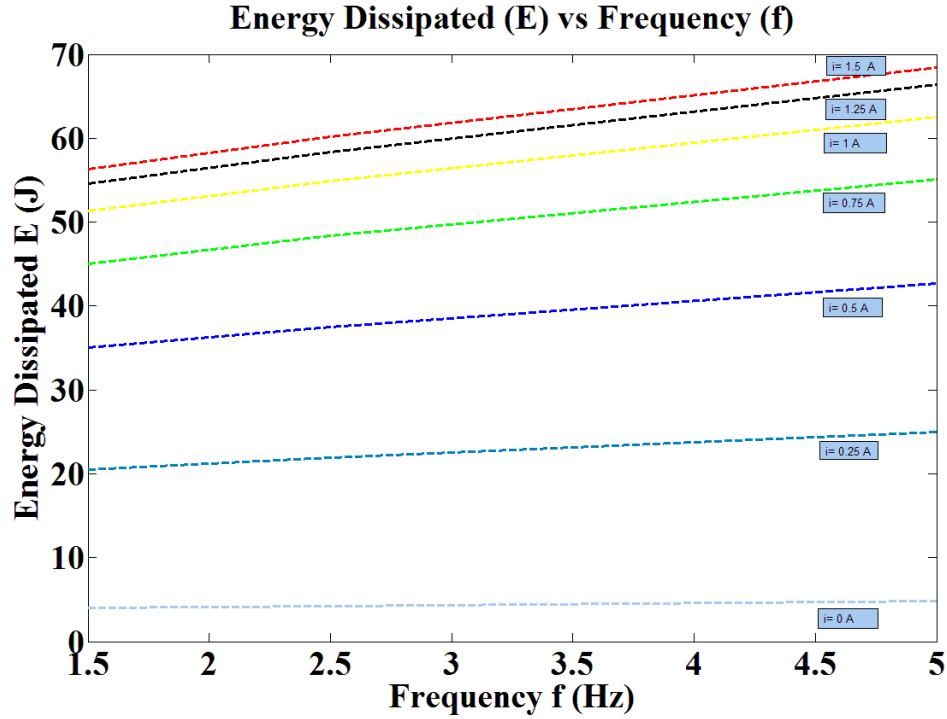
Figure 3.10 A graph of energy dissipated versus frequency

The variation of the dissipated energy in one cycle for the increasing values of the currents and frequencies can be observed from figures 3.9 and 3.10, respectively.

3.3.3 Simulation results for the equivalent viscous damping coefficients

From the obtained numerical values of the dissipated energy for each frequency and current, the equivalent damping coefficient can be calculated from the equations (3.3)-(3.7) for each case in order to linearize the MR damper. The relationship between the C_{eq}, with increasing levels of the current and frequency can also be established. The values of the C_{eq} are obtained from the previously calculated values of the dissipated energy and are summarized in the following tables.

Table 3.4 *Ceq* values for input frequency of 1.5 Hz for increasing current levels

No.	Current I (Amp.)	Energy Dissipated E (J)	C_{eq} (N-s/m)
1	0	3.9739	3435.86
2	0.25	20.4856	17712
3	0.5	35.0747	30328.31
4	0.75	45.3059	39175.01
5	1	51.3764	44424.03
6	1.25	54.6267	47234.5
7	1.5	56.2719	48657.06

Table 3.5 *Ceq* values for input frequency of 2.5 Hz for increasing current levels

No.	Current I (Amp.)	Energy Dissipated E (J)	C_{eq} (N-s/m)
1	0	4.2471	2200
2	0.25	21.8857	11353.85
3	0.5	37.4788	19443.24
4	0.75	48.4149	25116.67
5	1	54.9031	27784.96
6	1.25	58.3772	30284.91
7	1.5	60.1355	31197.08

Table 3.6 *Ceq* values for input frequency of 5.0 Hz for increasing current levels

No.	Current I (Amp.)	Energy Dissipated E (J)	C_{eq} (N-s/m)
1	0	4.8338	1254.55
2	0.25	24.9276	6465.80
3	0.5	42.6509	11062.92
4	0.75	55.0935	14290.32
5	1	62.4760	16205.22
6	1.25	66.4289	17230.53
7	1.5	68.4297	17749.51

The tabulated data provides the values for the linearized viscous damping coefficient of the MR damper for each operating frequency and current.
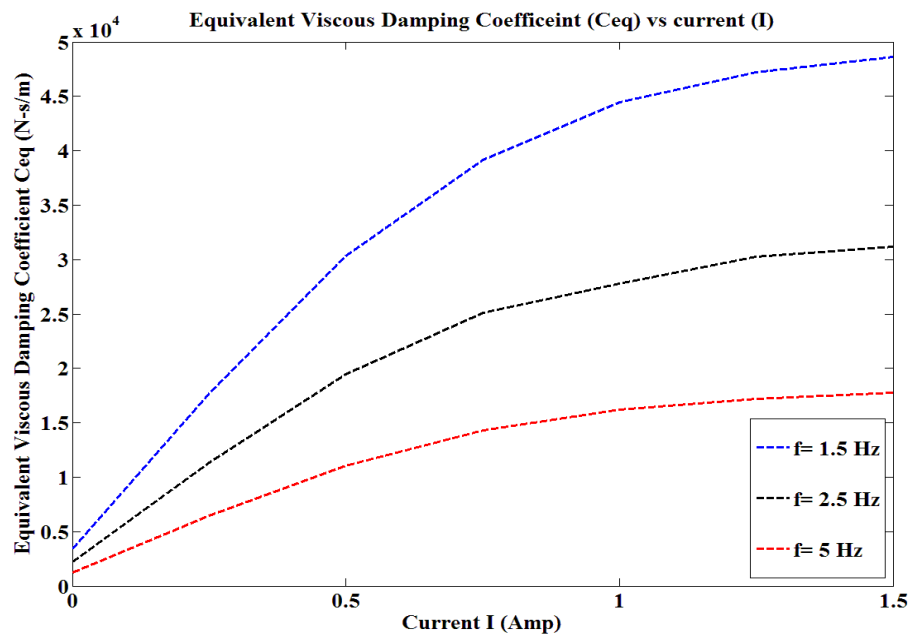
Figure 3.11 A graph of equivalent viscous damping coefficient versus current
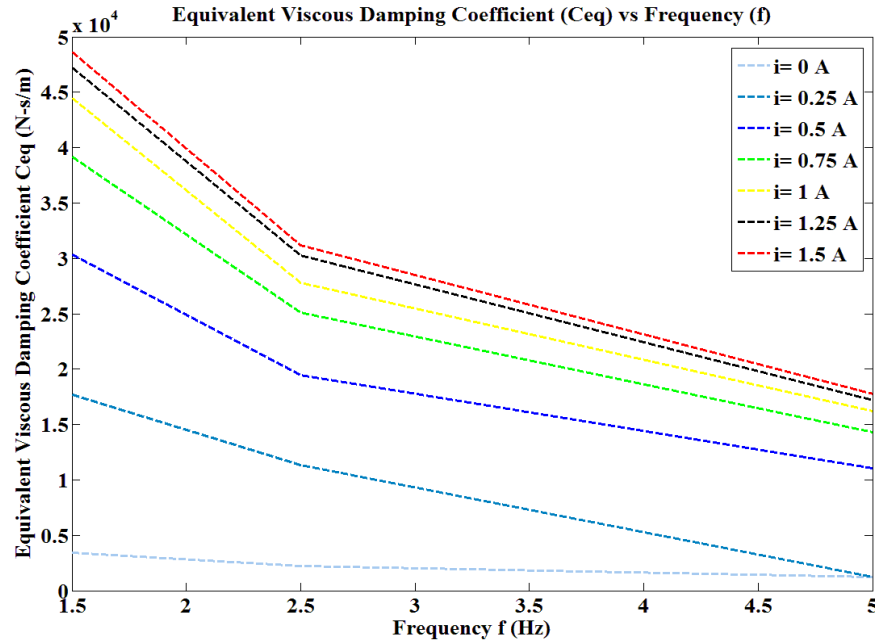
Figure 3.12 A graph of equivalent viscous damping coefficient versus frequency

The graphical relationships between the calculated C_{eq} and the varying frequencies and currents can provide a better means for analysing the obtained numerical data. The variations of C_{eq} with the varying currents and frequencies are depicted in figures 3.11 and 3.12.

3.4 Discussions

The obtained simulation results play an important role in understanding the energy dissipation behaviour of the Magnetorheological damper. The important conclusions that can be drawn from the results are described as follows.

- Figs. 3.3-3.5 depict the force-displacement characteristics of the MR damper for a sinusoidal excitation. The force-displacement hysteretic characteristic is elliptical in nature and follows a clockwise path. Initially, at zero current, the MR damper behaves like a linear viscous damper. As the current increases, the range of the MR damper force increases. For small increase in current, a considerable increase

in the damper force can be observed from the simulation results. It is necessary to depict the force-displacement characteristics of the MR damper accurately, as this characteristic is important in calculating the dissipated energy by integrating the area under the elliptical loop.

- The energy dissipation characteristics of the MR damper for sinusoidal excitations can be observed from the figs. 3.6-3.8. It can be seen that the amount of energy dissipated in one cycle increases with increase in frequency. The energy dissipation curves follow a sinusoidal pattern. The current also has a significant effect on the dissipated energy. From the numerical values summarized in tables 3.1-3.3, it can be concluded that the rate of energy dissipation increases with small increase in current levels. The highest amount of energy is dissipated when the input frequency is 5 Hz and a current of 1.5 A is applied in a circuit.

- From the obtained numerical data, the graphical relationships depicting the variation of the dissipated energy with the increasing current and frequency levels are plotted which can be seen from figs. 3.9 and 3.10. For each input frequency, the energy dissipated increases initially linearly for small values of currents. However, the relationship is no longer linear when the current increases above 0.5 A. A sharp rise in the dissipated energy can be observed for the current levels smaller than 1 A. As soon as the current increases above 1 A, the rise in the dissipated energy is not sharp towards the end of the cycle. Figure 3.10 depicts the plot of the dissipated energy against the frequency variations. The energy dissipation behaviour follows a linear pattern with increasing frequencies.

The numerical values of the calculated equivalent viscous damping coefficients are presented in tables 3.4-3.6. Based on this numerical data, the graphs of the equivalent viscous damping coefficient, C_{eq}, are plotted against the increasing levels of the current and the frequency. Figure 3.10 depicts the relationship between the equivalent viscous damping coefficient and the current. For the highest frequency of 5 Hz, the value of the C_{eq} obtained is the lowest at 0 A. As the current increases, the C_{eq} value also increases for each operating frequency. The highest values of the C_{eq} are obtained for the lowest frequency of 1.5 Hz. The relationship between the varying levels of the frequency and the C_{eq} can be observed from figure 3.11.

3.5 Summary

This chapter dealt with the analysis of the energy dissipation behavior of the Magnetorheological dampers using Spencer model. The basic principles of the energy dissipation analysis were reviewed initially, followed by deriving the equations for calculating the dissipated energy over one complete cycle by the MR damper. For this purpose, the force-displacement characteristics of the MR damper were plotted using Spencer dynamic model. From the obtained force-displacement characteristics, the dissipated energy was calculated for each operating frequency and current level. In order to linearize the MR damper, the equivalent viscous damping coefficients were calculated. The graphical relationships between the dissipated energy and the varying currents and frequencies were established.

Moreover, the graphs depicting the relationship of the equivalent viscous damping coefficient with varying frequencies and currents were also plotted.

The results obtained in the present chapter as well as the previous chapter validate the applicability of the Spencer model for modeling the dynamic behaviour of the MR dampers. The model could analyze the energy dissipation behaviors which are extremely important to understand before using the MR dampers for the vibration mitigation applications.

CHAPTER 4

SEMI-ACTIVE CONTROL OF AIRCRAFT LANDING GEAR SYSTEM USING H$_\infty$ AND LINEAR QUADRATIC REGULATOR (LQR) CONTROL APPROACH

4.1 Introduction

Most of the non-fatal aircraft accidents occur during landing. The landing gear plays an important role by acting as an intermediate cushioning element between the aircraft body and the runway. During the touchdown, large magnitude vibrations may get induced in the aircraft fuselage through the landing gear because of the harsh landing conditions. The landing gear shock absorbers must absorb the impact kinetic energy to maximum extent and dissipate this energy as quickly as possible in order to prevent large magnitude vibrations from getting transmitted to the fuselage. The oleo-pneumatic shock absorbers used in today's aircraft are the most efficient means of accomplishing such reduction in vibrations. Also, they exhibit good rate of energy dissipation. Along with the vertical energy dissipation during the impact, the landing gear must also be able to provide the required stability and maneuverability after the impact, which requires variable damping. However, the oleo-pneumatic shock absorber is unable to provide variable damping. Consistent attempts have been made to implement the semi-active control strategies in aircraft landing gears to obtain the improved rate of energy dissipation during landing [1], [2].

It is evident from the reviewed literature that the semi-active suspension systems have the advantage over the conventional passive and the active suspension systems.

Semi-active systems are robust, easy to build and are more efficient. Moreover, these systems eliminate the need for high power actuators. In early semi-active suspension systems, the goal of developing the required damping force could be achieved by varying the orifice area of the conventional damper thereby resisting the fluid flow according to the damping requirements. By using the Magnetorheological damper as an actuating mechanism, an efficient semi-active system can be built as these dampers can provide the controllable forces for nominal current thereby eliminating the need for large power supply [86]. Moreover, there are numerous mathematical models available for modeling the hysteretic dynamic behavior and the energy dissipation behavior of the MR damper. As evident from the previous chapters, Spencer model could describe the non-linear dynamic behavior of the MR damper satisfactorily thereby facilitating the design of the controller.

Various mathematical models of the aircraft system are available for the vibration analysis depending upon the particular landing gear configuration. Landing gear systems are classified depending upon the number of wheels carried by each landing gear and the pattern in which the wheels are arranged. Most of the aircraft have the tri-cycle landing gear configuration with two main landing gears at the back and one nose landing gear at the front. The number of wheels per landing gear is dependent on the aircraft weight and the loading conditions [2] .Hua-Lin et al [20], Wang et al. [27], Sivakumar & Haran [28] and Zapateiro et al [29], simulated two degrees of freedom (DOFs) aircraft model for the vibration analysis during landing impact. The advantage of this model is the simplicity and the ease with which a control strategy can be developed. This model takes into account only the vertical motion of the aircraft after landing. However, during landing,

the aircraft also undergoes pitch and roll motions which must be identified in the analysis from the stability point of view. Ghiringhelli and Gauldi [61], [60] simulated a multi-body aircraft model to analyze the response during the impact.

In this chapter, a methodology is developed for building the semi-active MR suspension for the aircraft landing gear system. A brief description of the contents of this methodology is as follows.

- Three degrees of freedom (3 DOF) aircraft model is developed that takes into consideration the bounce, pitch and roll motions of the aircraft during the landing impact. The aircraft has a tri-cycle landing gear configuration with one wheel per landing gear.

- Initially, the equations of motion for a 3 DOF aircraft with a passive suspension system are derived and the vibration analysis is carried out during the landing impact for different sink velocities. The purpose of this analysis is to validate the developed model.

- This is followed by the development of a semi-active suspension for a 3 DOF aircraft model for the purpose of suppressing the excessive fuselage vibrations during landing. For building the efficient semi-active landing gear suspension, MR damper is used as an actuation mechanism for generating the required damping force for each landing scenario and the damper characteristics are defined by Spencer model. Two different control approaches, namely, the Linear Quadratic Regulator (LQR) and the robust H_∞ are adopted for developing the semi-active controlled suspension system.

4.2 System Dynamics and Modeling

Today's aircraft are equipped with the conventional oleo-pneumatic dampers which have a good rate of energy dissipation. However, these dampers are not able to provide variable damping forces according to the different operating conditions which can reduce the damper efficiency over its lifetime. The implementation of semi-active dampers in the aircraft landing gears would be able to provide the variable rate of energy dissipation. Moreover, by adjusting the damping force to a desirable range, it is possible to control the excessive vibrations from getting transmitted to the aircraft fuselage, especially during the landing phase. For other aircraft operational phases such as taxiing, a lower damping force is sufficient which can be easily adjusted just by reducing the current.

In this study, a 3 DOF aircraft model is developed for the analysis of the dynamic behavior of the aircraft during the landing impact. As the aircraft has a tri-cycle landing gear system, it is assumed that the MR damper replaces the conventional oleo-pneumatic damper in all the three landing gears. According to the methodology suggested by Batterbee et al [10] for the design of the MR damper based landing gear, the total force generated inside the damper is a combination of the gas spring force, a viscous damping force and a controllable MR force. The gas spring force acts as a spring element and also provides the necessary stiffness in order to support the aircraft weight. The current flowing inside the magnetic circuit embedded in a damper does not completely magnetize the full volume of the MR fluid. The volume of the fluid which remains unaffected acts as a viscous fluid with Newtonian behavior thus providing the viscous damping effect. By magnetizing the specific volume of the MR fluid, a controllable MR force can be achieved. This force is the only adjustable damping force which can be achieved

according to the requirements by implementing the controller. Spencer dynamic model described in section (2.3.1) can be used for calculating the controllable MR force. Therefore, while deriving the equations of motion, the factors, viscous damping force as well as the gas spring force has to be taken into consideration along with the controllable MR force. The developed model takes into account the bounce, pitch and roll motions of aircraft upon landing and is a good approximation of the real model considering the landing impact.

As shown in Figure 4.1, the rotation of an aircraft around the *x*-axis passing from tail end to nose end is called roll. The vertical motion of an aircraft about the equilibrium position in *z*-direction is called bounce and the rotation of an aircraft around the horizontal *y*-axis is called pitch. The precision landing of an aircraft depends upon the factors such as sink speed, runway roughness, weather conditions and the pilot skills [2]. In reality, it is not possible to have an ideal situation during each landing scenario which may induce the uncontrollable levels of bounce, pitch and roll motions that are undesirable for passenger safety and comfort. Therefore, it is necessary to analyze these aircraft motions from the time when aircraft lands to the time when it attains the safe taxiing speed. Application of the Newton's second law of motion yields the following equations of motion for the three DOF aircraft system.
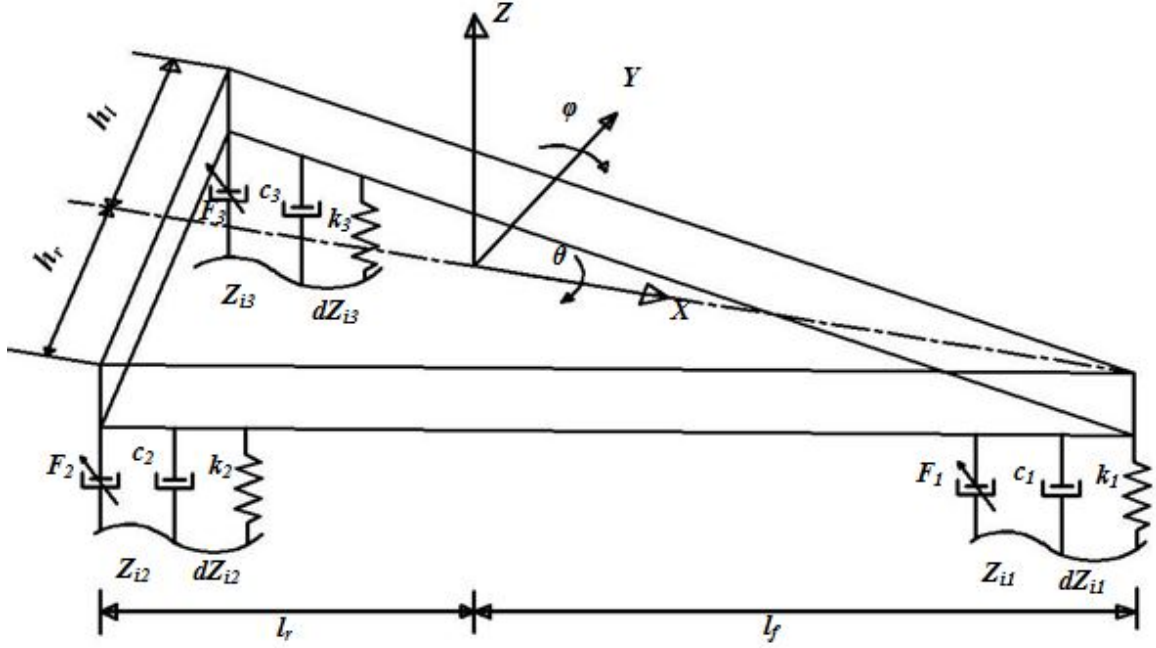
Figure 4.1 Schematic of 3 DOF aircraft model

$$m\ddot{z} + k_1(z - l_f\varphi - z_{i1}) + k_2(z + l_r\varphi - h_r\theta - z_{i2}) +$$
$$k_3(z + l_r\varphi + h_l\theta - z_{i3}) + c_1(\dot{z} - l_f\dot{\varphi} - \dot{z}_{i1}) +$$
$$c_2(\dot{z} + l_r\dot{\varphi} - h_r\dot{\theta} - \dot{z}_{i2}) + c_3(\dot{z} + l_r\dot{\varphi} + h_l\dot{\theta} - \dot{z}_{i3})$$
$$= -F_1 - F_2 - F_3$$
(4.1)

$$I_x\ddot{\theta} - k_2h_r(z + l_r\varphi - h_r\theta - z_{i2}) - k_3h_l(z + l_r\varphi + h_l\theta - z_{i3})$$
$$-c_2h_r(\dot{z} + l_r\dot{\varphi} - h_r\dot{\theta} - \dot{z}_{i2}) - c_3h_l(\dot{z} + l_r\dot{\varphi} + h_l\dot{\theta} - \dot{z}_{i3})$$
$$= F_3h_l - F_2h_r$$
(4.2)

$$I_y\ddot{\varphi} - k_1l_f(z - l_f\varphi - z_{i1}) - k_2l_r(z + l_r\varphi - h_r\theta - z_{i2})$$
$$-k_3l_r(z + l_r\varphi + h_l\theta - z_{i3}) - c_1l_f(\dot{z} - l_f\dot{\varphi} - \dot{z}_{i1}) -$$
$$c_2l_r(\dot{z} + l_r\dot{\varphi} - h_r\dot{\theta} - \dot{z}_{i2}) - c_3l_r(\dot{z} + l_r\dot{\varphi} + h_r\dot{\theta} - \dot{z}_{i3})$$
$$= (F_2 + F_3)l_r - F_1l_f$$
(4.3)

where, m, I_x and I_y are the mass of aircraft fuselage, mass moment of inertia about x-axis and mass moment of inertia about y-axis, respectively. Angle θ represents the angle of

roll whereas φ represents the angle of pitch at the time of landing, k_1, k_2 and k_3 represent the spring constants of the nose landing gear shock absorber, the left main landing gear shock absorber and the right main landing gear shock absorber, respectively. Constants c_1, c_2 and c_3 represent the damping coefficients for nose landing gear shock absorber, left main landing gear shock absorber and right main landing gear shock absorber, respectively. The distance of the nose landing gear from center of gravity (C.G.) is represented by l_f whereas l_r represents the distance of main landing gear from C.G. h_l is the distance of the left main landing gear from the center point and h_r is the distance of the right main landing gear from the center point. The MR damper forces corresponding to the nose gear, the left main landing gear and the right main landing gear are represented by F_1, F_2 and F_3, respectively.

4.2.1 Formulation of the MR damper forces

The Magnetorheological damper is implemented as an actuation mechanism for developing the semi-active suspension system. The MR damper generates the required forces according to the operating conditions. The MR damper forces F_1, F_2 and F_3 in equations (4.1)-(4.3), correspond to the nose gear, the left main gear and the right main gear and act as control input. To formulate the MR damper force in each landing gear, Spencer dynamic model is used. The dynamic equations of the model are derived as explained in section 2.3.1 and the parameters are selected from [87] for describing the dynamic behavior of the MR damper. Spencer model described by Yang et al [87] has a large force producing capacity of 200 KN. Since the required forces for absorbing the high impact energy during the aircraft landing are higher, a large capacity MR damper model is selected in order to build an efficient semi-active landing gear suspension.

However, for accurately predicting the MR damper behaviour, Yang et al [87] adopted a curve fitting approach for establishing a relationship between the current and the MR damper force instead of using the non-linear current function formulated in equation (2.2). Referring to the model described in section 2.3.1 and in [87], the overall model formulation can be done as follows.

$$F_D = \alpha p + c_0(\dot{z} - \dot{q}) + k_0(z - q) + k_r(z - z_i) \tag{4.4}$$

$$\dot{p} = -\gamma p |p|^{n-1} |\dot{z} - \dot{q}| - \beta(\dot{z} - \dot{q})|p|^n + A_1(\dot{z} - \dot{q}) \tag{4.5}$$

$$\dot{q} = \frac{1}{c_0 + c_r}\left(\alpha p + c_0\dot{z} + k_0(z - q)\right) \tag{4.6}$$

$$\alpha(i) = 16566i^3 - 87071i^2 + 168326i + 15114 \tag{4.7}$$

$$c_0(i) = 437097i^3 - 1545407i^2 + 1641376i + 457741 \tag{4.8}$$

$$c_r(i) = -936310i^3 + 5334183i^2 + 48788640i - 2791630 \tag{4.9}$$

The force generated by the MR dampers embedded in the main gears and the nose gear is given by equation (4.4) which depends on the parameters α, c_0 and c_r. As explained previously, the parameter related to the MR fluid yield stress is designated by α and it is a third order polynomial function of current which is presented in equation (4.7). The viscous damping coefficient at larger velocities is represented by c_0. The dashpot represented by c_r is included in the model to account for the roll-off effect, which is observed at low velocities. The relationship between the damping coefficient c_0 and c_r and the current i is represented by the third order polynomial function as shown in equations (4.8) and (4.9), respectively. The parameters of the selected Spencer model are summarized in the following table.

Table 4.1 Spencer model parameters for MR damper

Symbol	Entity	Numerical value
k_0	Control stiffness at larger velocities	137810 N/m
k_r	MR damper accumulator stiffness	617.31 N/m
n	A constant for adjusting the slope of the hysteresis curve	10
A_1	A constant for adjusting the slope of the hysteresis curve	2679 m^{-1}
β	A constant for adjusting the slope of the hysteresis curve	647.46 m^{-1}
γ	A constant for adjusting the slope of the hysteresis curve	647.46 m^{-1}

4.3 Synthesis of the Controllers

Control systems theory has been applied for improving the performance efficiency of the industrial machinery for a long time. Intensive research programs are being carried out for improving the efficiency as well as the life span of the mechanical systems by using electronic controls. The purpose of this research is to facilitate the human life by getting rid of the routine and repetitive chores away from human operator and automate them. All the control strategies developed so far find their foundation in the feedback theory which is the primary reason for their wide application range. Controls engineering concepts can be applied in various fields such as the automotive engineering, aircraft engineering, building and civil engineering, electrical engineering and many others [88]. The applications involving the use of the control strategies for developing the smart

dampers for the vehicles and civil structures have gained a tremendous importance in recent past. A few implementations of the control strategies for developing the smart aircraft suspensions have also been reported. However, none of the aircraft has been equipped with such system till date.

In reality, the mechanical systems are represented in the form of mathematical models for the ease of analysis. The model cannot predict the behavior of the actual system accurately. In case of uncertainties in the operating conditions, the behavior of the model can be different from the actual system. This fact has to be taken into consideration while designing the control laws for a particular system which accounts for the robustness analysis. Robustness refers to the stability of the system under disturbances. Therefore, it is necessary to develop a robust controller for the system in order to predict its behavior as accurately as possible under varying disturbances in actual practice [89].

Linear quadratic regulator (LQR) and the H_∞ control strategies are amongst the most widely used control strategies for developing the semi-active suspension system for road vehicles [90]-[92]. Kumar and Vijayarangan [91] implemented the LQR controller for a quarter car model by considering the ride quality, road holding and suspension travel as the performance criterion. Similar approach can also be implemented to design a semi-active landing gear system for aircraft. Son et al. [93] used a model based H_∞ controller for semi-active vehicle suspension to improve ride quality for irregular road disturbances and proved the effectiveness of H_∞ controller for reducing the vertical accelerations of a sprung mass over wide range of excitation conditions. In addition, the application of the robust controller for developing a shimmy damper was also reported

[94]. The H$_\infty$ controller also proved to be a better control strategy for a semi-active landing gear suspension [29] because of its ability to deal with the uncertainties and nonlinearities in a systematic way.

In this analysis, two control approaches namely, the linear quadratic regulator (LQR) and the H$_\infty$ are adopted for controlling the bounce of the landing aircraft subjected to disturbances for the purpose of improving the landing performance during each landing scenario for the passenger safety. During each landing scenario, the vibrations are inevitably transferred to the fuselage which may affect passenger safety. The transmissibility of vibrations depends upon the effectiveness of the damper. The performance of the passive damper is poor during hard landing scenarios. The semi-active controlled suspension system can reduce the fuselage vibrations for larger sink velocities during hard landing scenarios. The controller approaches aim at minimizing the bounce velocity of the fuselage. For facilitating the formulation of the design of the controllers, a state-space approach is adopted which is explained in the following section.

4.3.1 Formulation of the H$_\infty$ controller using state-space approach

For the systems involving complicated dynamics, the task of controller design becomes critical. A state-space modeling approach can provide a solution to simplify the complicated dynamics for the ease of controller design. The state-space approach is a time domain modeling which can be applied to multivariable systems and also time-variant systems. The basic principle behind this modeling technique is to represent a physical system as a set of first order differential equations. The state of a system describes the condition of that system at any given time. For describing the dynamic behavior of a system at any given time, it is necessary to represent the system as a set of

72

minimum number of states called the state variables. Based on the past behavior of the system, the state predicts the future behavior patterns at a particular time. The number of states is twice that of the number of degrees of freedom of a mechanical system [95], [96].

The state-space approach can be adopted for representing the 3 DOF aircraft model considered in this analysis in order to simplify the process of controller design. The state-space modeling approach for a simple system is presented in Appendix A. In order to represent the developed model in the state-space format, first consider the equations of motion derived in the equations (4.1)-(4.3).
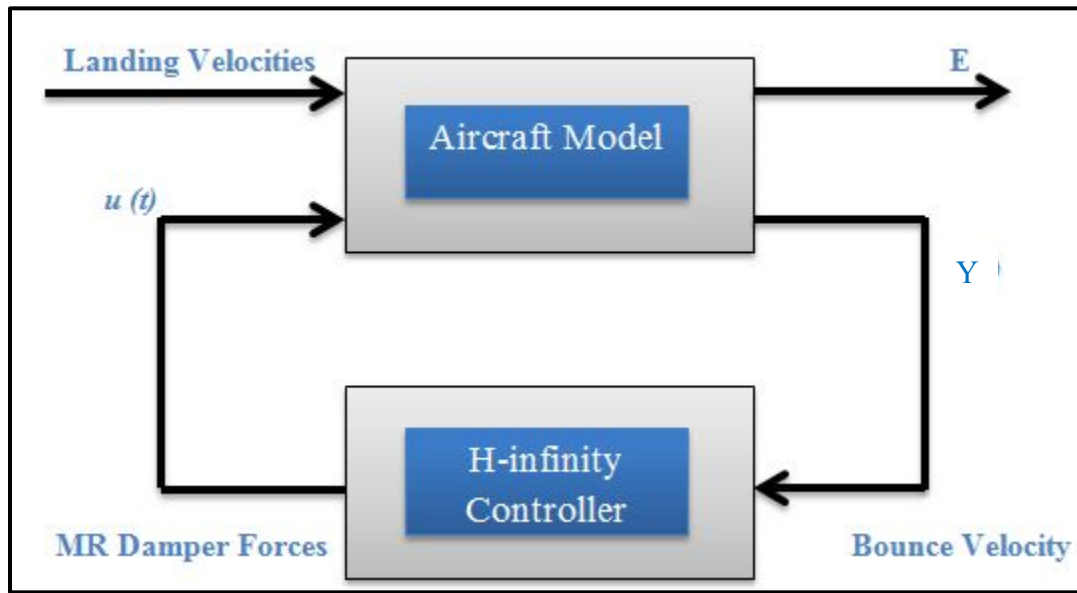

Figure 4.2 Block diagram of H-infinity control approach

Based on the governing equations of aircraft, the system can be represented in state-space as follows,

$$\dot{X} = AX + Bu + Gw$$
$$Y = C_1 X + D_{11} u + D_{12} w \qquad (4.10)$$
$$E = C_2 X + D_{22} u$$

where, $X \in R^6$ represents a state vector as shown in equation (4.11) and $u \in R^3$ represents the MR damper forces in each of the main landing gears and a nose landing gear as a control input. Vector $w \in R^6$ is the disturbance vector due to the landing displacement and velocities as shown in equation (4.13). The system matrix $[A] \in R^{6 \times 6}$ is represented by equation (4.14), matrix $[B] \in R^{6 \times 3}$ defines the input for the system and the matrix $[G] \in R^{6 \times 6}$ defines the source of disturbances for each landing gear. The matrix $[C_1] \in R^{1 \times 6}$ and the matrix $[C_2] \in R^{2 \times 6}$ represent the output of the plant and C_1 is also input to the controller, D_{11}, D_{12} and D_{22} are null matrices in the above governing equations of the plant.

$$X = \begin{bmatrix} z & \theta & \varphi & \dot{z} & \dot{\theta} & \dot{\varphi} \end{bmatrix} \tag{4.11}$$

$$u = \begin{bmatrix} F_1 & F_2 & F_3 \end{bmatrix} \tag{4.12}$$

$$w = \begin{bmatrix} Z_{i1} & Z_{i2} & Z_{i3} & \dot{Z}_{i1} & \dot{Z}_{i2} & \dot{Z}_{i3} \end{bmatrix} \tag{4.13}$$

$$A = \begin{bmatrix} 0_{3\times3} & I_{3\times3} \\ -M^{-1}K & -M^{-1}C_v \end{bmatrix} \tag{4.14}$$

$$B = \begin{bmatrix} 0_{3\times3} & M^{-1}b_1 \end{bmatrix}^T \tag{4.15}$$

$$G = \begin{bmatrix} 0_{6\times6} & -M^{-1}g_1 \end{bmatrix}^T \tag{4.16}$$

$$C_1 = \begin{bmatrix} 0_{2\times4} & I_2 \end{bmatrix} \tag{4.17}$$

$$C_2 = \begin{bmatrix} 0_{1\times3} & 0 & 1 & 0 \end{bmatrix} \tag{4.18}$$

where, the matrices $[C_v]$, $[K]$, $[b_l]$ and $[g_l]$ are represented as follows,

$$M = \begin{bmatrix} m & 0 & 0 \\ 0 & I_x & 0 \\ 0 & 0 & I_y \end{bmatrix} \quad (4.19)$$

$$K = \begin{bmatrix} k_1 + k_2 + k_3 & k_3 h_l - k_2 h_r & k_2 l_r - k_1 l_f + k_3 l_r \\ k_3 h_l - k_2 h_r & k_2 h_r^2 + k_3 h_l^2 & k_3 h_l l_r - k_2 h_r l_r \\ l_r(k_2 + k_3) - k_1 l_f & l_r(k_3 h_l - k_2 h_r) & k_1 l_f^2 + l_r(k_2 l_r + k_3 l_r) \end{bmatrix} \quad (4.20)$$

$$C_v = \begin{bmatrix} c_1 + c_2 + c_3 & c_3 h_l - c_2 h_r & c_2 l_r - c_1 l_f + c_3 l_r \\ c_3 h_l - c_2 h_r & c_2 h_r^2 + c_3 h_l^2 & c_3 h_l l_r - c_2 h_r l_r \\ l_r(c_2 + c_3) - c_1 l_f & l_r(c_3 h_l - c_2 h_r) & c_1 l_f^2 + l_r(c_2 l_r + c_3 l_r) \end{bmatrix} \quad (4.21)$$

$$b_1 = f \times \begin{bmatrix} -1 & -1 & -1 \\ 0 & -h_r & h_l \\ -l_f & l_r & l_r \end{bmatrix} \quad (4.22)$$

$$g_1 = \begin{bmatrix} k_1 & k_2 & k_3 & c_1 & c_2 & c_3 \\ 0 & k_2 h_r & -k_3 h_l & 0 & c_2 h_r & -c_3 h_l \\ k_1 l_f & -k_2 l_r & -k_3 l_r & c_1 l_f & -c_2 l_r & -c_3 l_r \end{bmatrix} \quad (4.23)$$

Based on the state-space of the plant and controller, the controller can be presented as shown in equation (4.24). The controller is designed in two steps: (i) solving Riccati equations (ii) defining controller structure in state-space format.

For the controllable pair of A and B, and the observable pair of A and C_1, the H$_\infty$ controller can be designed by solving the following Riccati equations [97]:

$$A^T M_1 + M_1 A + C_1^T C_1 - M_1 B B^T M_1 + \frac{1}{\eta^2} M_1 G G^T M_1 = 0 \tag{4.24}$$

$$A^T N_1 + N_1 A + G G^T - N_1 C_2^T C_2 N_1 + \frac{1}{\eta^2} N_1 C_1^T C_1 N_1 = 0 \tag{4.25}$$

where, matrices M_1 and N_1 are the solutions of Riccati equations. Those matrices should satisfy the following controller criteria.

$$\rho(M_1 N_1) < \eta^2 \tag{4.26}$$

where, η is controller performance index which should be a real positive number.

Based on the M_1 and N_1 matrices, the controller is presented in state-space as shown in equations (4.27) and (4.28), [97]. The output of control system is the input to the plant.

$$\dot{\xi} = \Delta(\xi, Y)$$
$$u = F(\xi) \tag{4.27}$$

$$\dot{\xi} = A_{H\inf} \xi + ((I - \eta^2 N_1 M_1)^{-1} N_1 C_2^T) Y$$
$$F = (-B B^T M_1) \xi \tag{4.28}$$

where, A_{Hinf} is shown as follows:
$$A_{H\inf} = A + \eta^{-2} G G^T M_1 - B B^T M_1 - (I - \eta^{-2} N_1 M_1)^{-1} N_1 C_2^T C_2 \tag{4.29}$$

Equations (4.10)-(4.29) summarize the synthesis of the robust H_∞ controller for the developed 3 DOF aircraft model. In order to validate the performance capability of the designed controller, the aircraft response is simulated using MATLAB/SIMULINK for a wide range of operating conditions during landing.

4.3.2 Formulation of the Linear Quadratic Regulator (LQR) controller using state-space approach

Linear quadratic regulator is a simple design methodology that acts as a basis for many control design approaches for linear systems [95], [98]. The advantages of the LQR method are that it is easy to compute and guarantees the stability of the closed-loop systems. This method is based on the conventional feedback control theory and provides an optimal control which can be effectively utilized for the variety of systems because of the simplicity in computations. Based on the state-space plant presented in the above sections, the block diagram of the LQR is as shown below.
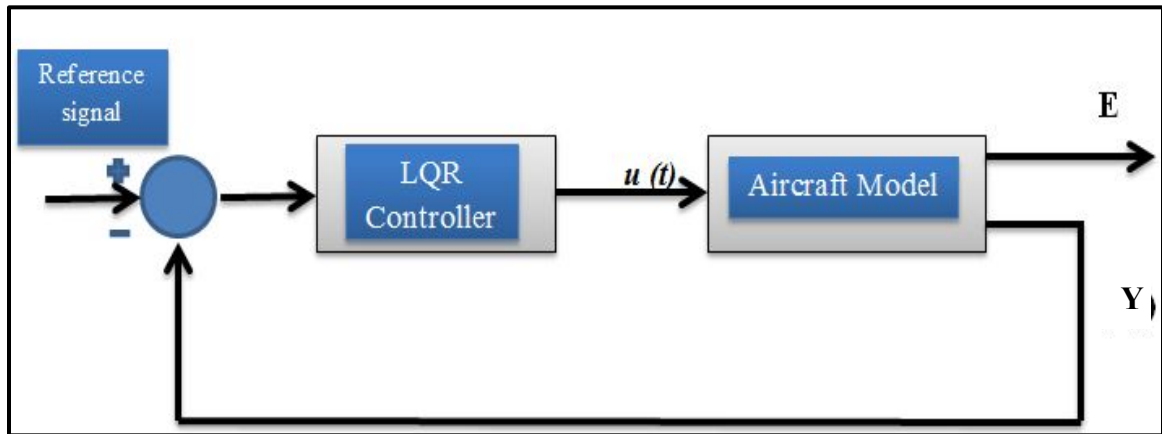
Figure 4.3 Block diagram of LQR control approach

The LQR control approach changes the system dynamics in order to obtain the gain required for the desired system response. The LQR controller operates by changing the location of poles of the system to the optimal place. The parameters of the dynamic system such as the overshoot, the time response and steady-state response depend upon the optimal location of the poles of the system. The system dynamics is controlled by the LQR by adjusting a matrix gain which is given by equation (4.30) which represents the performance index. The performance index function can be treated as an energy function

and the objective of the LQR control problem is to minimize this function. In other words, the goal is to minimize the energy of the closed-loop system. As the function J is an infinite integral of X, it can be interpreted from the equation (4.30) that the state X approaches zero as the time approaches infinity thereby validating the system stability.

The purpose of the LQR design is to maintain the deviation of the state within the acceptable range with less control effort. The control problem can be solved by minimizing the performance index function J in equation (4.30) by appropriately selecting the matrices $[Q]$ and $[R]$. The selection of the matrices $[Q]$ and $[R]$ is very essential for achieving the optimal performance of the controller. The size of matrix $[R]$ depends on the number of inputs whereas the size of the matrix $[Q]$ can be determined from the number of states. For the problem defined in this study, the state-space plant represents six states since the system has 3 DOF. The number of excitation inputs applied is three since each of three landing gears is excited by a step input. Therefore, the matrix $[Q]$ will represent a 6×6 matrix and the matrix $[R]$ will represent a 3×3 matrix. Initially, these matrices can be selected as the diagonal matrices as shown in equations (4.31) and (4.32). The elements of these matrices must be selected by trial and error method in such a way that the matrix $[Q]$ must be at least positive semi-definite matrix with size of 6×6 and matrix $[R]$ must be a positive definite matrix with size of 3×3. Selection of the matrices $[Q]$ and $[R]$ as the positive semi-definite matrix and positive definite matrix, respectively yields the solution which represent a positive definite Riccati matrix $[S]$. This selection criterion ensures that the homogeneous system is asymptotically stable.

$$J = \frac{1}{2}\int_0^\infty (X^T(t)QX(t) + u^T(t)Ru(t))dt \tag{4.30}$$

$$[Q] = \begin{bmatrix} q_1 & 0 & 0 & 0 & 0 & 0 \\ 0 & q_2 & 0 & 0 & 0 & 0 \\ 0 & 0 & q_3 & 0 & 0 & 0 \\ 0 & 0 & 0 & q_4 & 0 & 0 \\ 0 & 0 & 0 & 0 & q_5 & 0 \\ 0 & 0 & 0 & 0 & 0 & q_6 \end{bmatrix} \tag{4.31}$$

$$[R] = \begin{bmatrix} r_1 & 0 & 0 \\ 0 & r_2 & 0 \\ 0 & 0 & r_3 \end{bmatrix} \tag{4.32}$$

If the selected $[Q]$ is large, the state must be smaller for minimizing the cost function J which indicates that the system response becomes steady state in less time. On the other hand, selecting larger $[R]$ makes system more optimal. In this case, the system state decays to zero slowly, however, the control effort required is less. Therefore, the parameters of these matrices should be selected by trial and error based on the desired controller force and the maximum available energy of the MR damper. The selected $[Q]$ and $[R]$ weighting matrices based on the dynamic characteristic of the system for required control performance are presented in equations (4.33) and (4.34). The solution to the cost function J can be obtained from equation (4.35) which is called as the Algebraic Riccati equation (ARE) [95].

$$[Q] = \begin{bmatrix} 9 & 0 & 0 & 0 & 0 & 0 \\ 0 & 9 & 0 & 0 & 0 & 0 \\ 0 & 0 & 9 & 0 & 0 & 0 \\ 0 & 0 & 0 & 9 & 0 & 0 \\ 0 & 0 & 0 & 0 & 9 & 0 \\ 0 & 0 & 0 & 0 & 0 & 9 \end{bmatrix}$$ (4.33)

$$[R] = \begin{bmatrix} 0.2 & 0 & 0 \\ 0 & 0.2 & 0 \\ 0 & 0 & 0.2 \end{bmatrix}$$ (4.34)

The Riccati equation can be solved using different numerical procedures. The simplest method is to utilize MATLAB function when the numerical values of the other matrices are known. Therefore, for this case the matrices [A] and [B] represented in the equations (4.14) and (4.15), respectively, and the selected matrices [Q] and [R] are substituted in the Algebraic Riccati equation (4.35) to solve for the matrix [S] which will represent a symmetric positive semi-definite matrix and is the final solution of the equation (4.35).

$$AS^T + SA + SBR^{-1}B^T S + Q = 0$$ (4.35)

After obtaining the solution of the Riccati equation, the optimal gain of LQR can be obtained from the equation (4.36) which finally changes the location of system closed loop poles to the optimal one.

$$K_{LQR} = R^{-1}B^T S$$ (4.36)

Based on the solution of the Riccati equations and the selected matrix [R], the value of the gain matrix $[K_{LQR}]_{3\times6}$ can be obtained as follows,

$$K_{LQR} = \begin{bmatrix} 3.1915 & -1.3696 & 6.5204 & 2.1971 & -0.0538 & -0.9809 \\ -0.9107 & 0.3533 & 19.2777 & 2.9021 & -1.3670 & 3.6651 \\ -1.5674 & 1.1426 & 17.8890 & 2.9025 & 1.3795 & 3.8388 \end{bmatrix}$$

The system matrix for this new gain can be obtained by equation (4.37), [99]. The controller input of the LQR controller is presented in equation (4.38).

$$A_{LQR} = A - BK_{LQR} \tag{4.37}$$

$$u = K_{LQR}x \tag{4.38}$$

The stability analysis of the designed system can be performed using the eigenvalues of the system matrices $[A]$ and $[A_{LQR}]$. The eigenvalues of these matrices represent the poles of the system and reflect important information which provides a consolidated theory for analyzing the system stability.

Table 4.2 Representation of poles of the system matrices

NO	Eigenvalues of matrix [A]	Eigenvalues of matrix [A$_{LQR}$]
1	-2.3586 + 5.6545i	-35.5666
2	-2.3586 - 5.6545i	-2.5244
3	-9.0654 + 6.3672i	-4.8724 + 5.7544i
4	-9.0654 - 6.3672i	-4.8724 - 5.7544i
5	-7.0617 + 6.9356i	-8.3016 + 5.3904i
6	7.0617 - 6.9356i	-8.3016 - 5.3904i

In equation (4.38), K_{LQR} represents the optimal pole placement gain which shifts the poles of system to the left half plane close to real axis. As long as the poles of the system are in left half plane, the system is said to be asymptotically stable. For the case analyzed in this study, it can be observed from the following table that the system poles lie in left half plane which ensures system stability during landing procedure. Therefore, it becomes necessary in LQR problem to identify the eigenvalues of the system matrices for stability analysis under different inputs. The following table identifies the eigenvalues of the system matrices before and after the application of control.

4.4 Summary

In the presented chapter, the equations of motion for a 3 DOF aircraft model are derived considering the bounce, pitch and roll motions. A methodology is presented for developing the semi-active suspension system for the aircraft model implementing two different control strategies. The landing gear is equipped with the magnetorheological damper replacing the existing Oleo-pneumatic damper. The MR damper provides an effective actuation mechanism by providing the required damping forces for different operating conditions. The dynamic behavior of the MR damper is analyzed using Spencer model and the parameters of the model are selected from the literature. For designing the robust controller, a state-space modeling approach is adopted and the mathematical equations for synthesizing the robust H_∞ controller and the LQR controller are derived.

The remaining part of the study will deal with analyzing the performance of the developed semi-active MR landing gear. In the next chapter, initially, the performance of the robust H_∞ controller is compared with the LQR controller for a particular sink velocity with the goal of selecting the best control approach amongst the two. Later, the vibration

response of the aircraft for the uncertainties during landing is simulated to validate the applicability of the designed semi-active system in worst landing scenarios.

CHAPTER 5

PERFORMANCE ANALYSIS OF THE AIRCRAFT WITH SEMI-ACTIVE MAGNETORHEOLOGICAL LANDING GEAR

5.1 Introduction

The primary objective of this study is to develop a methodology for designing a semi-active suspension for the aircraft landing gear for improving the passenger safety during the aircraft operations. The goal of designing a smart suspension system for the aircraft landing gear was achieved through the numerical methodologies adopted in the previous chapters.

This chapter deals with the validation of the designed semi-active system for the developed 3 DOF model through simulation approach. Initially, the vibration response of the passive system is compared with the semi-active system designed using both the control approaches presented in chapter 4 for a particular sink velocity. Later, the performance of the controllers is compared for the same sink velocity but taking into consideration the runway unevenness, which would provide a basis for the selection of the appropriate controller out of the two suggested ones. Once the selection process of the control approaches is completed, it is used for controlling the vibrations of the aircraft for higher landing velocities considering the runway roughness and other adverse operating conditions. Moreover, the analysis also takes into consideration the pilot inaccuracies which sometimes may cause damage during landing.

5.2 Simulation of Actual Aircraft Landing

The simulation studies are performed using MATLAB/SIMULINK for 3 DOF aircraft model. The parameters used for simulating the response of an aircraft during the landing procedure are summarized in the following table [100].

Table 5.1 Aircraft parameters for simulation

Symbol	Entity	Numerical value
m	Mass of aircraft fuselage	3345 kg
I_x	Mass moment of inertia in roll	56465.3 kg.m^2
I_y	Mass moment of inertia in pitch	200879 kg.m^2
k_1	Stiffness of the nose landing gear suspension	102095 N/m
k_2	Stiffness of the left main landing gear suspension	102095 N/m
k_3	Stiffness of the right main landing gear suspension	102095 N/m
c_1	Damping coefficient of the nose landing gear	1.9822e4 N.s/m
c_2	Damping coefficient of the left main landing gear	1.9822e4 N.s/m
c_3	Damping coefficient of the right main landing gear	1.9822e4 N.s/m
l_f	Distance of nose landing gear form C.G.	11.6 m
l_r	Distance of main landing gears form C.G.	1.2 m
h_l	Distance of the right main landing gear from center point p	5.2 m
h_r	Distance of the right main landing gear from center point p	5.2 m
f	Actuator constant	10000
η	Controller preformance index	0.10

In order to simulate the actual landing scenario, it is assumed that the aircraft lands with the initial vertical sink velocity of 0.8 m/s. The main landing gears will touch the ground first followed by the nose landing gear. To deal with adverse conditions during landing, the pilot inaccuracies are taken into consideration. During each landing, it is not always possible that both the main landing gears touch the ground at the same time. Because of the pilot inaccuracies, it is possible that one of the main landing gears touches the ground prior to the other gear. However, the runway roughness is not taken into consideration for the first simulation. This approach simulates the landing of an actual aircraft allowing the sequential touching of the three wheels. A switching technique is developed in the simulation of the landing procedure which enables the system to switch from the single degree of freedom to three degrees of freedom system in order to simulate the sequential touching of the two wheels of the main landing gears and the nose landing gear wheels with the ground. The landing scenario for the sink velocity of 0.8 m/s can be visualized from figure 5.1.
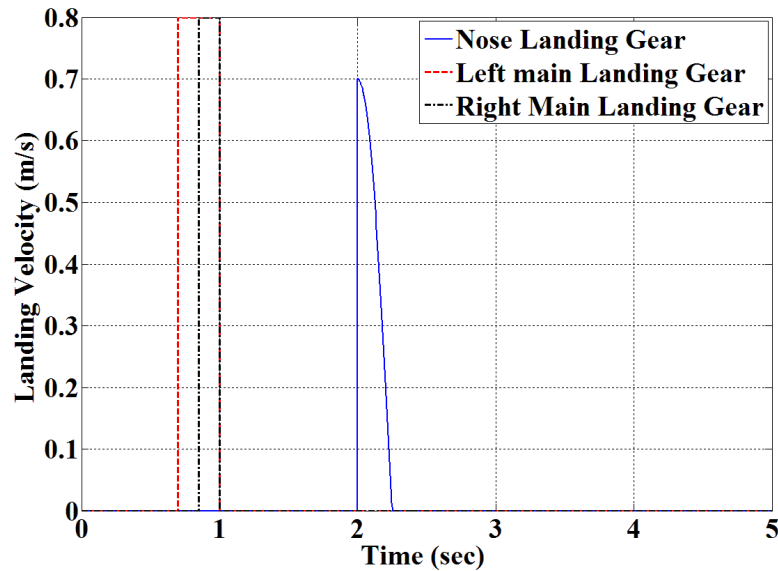

Figure 5.1 Landing scenario for initial sink velocity of 0.8 m/s

The left main landing gear touches the ground first followed by the right one with a delay of 0.15 seconds. The initial sink velocities are represented by dash and dash-dot lines in Figure 5. The nose landing gear touches the ground with a delay of one second after the initial touchdown of the main landing gears. Initially, when only the left landing gear is in contact with the ground, the MR damper force, the viscous damping force and the stiffness corresponding to this gear only will be taken into account. Therefore, a single DOF model is used for the simulation. When the right main landing gear touches the ground, the model is switched to two DOFs. Finally, with the touchdown of the nose landing gear, the system switches to a three DOFs model. A switching technique is developed in the Simulink which enables the system to switch from the single DOF to two DOF and finally a three DOFs model during the simulation procedure. This completely represents the actual landing scenario assuming that the aircraft is landing on a smooth runway. The simulated vibration response of the aircraft with the semi-active system for a normal landing can be visualized from figures 5.2 and 5.3.
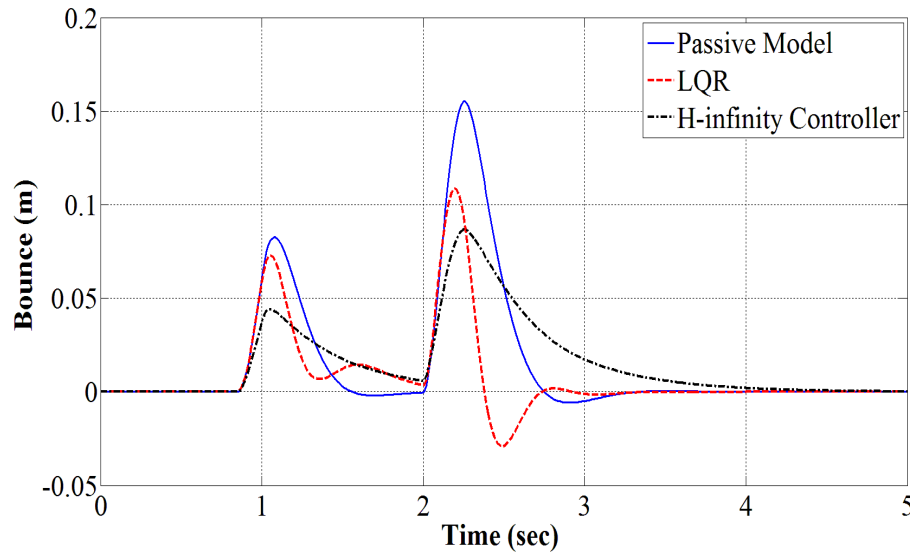

Figure 5.2 Performance comparison of passive and semi-active systems for bounce for sink velocity of 0.8 m/s
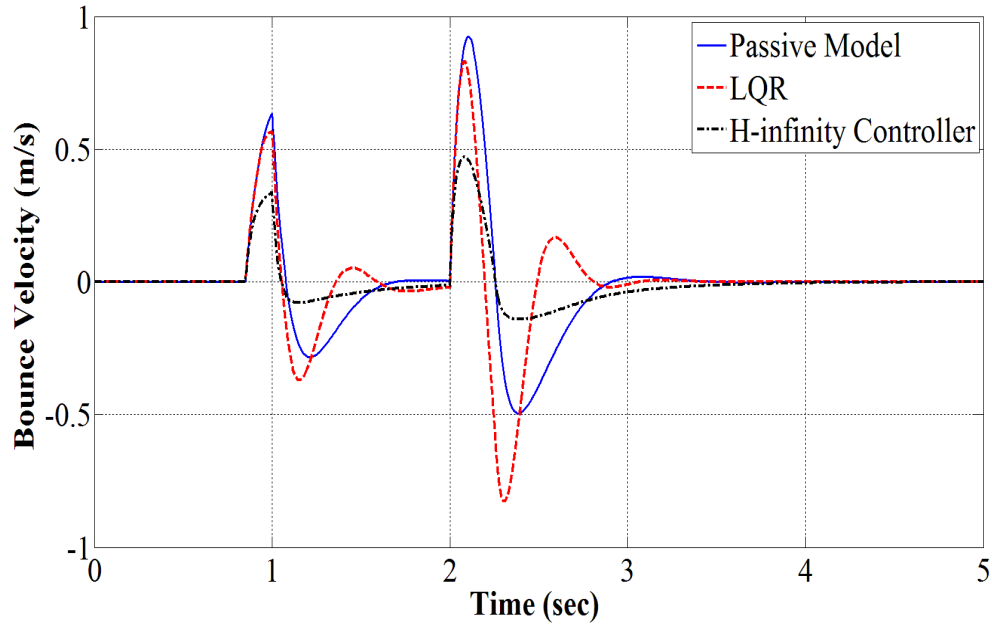
Figure 5.3 Performance comparison of passive and semi-active systems for bounce rate for sink velocity of 0.8 m/s

It can be interpreted from figures 5.2 and 5.3 that for a normal landing scenario where the sink velocity is 0.8 m/s, the semi-active system with the robust H_∞ controller is able to absorb the vibrations effectively as compared to the system with the LQR controller and the passive system. The implementation of the H_∞ controller reduced the peak of oscillations by approximately 46% which is observable from the bounce and the bounce rate responses. The LQR controller is not able to reduce the peak of oscillations as effectively as the H_∞. However, the LQR controller finds its advantages over the H_∞ if the settling time is considered as a criterion for the comparison. As the focus of this analysis is to reduce the peaks in bounce and bounce rate responses, the H_∞ controller has its edge over the LQR.

However, during the landing procedure, an aircraft is inevitably subjected to random excitations because of the roughness of an airstrip. Therefore, it becomes necessary to analyze the transmission of these random vibrations to the aircraft fuselage as

it is directly related to the ride comfort and structural safety. In order to study the transmission of random vibrations to the aircraft fuselage, it is assumed that the aircraft lands on a rough airstrip. To simulate the rough landing scenario, a random signal is generated in the form of a white noise and applied as input to one of the main landing gear wheels as a base excitation as shown in Figure 5.4.
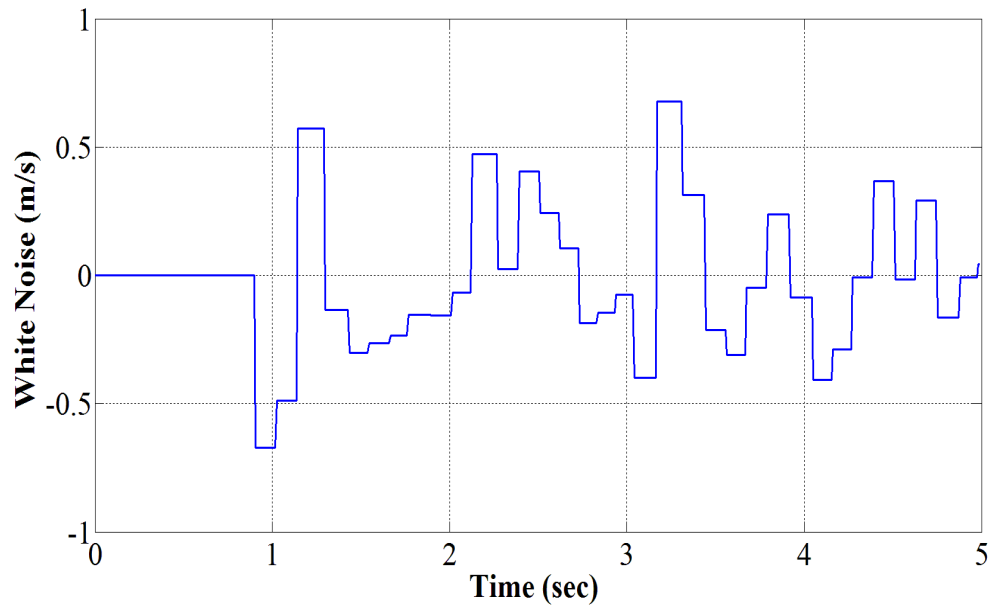

Figure 5.4 Noise signal under left main landing gear

To validate the robustness of the H_∞ controller, the response is simulated in Figures 5.5 and 5.6 for a rough landing case including the white noise and compared with the response of the semi-active system with LQR and the passive system. When a random signal is generated in the form of white noise during landing and provided as input for the left main gear, large amplitude vibrations are transmitted to the fuselage. However, for this case, the H_∞ controller is able to reduce the peaks in both the responses significantly. On the other hand, the semi-active system with the LQR controller fails to absorb the vibrations effectively.

Figure 5.5 Performance comparison of passive and semi-active systems for bounce considering noise signal under left main landing gear
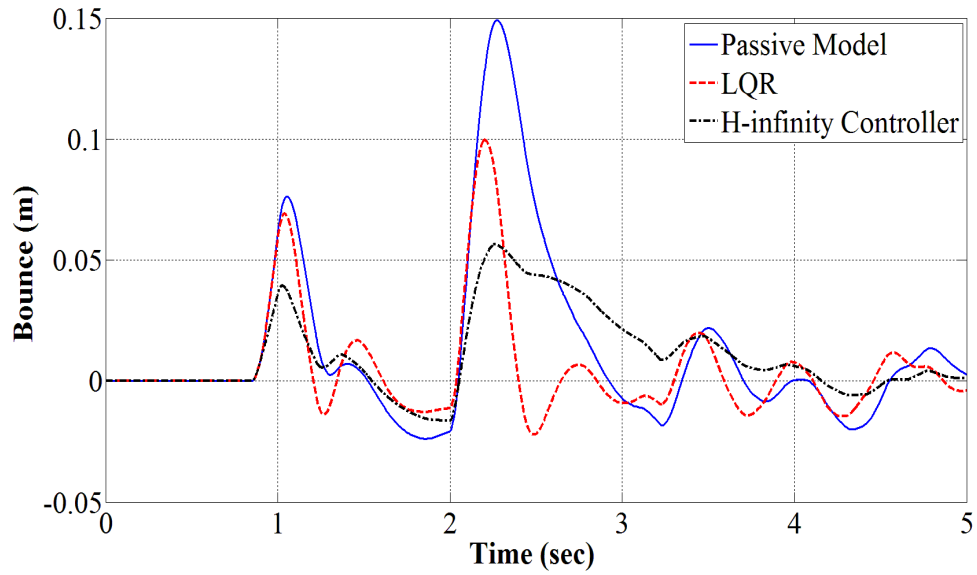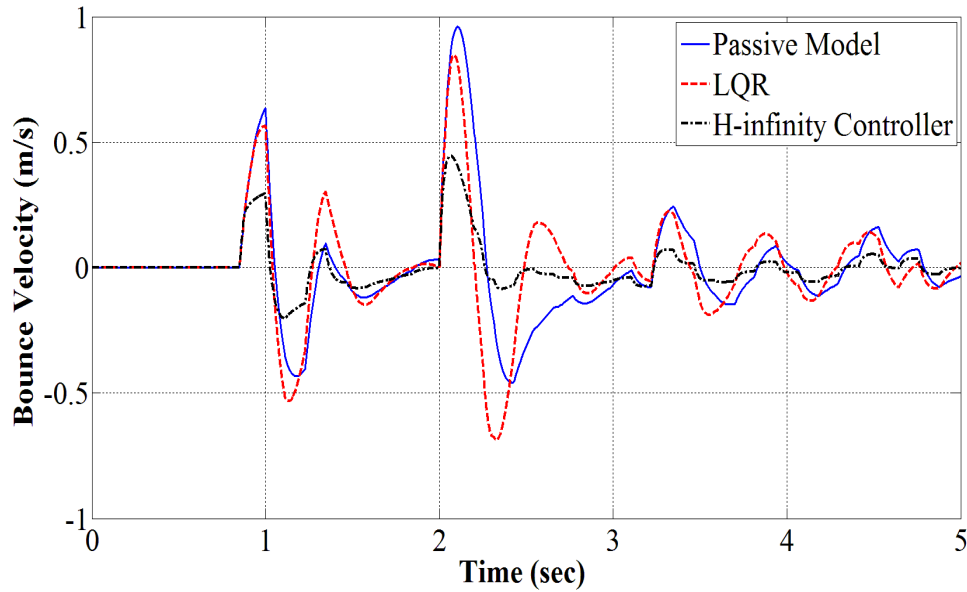

Figure 5.6 Performance comparison of passive and semi-active systems for bounce rate considering noise signal under left main landing gear

The reason for the better performance of the H_∞ controller in case of random vibration analysis lies in the fact that the H_∞ controller is designed to deal with any type of

disturbance and accordingly provides the required damping force for every case in order to suppress the vibrations.

Figures 5.7-5.9 compare the range of the MR damper force generated by the semi-active system considering both control strategies. The comparison shows the effectiveness of the H_∞ controller in applying the MR damper actuation force as soon as the system is excited thereby absorbing the vibrations getting transferred to the fuselage effectively. In case of the LQR controller, the delay in the application of the actuation force can be observed which deteriorates the performance of this controller for the rough landing scenarios. Therefore, the obtained results are clear indicators of the effectiveness and robustness of the H_∞ controller for any landing situation.
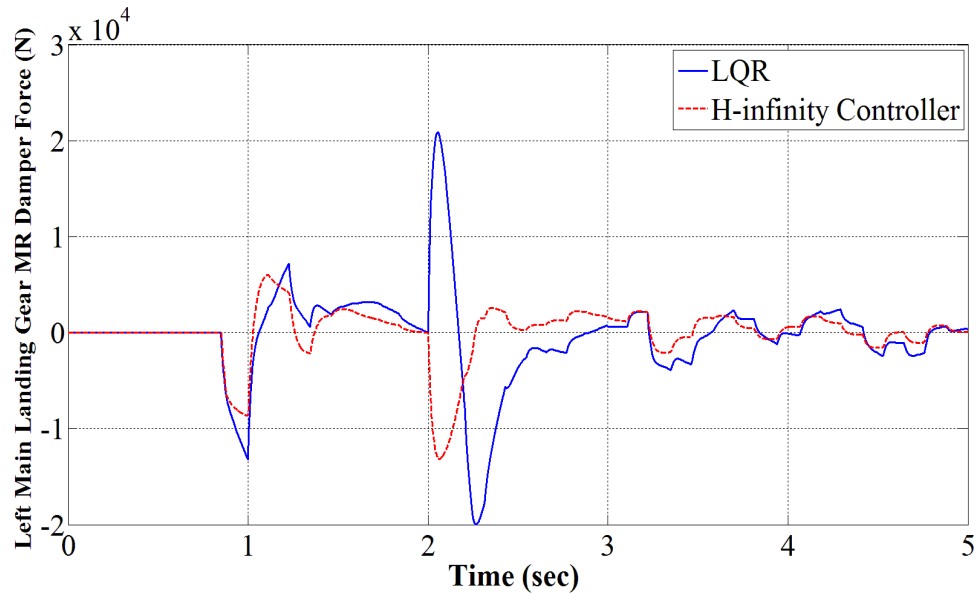
Figure 5.7 MR damper force for left main landing gear for sink velocity of 0.8 m/s
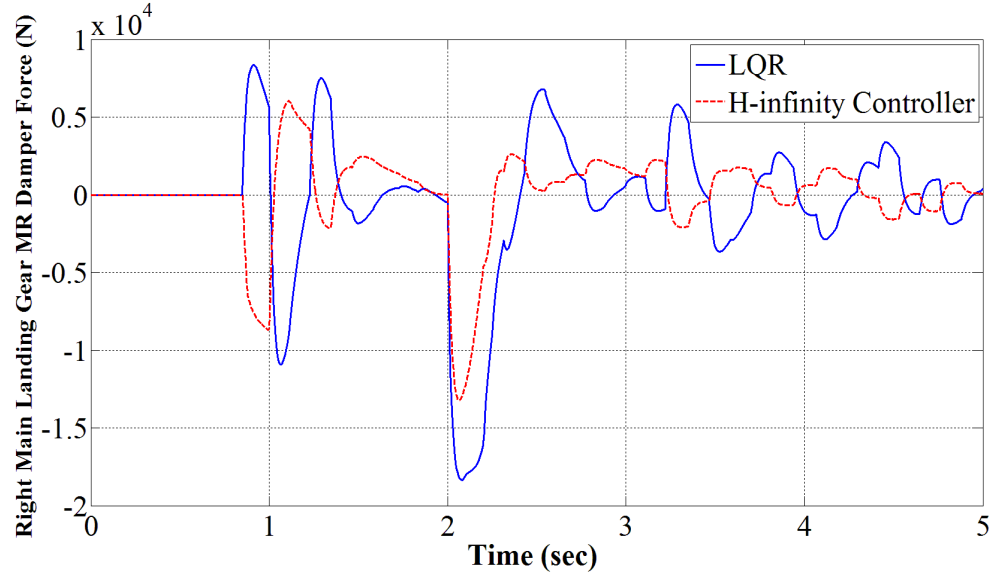
Figure 5.8 MR damper force for right main landing gear for sink velocity of 0.8 m/s
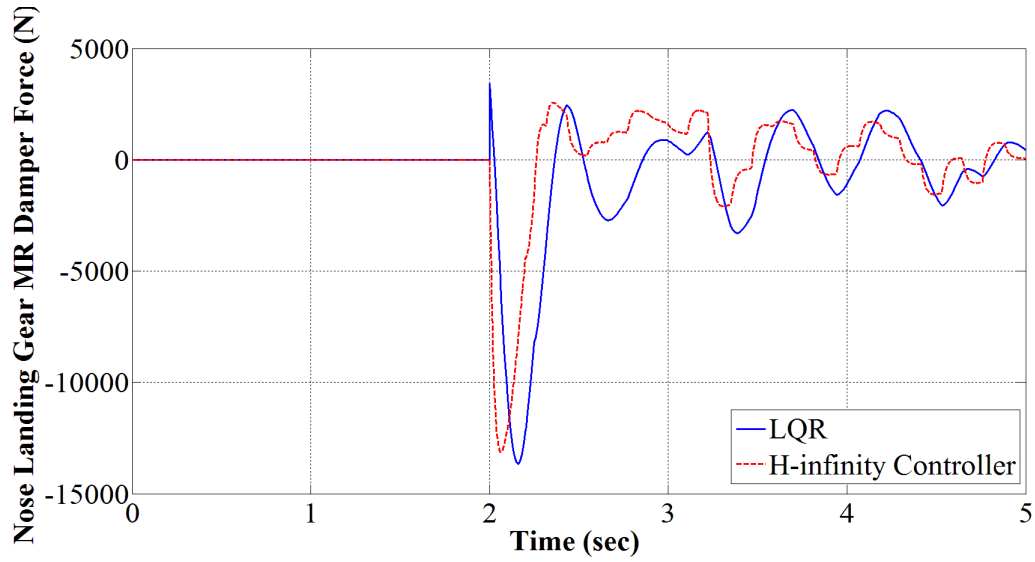
Figure 5.9 MR damper force for nose landing gear for sink velocity of 0.8 m/s

The robustness of the semi-active system with the H_∞ controller is confirmed from the obtained results. It can be interpreted that the H_∞ controller is adaptable to the uncertainties during landing thereby is capable of reducing the fuselage vibrations effectively. On the other hand, though the LQR controller works well for the normal landing case, it fails to absorb the fuselage vibrations when the aircraft is subjected to

uncertainties in landing situations. The effectiveness of the semi-active system with H_∞ controller will be demonstrated in the next sections by predicting its ability to absorb the fuselage vibrations for higher sink velocities considering the runway roughness.

5.3 Performance of the Semi-active System with H_∞ Controller for Different Landing Conditions

For simulating the landing performance of the aircraft and validating the effectiveness of the H_∞ control approach, four different landing scenarios are considered each with increasing sink velocity. The sink velocities selected for simulating the response are 1.5 m/s, 2.5 m/s and 3.6 m/s. For the fourth case, the sink velocity considered is 3.6 m/s but with the consideration of the runway unevenness for simulating the worst landing.

5.3.1 Landing performance for sink velocity of 1.5 m/s

For the first case the aircraft is assumed to be landing with a sink velocity of 1.5 m/s on a smooth runway. The landing scenario is depicted in figure 5.10. The left main landing gear touches the ground first followed by the right main gear after a delay of 0.15 seconds. The nose gear touches the ground 2 seconds after the initial touchdown. The landing scenario can be observed from figure 5.10.
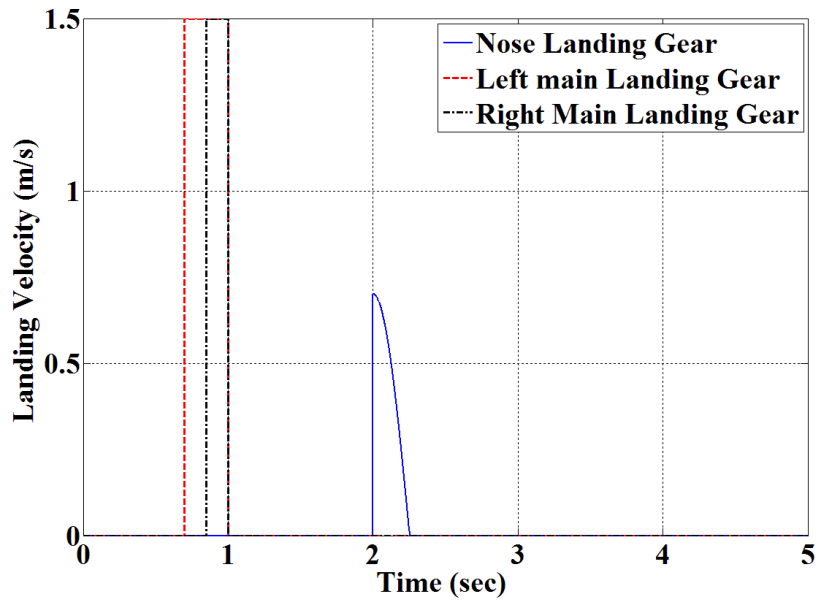
Figure 5.10 Landing scenario for initial sink velocity of 1.5 m/s

The landing performance of the aircraft for the sink velocity is depicted in figures 5.11 and 5.12.
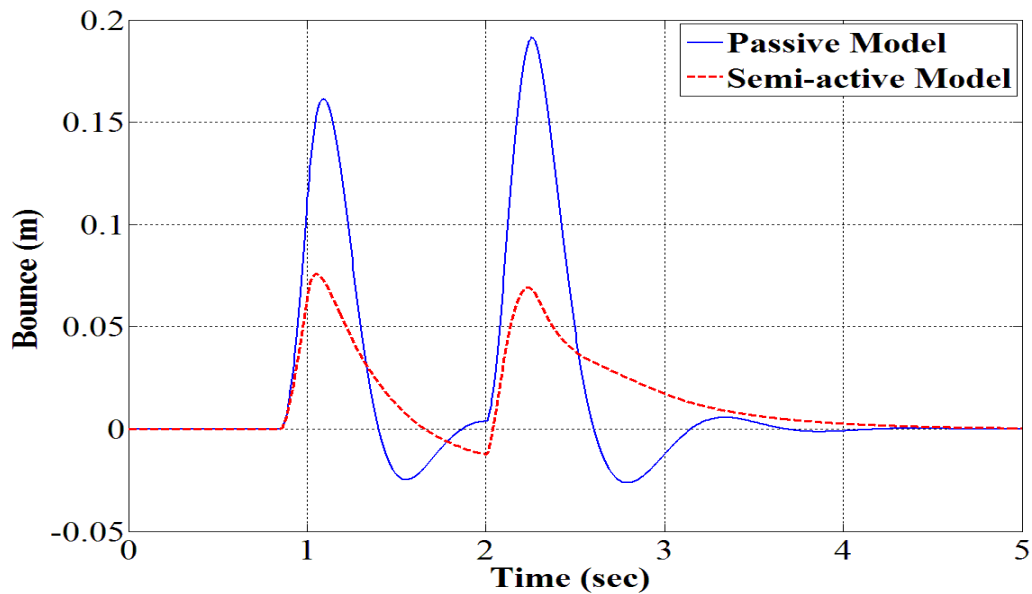
Figure 5.11 Performance comparison of passive and semi-active systems for bounce for sink velocity of 1.5 m/s
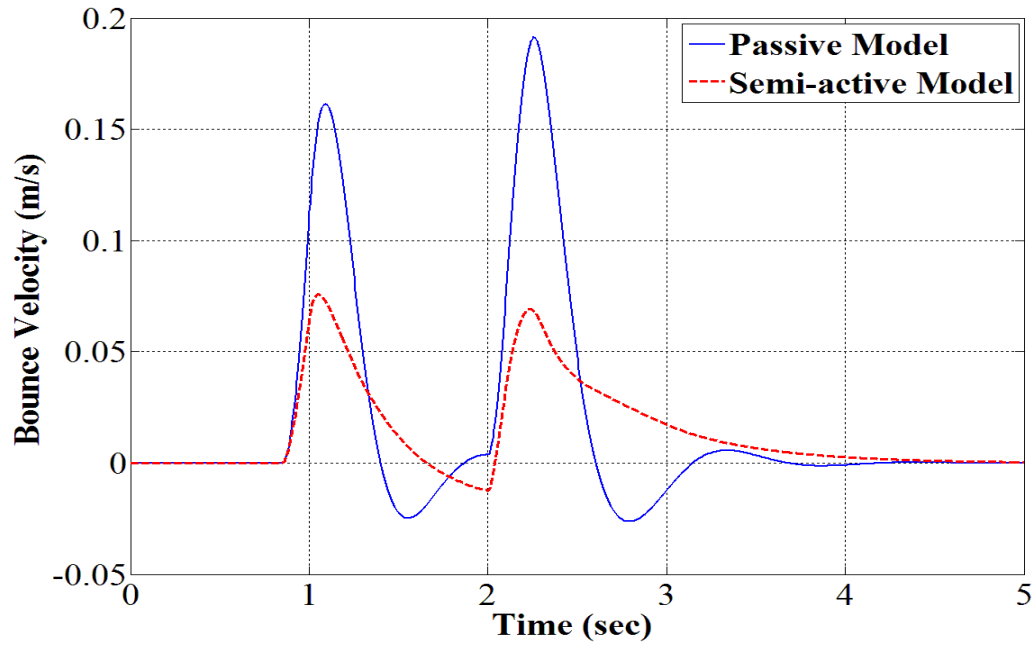
Figure 5.12 Performance comparison of passive and semi-active systems for bounce rate for sink velocity of 1.5 m/s

For this case since the aircraft lands with a higher sink velocity of 1.5 m/s as compared to the previous case, an increase in the peaks of the bounce response can be observed. The H_∞ controller could significantly reduce the fuselage vibrations for this sink velocity similar to the case of normal landing. The percentage reduction in the peaks of the bounce and the bounce rate response is 46% which is significant.
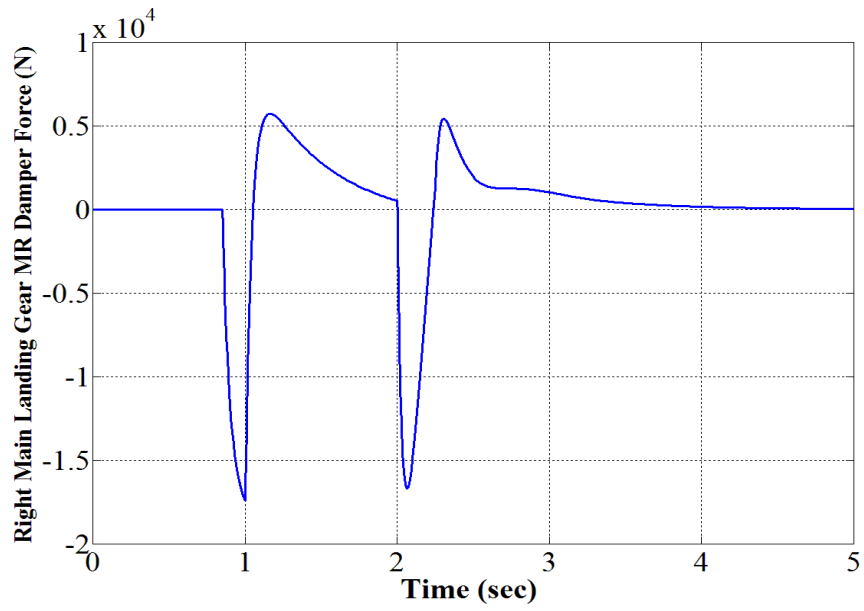
Figure 5.13 MR damper force for right main landing gear for sink velocity of 1.5 m/s
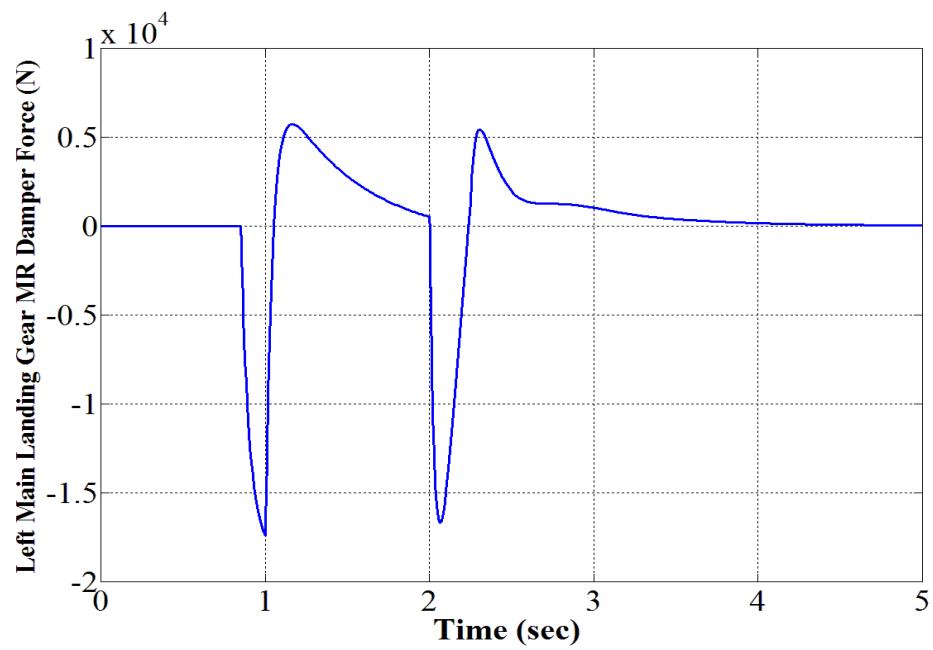
Figure 5.14 MR damper force for left main landing gear for sink velocity of 1.5 m/s

Figure 5.15 MR damper force for nose landing gear for sink velocity of 1.5 m/s

It can be interpreted that the designed controller can effectively detect the required MR damper force for damping out the excessive vibrations by detecting the sink velocity each time during landing. The required range of force generated by each MR damper corresponding to the two main gears and a nose gear can be observed from figures 5.13-5.15. As the main wheels touch the ground, the MR damper generates a force of approximately 18 kN for damping out the fuselage vibrations. As soon as the nose wheel touches the ground, the MR damper corresponding to it generates a force of approximately 15 kN for vertical vibration reduction.

5.3.2 Landing performance for sink velocity of 2.5 m/s

In this case, the lading velocity is increased to 2.5 m/s considering identical landing conditions. The sequence in which the three wheels touch the ground is similar to the one in the previous cases. Again, the aircraft is assumed to be landing on the smooth airstrip. Figure 5.16 depicts the landing scenario for the sink velocity of 2.5 m/s.
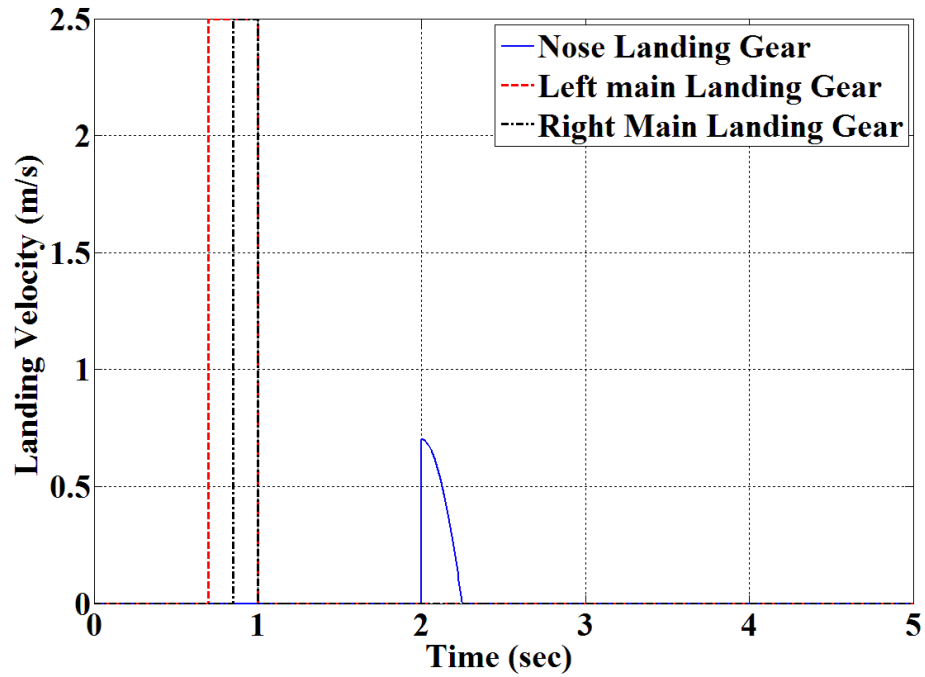
Figure 5.16 Landing scenario for initial sink velocity of 2.5 m/s

Although there is an increase in the landing velocity, the semi-active system performs efficiently during landing and absorbs the vibrations getting transmitted to the fuselage which can be observed from figures 5.17 and 5.18. It can be interpreted that the peak amplitudes increase with increase in the sink velocity. However, the designed semi-active system with the robust controller could reduce the peaks by approximately 46% similar to the first two cases and is capable of stabilizing the aircraft in the shortest possible time after landing.

98
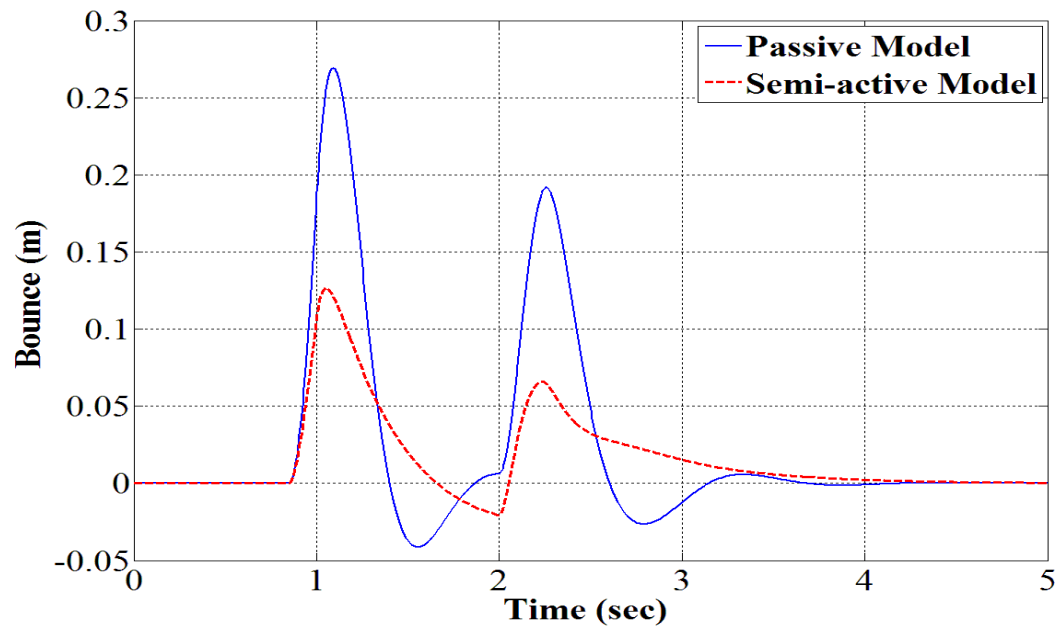
Figure 5.17 Performance comparison of passive and semi-active systems for bounce for sink velocity of 2.5 m/s
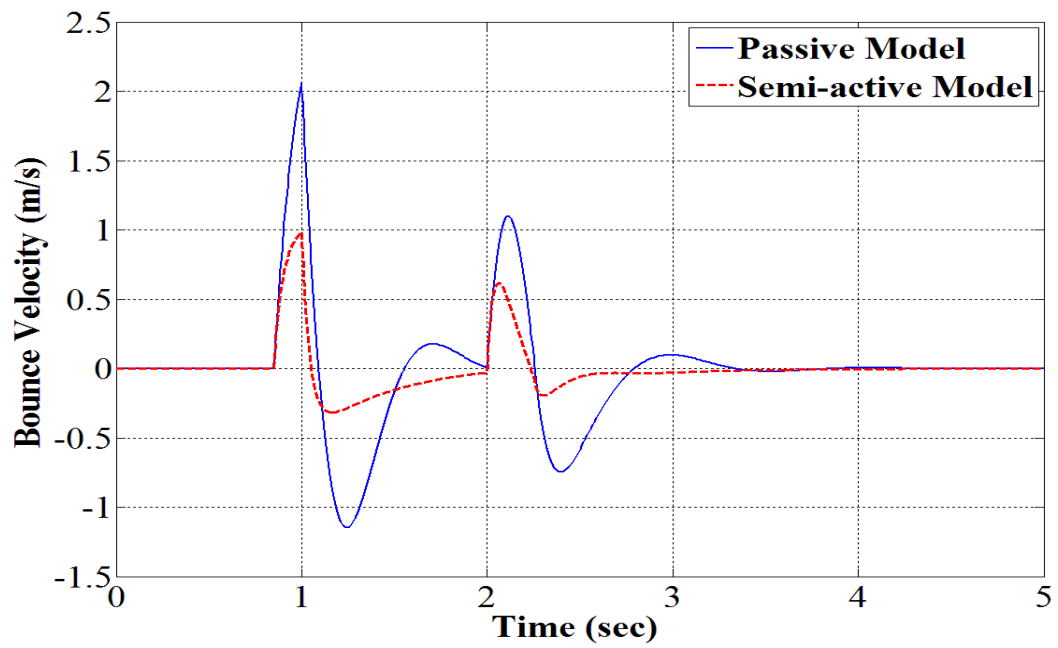
Figure 5.18 Performance comparison of passive and semi-active systems for bounce rate for sink velocity of 2.5 m/s

As the input to the controller is the bounce velocity, the required MR forces for reducing the fuselage vibrations will increase with the velocity.
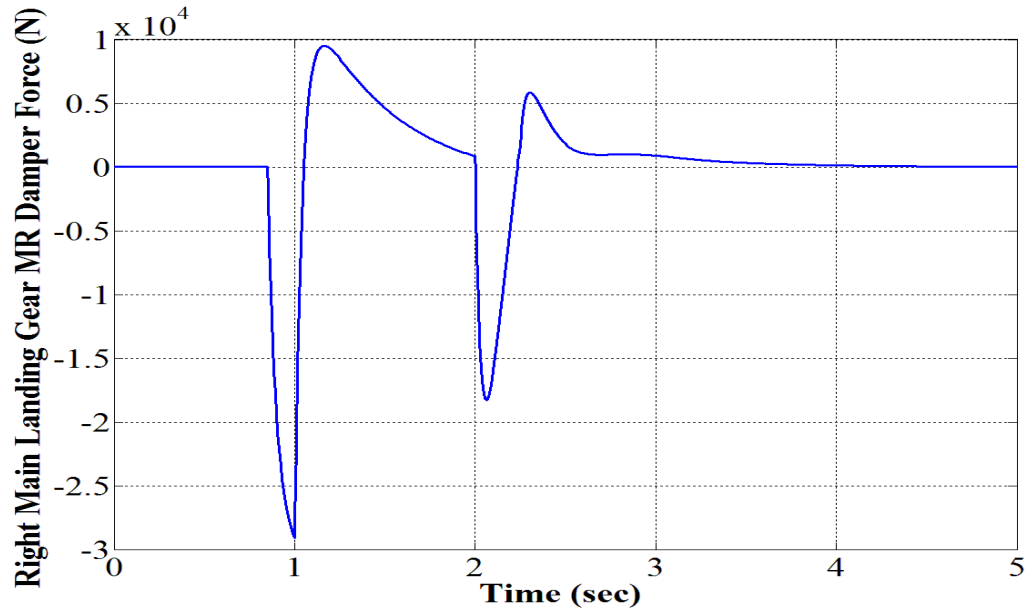
Figure 5.19 MR damper force for right main landing gear for sink velocity of 2.5 m/s

Figure 5.20 MR damper force for left main landing gear for sink velocity of 2.5 m/s
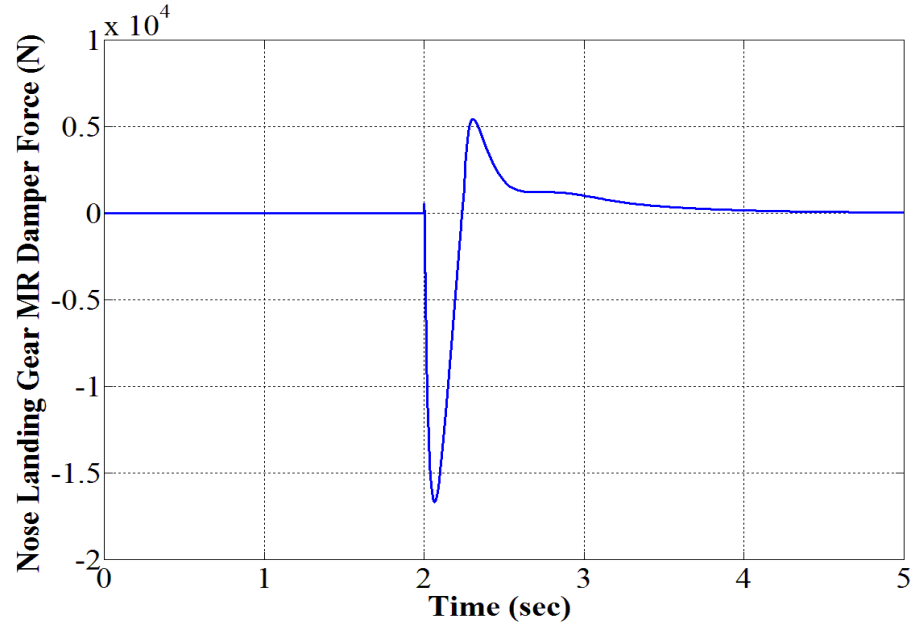
Figure 5.21 MR damper force for nose landing gear for sink velocity of 2.5 m/s

Figures 5.19-5.21 depict the required MR damper force for a sink velocity of 2.5 m/s. Compared to the previous case, the required forces are higher. To damp out the excessive vibrations effectively, the force generated by the MR damper in the main landing gears is approximately 30 kN whereas the MR damper generates a force of approximately 18 kN as the nose wheel touches the ground with a smaller velocity.

5.3.3 Landing performance for sink velocity of 3.6 m/s considering runway unevenness

It can be observed from results that the landing performance of the aircraft equipped with the semi-active suspension system with the H_∞ controller is better compared to the one equipped with the passive suspension system. However, all the above cases are for the normal landing conditions where the aircraft is assumed to be landing with the normal velocities. In reality, the aircraft might exceed the regulation limits of the sink velocity

during landing because of the pilot inaccuracies. Moreover, the airstrip is not always smooth because of the weather conditions which may cause excessive fuselage vibrations and sometimes a crash at the time of landing. The objective of designing the semi-active suspension for the aircraft is to prevent it from such uncertain hazards during landing, especially. Although the designed control system works well for the cases analyzed above, it is extremely important to design for the worst landing scenarios. Therefore, for this case it is assumed that the aircraft lands with a sink velocity of 3.6 m/s on a rough airstrip. Similar to the first case, a disturbance signal is applied as an input to the left main landing gear in the form of white noise. This means that the left main gear lands on a bump with the sink velocity of 3.6 m/s. The landing scenario and the generated noise signal can be visualized from figures 5.22 and 5.23, respectively.
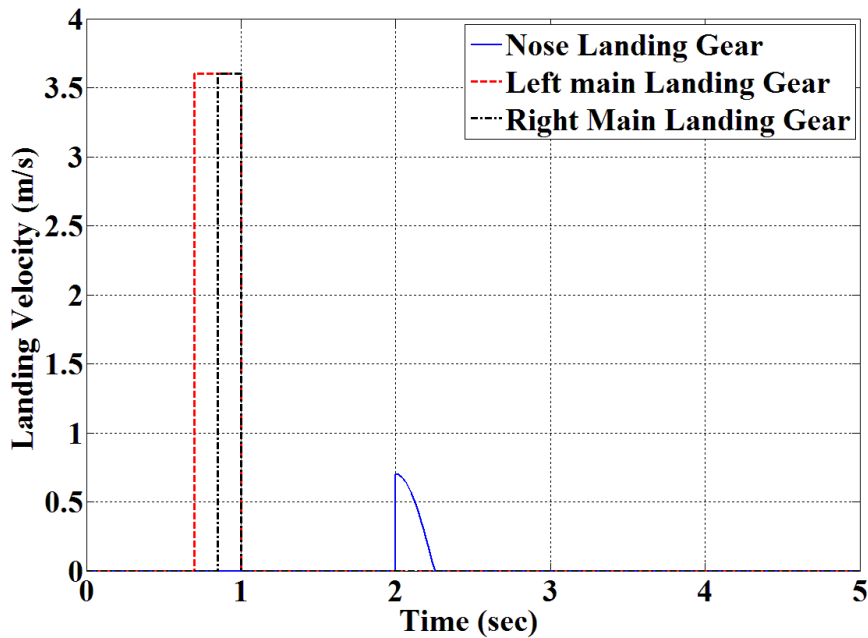
Figure 5.22 Landing scenario for initial sink velocity of 3.6 m/s
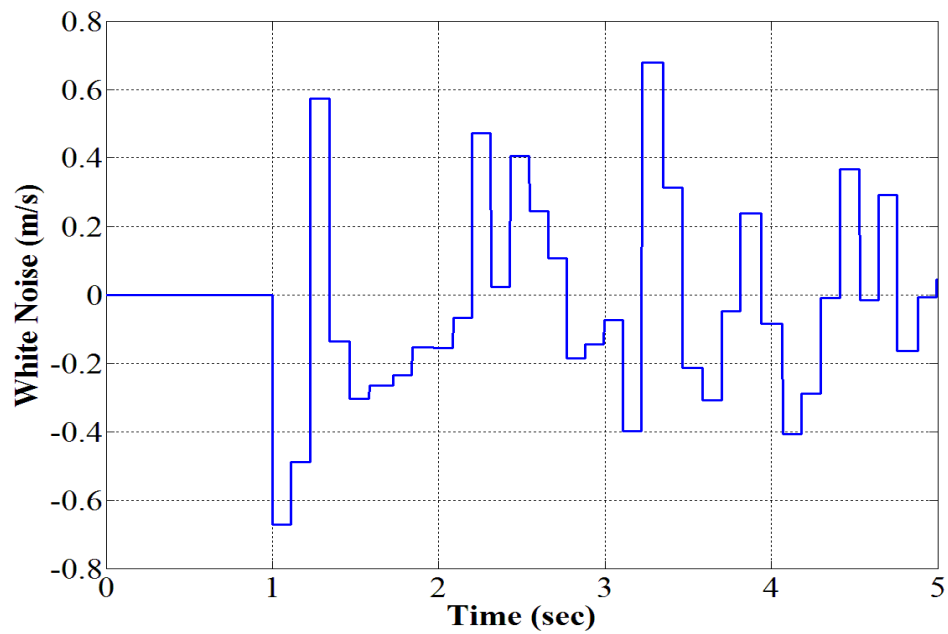
Figure 5.23 Noise signal under left main landing gear at sink velocity of 3.6 m/s

The landing performance of the aircraft for the worst landing case is simulated in figures 5.24 and 5.25.
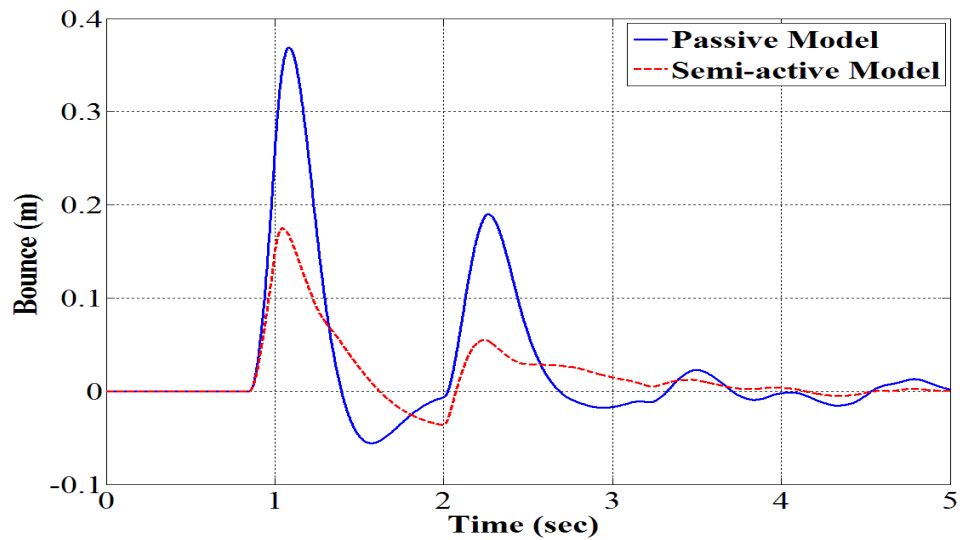
Figure 5.24 Performance comparison of passive and semi-active systems for bounce considering noise signal under left main landing gear at sink velocity of 3.6 m/s
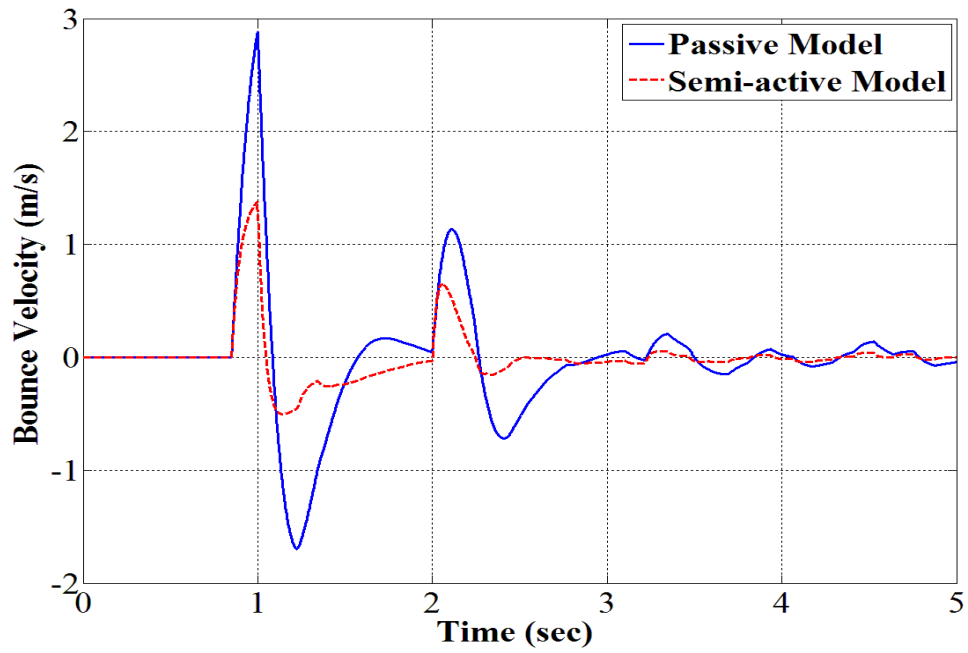
Figure 5.25 Performance comparison of passive and semi-active systems for bounce rate considering noise signal under left main landing gear at sink velocity of 3.6 m/s

Figures 5.26-5.29 depict the MR damper force range for the worst landing case.
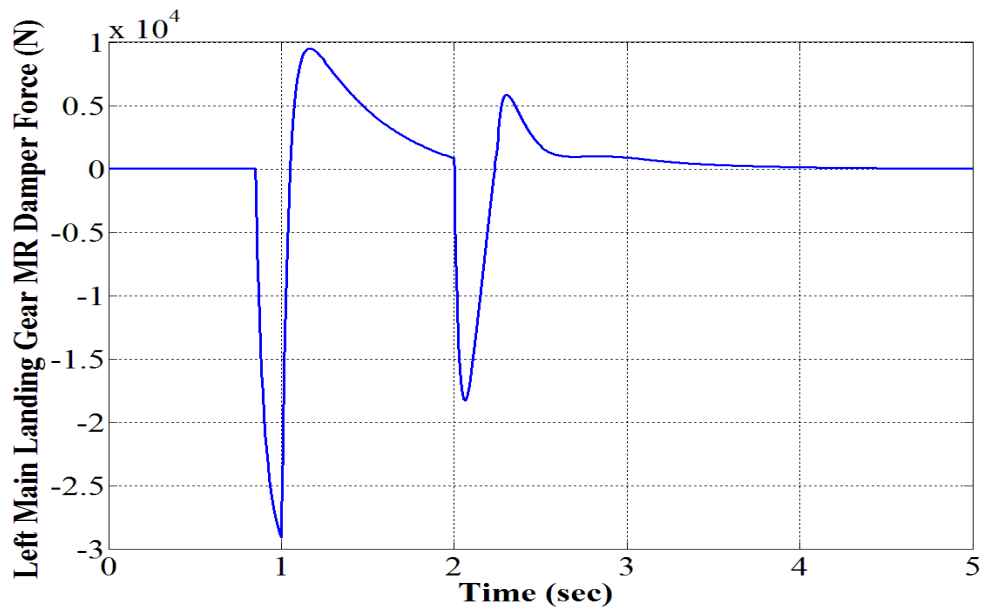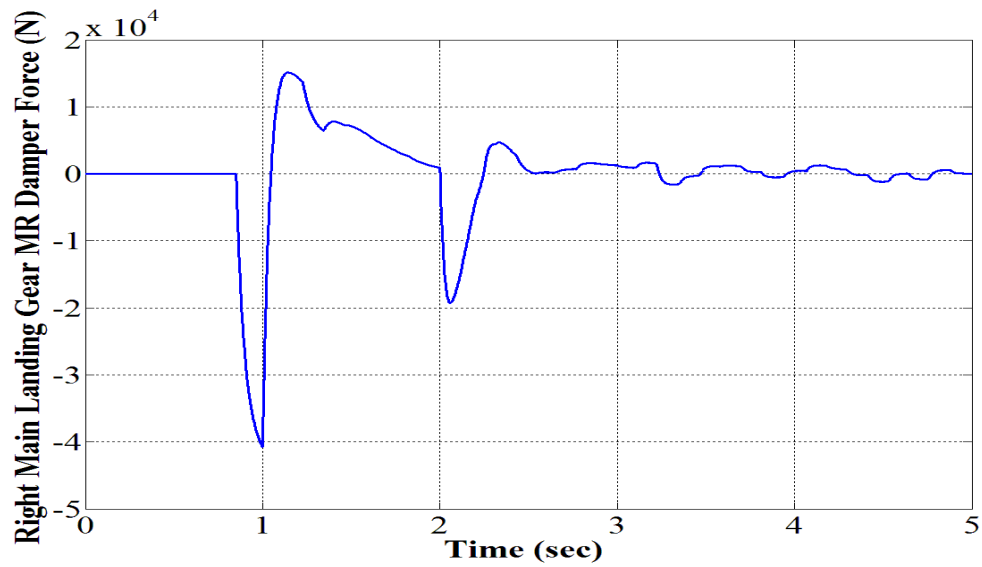

Figure 5.26 MR damper force for right main landing gear for sink velocity of 3.6 m/s

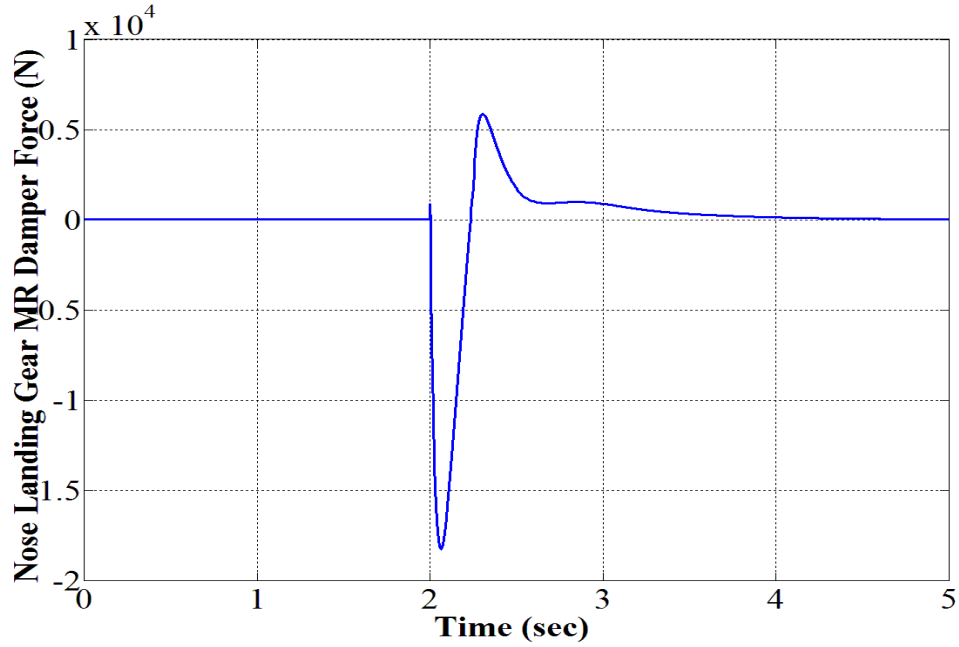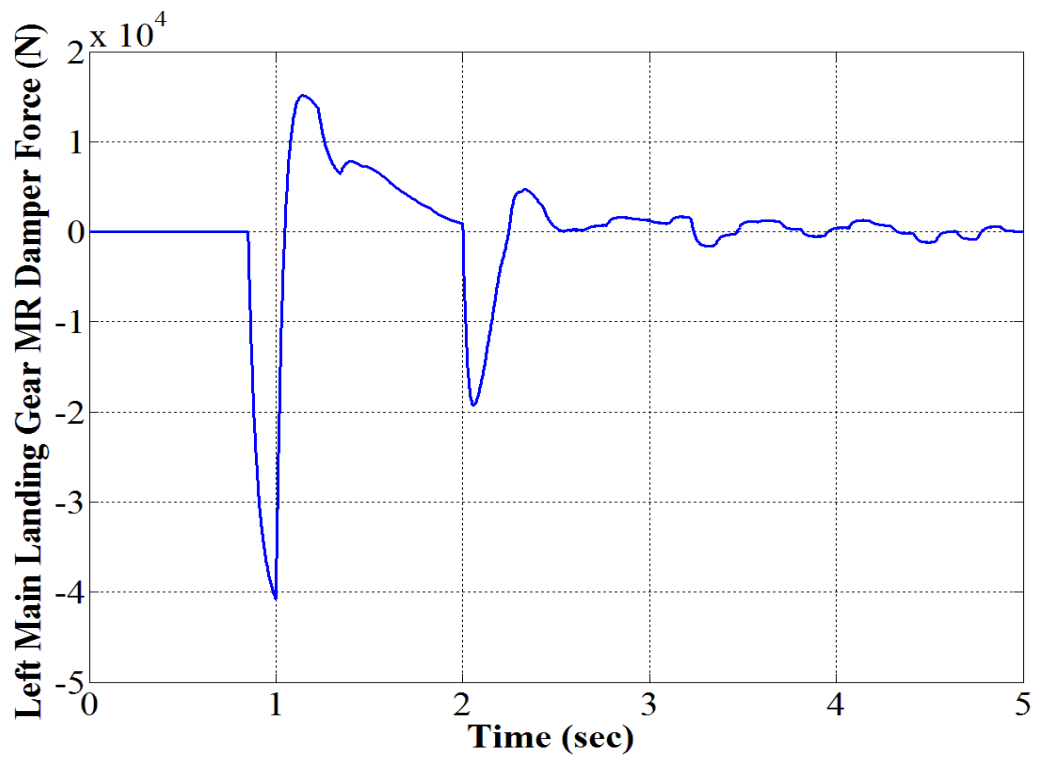**Figure 5. 27 MR damper force for left main landing gear for sink velocity of 3.6 m/s**
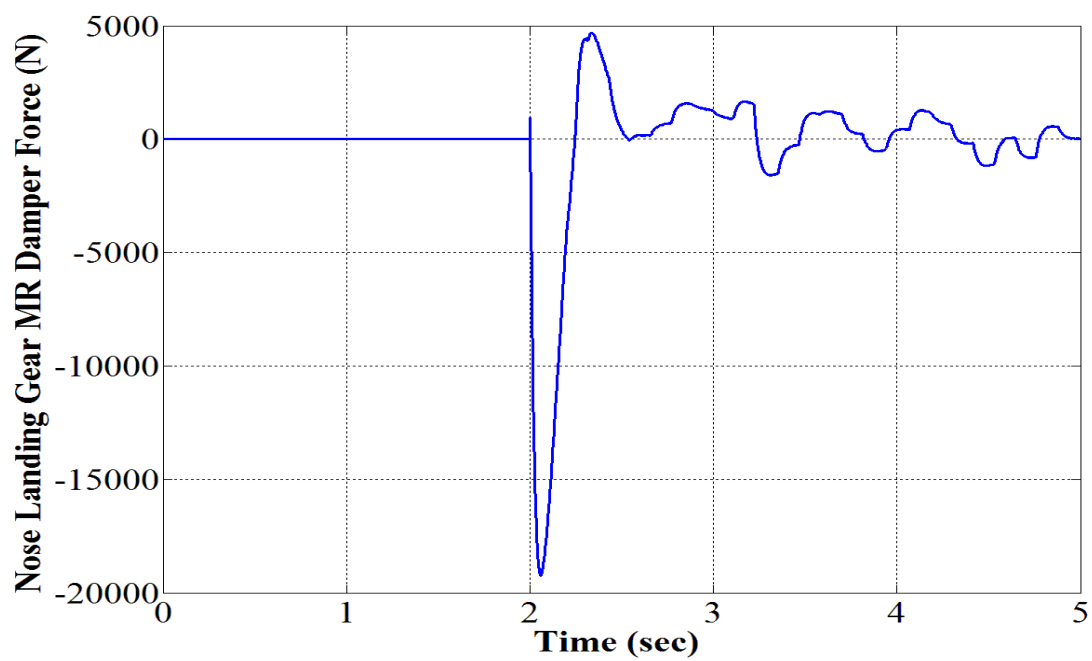
Figure 5.28 MR damper force for nose landing gear for sink velocity of 3.6 m/s

The bounce and the bounce rate responses depicted in the figures 5.24 and 5.25, respectively, clearly indicate the effectiveness of the designed semi-active system for the adverse landing conditions. The amplitude of the peaks increased as the aircraft landed on a rough airstrip with comparatively higher landing velocity. However, for the worst case landing also, the H_∞ controller could damp out the vibrations getting transmitted to the fuselage effectively. It can be observed from figures 5.26-5.28 that the required MR damper forces have increased compared to the previous cases of landing. The MR dampers embedded in two main landing gears and a nose gears are required to generate a force of approximately 40 kN and 20 kN respectively, to supress the fuselage vibrations during the possible worst landing case described above. Moreover, the aircraft takes considerably less time to stabilize after the initial impact.

It can be interpreted from the results that the designed semi-active suspension with the H_∞ controller is adaptable to the uncertainties during landing. The system can effectively reduce the fuselage vibrations both for the normal landing as well as the worst lading case. In real landing scenarios, if the aircraft exceeds its sink speed limit and lands on a rough airstrip, there is a possibility of accident during landing. From the results it can be observed that the designed system is able to supress the fuselage vibrations significantly not only for higher sink velocities but also in case of the other disturbance occurring during landing like runway roughness.

5.4 Summary

In this chapter, the performance analysis of the designed semi-active MR landing gear system is carried out by taking into consideration different landing scenarios. The simulated results prove that the use of robust H_∞ controller can significantly reduce the overshoot of the bounce and bounce rate responses which are related to the ride comfort of the aircraft after the initial landing impact. However, it is possible to carry out the LQR design at more than one operating points and attempt gain scheduling to further optimize the performance. Using robust control approach, the overshoot and settling time are significantly reduced. The simulation results prove the ability of the control strategy to generate required MR damper force for the initial landing scenario irrespective of the external environment. The robust analysis shows that the H_∞ controller is more efficient than the LQR not only for the ideal landing but also for the worst landing case. The H_∞ controller can accurately predict the required force corresponding to the MR damper current. Therefore, it can be interpreted that the semi-active MR damper suspension system using the H_∞ approach is able to absorb the excessive fuselage vibrations effectively during each landing. By considerably reducing the rate of bounce for the realistic landing scenario, the passenger safety and comfort are improved during the landing operation.

CHAPTER 6

CONCLUSIONS AND FUTURE RECOMMENDATIONS

6.1 Thesis Contributions

This study focuses on the development of the semi-active suspensions for the aircraft landing gears implementing a robust H_∞ control strategy and an optimal Linear Quadratic Regulator (LQR) control strategy. The primary goal of designing an intelligent suspension is to supress the excessive vibrations that are transferred to the aircraft fuselage during the landing phase which is considered as the most critical operational phase. This issue is directly related to the passenger safety and comfort. Therefore, the goal is to make the aircraft landing as smooth and as comfortable as possible. It is evident from the literature that the Magnetorheological dampers can form the basis for developing intelligent suspension systems for aircraft. The unique ability of these dampers to provide a variable damping effect at nominal currents makes them very attractive for the suspension applications. These dampers can provide a rapid interface between the mechanical systems and the electronic controls. Moreover, in case of failure, they have the capability to act as passive damping devices. Because of their unique characteristics, the MR dampers and their applications in engineering has been the focus of many research studies.

To fulfil the objectives of this study, a simulation approach was presented and a 3 DOF aircraft model was developed which took into consideration the bounce, pitch and roll motions of the aircraft during landing. The aircraft was assumed to be equipped with a conventional tri-cycle landing gear system with one wheel per landing gear. An actual

landing scenario was simulated using MATLAB/SIMULINK by providing a specific sink velocity and a time delay between the touchdown of the main wheels and the nose wheel. A semi-active Magnetorheological suspension system was developed using a robust H_∞ controller and an optimal LQR controller and the response of the aircraft was analyzed for different sink velocities during landing. The performance of the two controllers was compared for a particular landing scenario for the purpose of selecting the appropriate control approach. Finally, the applicability of the developed semi-active suspension system with the robust controller was tested by subjecting the landing aircraft to runway input. Based on the mathematical and the simulation studies done on the developed model, following are the important contributions of this study.

- Based on the available Spencer model, the analysis of the energy dissipation characteristics of the MR damper is carried out. The energy dissipation patterns for different input frequencies are analyzed and the mathematical equations for linearizing the MR damper through simulation approach are presented. The relationship between the dissipated energy and the current is depicted through simulations. Similarly, the relationship between the equivalent damping coefficient and the current is also established. The analysis of the energy dissipation patterns of the MR damper and the graphically depicted relationships with the applied inputs can give a better understanding of the behaviour of the damper in order to effectively use it for the variable damping applications.

- A 3 DOF aircraft model is developed for the vibration analysis which takes into consideration the bounce, pitch and roll motions of the aircraft. Most of the aircraft models developed in the previous studies were based on the conventional

quarter car model which could take into account only the vertical vibrations. However, the model developed in this study could be used to present the real aircraft equipped with a tri-cycle landing gear system. The effects of the roll and pitch motions on the vertical motion are also taken into consideration though these motions are not analyzed in this study. Since most of today's passenger aircraft use a conventional tri-cycle landing gear system, this model can be used for the simulation studies of the prototypes.

- The most important contribution is the simulation of the actual landing scenario for the developed 3 DOF aircraft model. A switching technique is developed in SIMULINK which enables the system to switch from a single degree of freedom to three degrees of freedom system in order to simulate the sequential touching of the two wheels of the main landing gears and the nose landing gear wheel during landing. This approach can provide a good approximation of the real landing scenarios in case of pilot inaccuracies and the other uncertainties.

6.2 Conclusions

The proposed study focused on the two important aspects; analyzing the behavior of the Magnetorheological dampers using parametric dynamic modeling approach and developing the semi-active MR landing gear suspension using the robust H_∞ and the LQR control strategies for reducing the fuselage vibrations. Based on the work done in this study, the important conclusions can be summarized as follows:

- The Magnetorheological dampers can provide an effective solution for developing the semi-active suspensions for the aircraft. Although a few applications of these dampers have been reported in vehicle engineering field, aircraft landing gears have not been equipped with such damper. MR fluids have the ability to make rapid and reversible transitions in their rheological properties. This fact makes the MR damper a powerful device for achieving the variable damping in suspension systems with minimal power requirements.

- Parametric dynamic modeling approach for studying the non-linear hysteretic characteristics of the MR dampers is a simple and robust modeling approach. The parametric modeling approach facilitates the numerical analysis as well as the simulation for studying the dynamic behavior of the MR dampers.

- It can be interpreted from the force-velocity characteristics that the MR dampers operate in two distinct regions namely, the post-yield and the pre-yield region. The force-velocity characteristics show hysteretic behavior which has to be predicted accurately for implementing the control laws. Spencer dynamic model can accurately depict the behavior of the MR damper by characterizing the post-

yield and the pre-yield hysteresis. The mathematical equations of Spencer model are easy to understand and implement in the simulation.

- The energy dissipation results were also simulated using Spencer model. The model could accurately predict the energy dissipation patterns of the MR damper for varying input frequencies.

- The MR damper can be an effective actuation mechanism for developing the semi-active suspension for the aircraft landing gears. The semi-active MR landing gear was developed using the H_∞ and the LQR control strategies. The simulated results showed that the use of robust H_∞ controller can significantly reduce the overshoot of the bounce and bounce rate response which is related to the ride comfort of the aircraft after the initial landing impact.

- Using robust control approach, the overshoot and settling time are significantly reduced. The simulation results proved the ability of the control strategy to generate the required MR damper force for the initial landing scenario irrespective of the external environment. The robust analysis showed that the H_∞ controller is more efficient than the LQR not only for the ideal landing but also for the rough landing case considering the uncertainties like runway roughness. The H_∞ controller can accurately predict the required MR damper force based on the bounce velocity. Therefore, a semi-active MR landing gear suspension system using the H_∞ approach is able to suppress the excessive fuselage vibrations effectively during each landing scenario. By considerably reducing the rate of bounce for the realistic landing scenario, the passenger safety and comfort are improved during the landing operation.

6.3 Future Recommendations

The analyses done in the research provided a stimulus for further extending the dimensions of knowledge in the field of the aircraft landing and the passenger safety associated with it. The concept of development of smart dampers for the aircraft landing gears is amongst the emerging research topics which, if implemented considering the engineering constraints, can effectively reduce the impact loads during the landing phase. The primary focus of all the research programs is to make human life pleasant, comfortable and safe. Considering the human life as the utmost important factor can give a tremendous impetus for making progress in this research field.

This field has wide open scope, and some recommendations are made for the future studies. A few of them are summarized as follows.

- In this study, a 3 DOF aircraft model is developed for the vibration analysis. A model considering the additional yaw DOF can be developed in order to consider the shimmy motion occurring during landing. The application of the smart MR damper for shimmy control is also recommended.

- Since the primary objective is to improve the ride comfort and passenger safety, it is necessary to model the human body sitting inside an aircraft as a spring-mass-damper system for analyzing the vibration transmissibility to the human body through the fuselage. The human body of a pilot inside a cockpit can be modeled for the transmissibility analysis as the safety of the pilot is extremely important. This analysis can provide an actual idea of the passenger comfort during landing.

- The smaller capacity and light weight MR dampers can be used for the aircraft seats to attenuate the vibrations during the landing impact. However, this

application would involve high cost as the number of MR dampers required for each aircraft would be high which could be quite expensive.

- It is recommended to consider the aerodynamic forces acting on the aircraft fuselage as well as the undercarriage during landing. This would provide a complete analysis from the aerodynamics point of view. Considering the effects of the factor such as the lift force, the drag force, the horizontal velocity and approach speed during landing could provide a better idea about the structural vibration analysis. Moreover, the presented study analyzed the aircraft landing under normal landing conditions and considered only the runway unevenness. However, it is necessary to analyze the cases where the aircraft is subjected to a cross wind landing scenario and other undesirable conditions.

- In this study, only the passenger aircraft is taken into consideration. It is recommended to extend the research for the fighter aircraft landing on the deck of the aircraft carrier. The vibration analysis problem can become interesting in this case since the movement of deck due to ocean waves and its effect on the aircraft landing would lead to a critical dynamics. The MR dampers can be also used for developing the semi-active suspensions for the Unmanned Aerial Vehicle (UAV).

- One of the recommended designs is to replace the oil in the oleo-pneumatic damper with the MR fluid and build the necessary current circuit to magnetize the fluid.

REFERENCES

[1] D. Howe, *Aircraft loading and structural layout*. London: Professional Engineering Publishing, 2004.

[2] N. S. Currey, *Aircraft landing gear design: Principles and practices*. Washington D.C.: American Institute of Aeronautics and Astronautics, Inc., 1988.

[3] Y. Xie et al., "Runway landing safety analysis: a case study of Atlanta Hartsfield airport," *Proc. The 22nd IEEE Digital Avionics Systems Conference*, vol. 1, pp. 1-12, 2003.

[4] H. Sheikhpour et al., "An approach on take-off and landing related aircraft accidents involving new considerations," *International Conference on Traffic and Transportation Engineering*, Singapore, 2012, pp. 49-53.

[5] G. W. H. Van Es, "Running out of runway analysis of 35 years of landing overrun accidents," National Aerospace Laboratory NLR, Amsterdam, Rep. NLR-TP-2005-498, 2005.

[6] F. Mirzatolooei and A. Bazzazi, "Analysis of orthopedic injuries in an airplane landing disaster and a suggested mechanism of trauma," *European Journal of Orthopaedic Surgery and Traumatology*, vol. 23, pp. 257-262, 2013.

[7] H. Wentscher et al., "Fuselage vibration control using semi-active front gear," Advisory Group for Aerospace Research and Development North Atlantic Treaty Organization (AGARD), Rep. R-800:5, 1996.

[8] A. Krauss, "The Design, qualification and maintenance of vibration-free landing gear," Daimler-Benz Aerospace AG, Munich, Rep. AGARD R-800, 1995.

[9] D. W. Young, "Aircraft landing gears-the past, present and future," *Proc. The Institute of Mechanical Engineers, Part D: Journal of Automobile Engineering*, vol. 200, pp. 75-92, 1986.

[10] D. C. Batterbee et al., "Magnetorheological landing gear: 1.a design methodology," *Smart Materials and Structures*, vol. 16, pp. 2429-2440, 2007.

[11] C. B. Asthana and R. B. Bhat, "Novel design of landing gear oleo strut damper using fluid for aircraft and UAV's," *Applied Mechanics and Materials*, vol. 225, pp. 275-280, 2012.

[12] M. Khani, "MR damper for landing gear system," MAsc thesis, Dept. Mechanical and Industrial Engineering., Concordia University., Montreal, QC, Canada, 2010.

[13] W. Kruger et al., "Aircraft landing gear dynamics: simulation and control," *Vehicle System Dynamics*: *International Journal of Vehicle Mechanics and Mobility*, vol. 28, pp. 119-158, 1997.

[14] H. H. Somm et al., "Adaptive landing gear for improved taxi performance," Boeing Aerospace Company, Seattle, Rep. AFFDL-TR-77-119, 1977.

[15] E. R. Wang, "Syntheses and analyses of semi-active control algorithms for a Magnetorheological damper for vehicle suspensions," Ph.D. dissertation, Dept. Mechanical and Industrial Engineering., Concordia University., Montreal, QC, Canada, 2005.

[16] D. L. Margolis, "A procedure for comparing passive, active and semi-active approaches to vibration isolation," *Journal of the Franklin Institute*, Vol. 315, pp. 225-238, 1983.

[17] H. Du et al., "Semi-active H_∞ control of vehicle suspension with magneto-rheological dampers," *Journal of Sound and Vibration*, vol. 283, pp. 981-996, 2005.

[18] E. R. Wang et al., "Semi-active control of vehicle vibration with MR-dampers," *Proc. 42nd IEEE Conference on Decision and Control*, vol. 3, pp. 2270-2275, 2003.

[19] M. Zapateiro et al., "Semiactive control methodologies for suspension control with magnetorheological dampers," *IEEE/ASME Trans. Mechatronics*, vol. 17, pp. 370-380, 2012.

[20] L. Hua-Lin et al., "Fuzzy PID control for landing gear based on magneto-rheological (MR) damper," *International Conference on Apperceiving Computing and Intelligence Analysis*., Chengdu., 2009, pp. 22-25.

[21] D. H. Wang and W. H. Liao, "Magnetorheological fluid dampers: a review of parametric modeling," *Smart Materials and Structures*, vol. 20, pp. 1-34, 2011.

[22] J. D. Carlson, "Commercial Magnetorheological fluid device," *International Journal of Modern Physics B*, Vol. 10, pp. 2857-2865, 1996.

[23] M. R. Jolly et al., "Properties and applications of commercial magnetorheological fluids," *Journal of Intelligent Material Systems and Structures*, vol. 10, pp. 5-13, 1996.

[24] M. Aslam et al., "Review of magnetorheological (MR) fluids and its applications in vibration control," *Journal of Marine Science and Application*, Vol. 5, pp. 17-29, 2006.

[25] J. D. Carlson and J. L. Sproston, "Controllable fluids in 2000 status of ER and MR fluid technology," *Proc. 7th International Conference on New Actuators*., Bremen, 2000, pp. 126-130.

[26] S. B. Choi et al, "Vibration control of a MR seat damper for commercial vehicles," *Journal of Intelligent Material systems and structures,* vol. 11, pp. 936-944, 2000.

[27] H. Wang et al., "An investigation of an active landing gear system to reduce aircraft vibrations caused by landing impacts and runway excitations," *Journal of Sound and Vibration,* vol. 317, pp. 50-66, 2008.

[28] S. Sivakumar and A. P. Haran, "Parametric analysis and vibration control of landing gear with PID controller," *European Journal of Scientific Research*, vol. 89, pp. 441-453, 2012.

[29] M. Zapateiro et al., "Landing gear suspension control through adaptive backstepping techniques with H_∞ performance," *Proc. The 18th IFAC World Congress., Milano.*, 2011, pp. 4809-4814.

[30] D. P. Raymer, *Aircraft design: a conceptual approach*. Washington D.C.: American Institute of Aeronautics and Astronautics, Inc., 1989.

[31] H. Hall, *Some theoretical studies concerning oleo damping characteristics.* London: Her Majesty's Stationery Office, 1966.

[32] W. I. Kordonsky, "Magnetorheological effect as a base of new devices and technologies, *Journal of Magnetism and Magnetic Materials*, Vol. 122, pp. 395-398, 1993.

[33] X. Zhu et al., "Magnetorheological fluid dampers: A review on structure design and analysis," *Journal of Intelligent Material Systems and structures*, vol. 23, pp. 839-873, 2012.

[34] J. Rabinow, "The magnetic fluid clutch," *AIEE* Transactions, vol. 67, pp. 1308-1315, 1948.

[35] S. B. Choi and Y. M. Han, *Magnetorheological fluid technology: applications in vehicle systems*. Boca Raton: CRC Press, 2012.

[36] O. Ashour, "Magnetorheological fluids: Materials, characterization and devices," *Journal of Intelligent Material Systems and Structures*, vol. 7, pp. 123-130, 1996.

[37] P. P. Phule, "Magnetorheological fluid, Phule," U.S. Patent 5 985 168, November 16, 1997.

[38] P. Phule, "Rheological properties of magnetorheological fluids," *Smart Materials and Structures*, vol. 11, pp. 140-146, 2002.

[39] J. D. Carlson, "MR fluid foam and elastomer devices," *Mechatronics*, vol. 10, pp. 555-569, 2000.

[40] M. Kciuk, "Properties and application of magnetorheological fluids," *Journal of Achievements in Smart Materials and Structures*, vol. 18, pp. 127-130, 2006.

[41] J. D. Carlson, "What makes a good MR fluid?," *Journal of Intelligent Material Systems and* Structures, vol. 13, pp. 431-435, 2002.

[42] Q. H. Nguyen and S. B. Choi. (2012). *Smart actuation and sensing systems-recent advances and future challenges* [online]. Available: http://www.intechopen.com.

[43] K. Kim and D. Jeon, "Vibration suppression in an MR fluid damper suspension system," *Journal of Intelligent Material Systems and Structures*, vol. 10, pp. 779-786, 1999.

[44] H. F. Lam and W. S. Liao, "Semi-active control of automobile suspension systems with magnetorheological dampers" *International Journal of Vehicle Design*, vol. 33, pp. 1-3, 2003.

[45] H. S. Lee and S. B. Choi, "Control and response characteristics of a magnetorheological fluid damper for passenger vehicles," *Journal of Intelligent Material Systems and Structures*, vol. 11, pp. 80-87, 2000.

[46] Y. Shen et al., "Semi-active vibration control schemes for suspension systems using magnetorheological dampers, *Journal of Sound and Vibration*, vol. 12, pp. 3-24, 2006.

[47] H. J. Yao, "Semi-active H_∞ control of seat suspension with MR damper," *Journal of Physics*: *Conference Series*, vol. 412, pp. 1-16, 2013.

[48] L. H. Zong et al., "Semi-active H_∞ control of high-speed railway vehicle suspension with magnetorheological dampers," *International Journal of Vehicle Mechanics and Mobility*, vol. 51, pp. 600-626, 2013.

[49] W. H. Liao and D. H. Wang, "Semi-active vibration control of train suspension systems via Magnetorheological dampers," *Journal of Intelligent Material Systems and Structures*, vol. 14, pp. 161–172, 2003.

[50] D. H. Wang and W. H. Liao, "Semi-active suspension systems for railway vehicles using magnetorheological dampers: part I. System integration and modeling," *Vehicle System Dynamics*, vol. 47, pp. 1305–1325, 2009.

[51] D. H. Wang and W. H. Liao, "Semi-active suspension systems for railway vehicles using magnetorheological dampers: part II. Simulation and analysis," *Vehicle System Dynamics*, vol. 47, pp. 1439–1471, 2009.

[52] S. J. Dyke, "Modeling and control of magnetorheological dampers for seismic response reduction," *Smart Materials and structures*, vol. 5, pp. 565-575, 1996.

[53] B. F. Spencer and S. Nagarajaih, "State of the art of structural control," *Journal of Structural Control*, vol. 129, pp. 845-856, 2003.

[54] I. Yuan and A. Hac, "Semi-active suspensions with adaptive capability," *Journal of Sound and Vibration*, vol. 180, pp. 475-492, 1995.

[55] N. D. Sims and R. Stanway, "Semi-active vehicle suspension using smart fluid dampers: a modeling and control study," *International Journal of Vehicle Design*, vol. 33, pp. 76-102, 2003.

[56] G. Mikulowski and J. Holnicki-szulc, "Adaptive aircraft shock absorbers," *AMAS workshop on Smart Materials and Structures*, vol. 3, pp. 63-72, 2003.

[57] W. Kruger, "Design and simulation of semi-active landing gears for transport aircraft," *Mechanics of Structures and Machines*, vol. 30, pp. 493-526, 2002.

[58] W. Dong et al., "GA-based model predictive control of semi-active landing gear," *Chinese Journal of Aeronautics*, vol. 20, pp. 47-54, 2007.

[59] Y. T. Choi and N. M. Wereley, "Vibration control of a landing gear system featuring ER/MR fluids," *Journal of Aircraft*, vol. 40, pp. 432-439, 2003.

[60] G. L. Ghiringhelli, "Testing of a semi-active landing gear control for a general aviation aircraft," *Journal of Aircraft*, vol. 37, pp. 606-616, 2000.

[61] G. L. Ghiringhelli and S. Gualdi, "Evaluation of a landing gear semiactive control system for complete aircraft landing," *Aerotecnica Missili e Spazio*, vol. 83, pp. 21-31, 2004.

[62] J. H. Kim and J. H. Oh, "Development of an above knee prosthesis using MR damper and leg simulator," *Proc. IEEE International Conference of Robotics and Automation*, vol. 4, pp. 3686-3691, 2001.

[63] H. Herr and A. Wilkenfeld, "User-adaptive control of a magnetorheological prosthetic knee," *Industrial Robot: An International Journal*, Vol. 30, pp. 42–55, 2003.

[64] W. H. Li, "Viscoelastic properties of MR fluids," *Smart Materials and Structure*, vol. 8, pp. 460-468, 1998.

[65] J. Wang and G. Meng, "Magnetorheological fluid devices: Principles, characteristics and applications in mechanical engineering," *Proc. The Institution of Mechanical Engineers, Part L: Journal of Materials Design and Applications*, vol. 215, pp. 165-174, 2001.

[66] D. H. Wang and T. Wang, "Principle, design and modeling of an integrated relative displacement self-sensing magnetorheological damper based on electromagnetic induction," *Smart Materials and Structures*, vol. 18, pp. 950-970, 2009.

[67] S. B. Choi et al., "A hysteresis model for the field-dependent damping force of a Magnetorheological damper,'' *Journal of Sound and Vibration*, vol. 245, pp. 375–383, 2001.

[68] G. Jin et al., "Modeling MR-dampers: A nonlinear blackbox approach," *Proc. IEEE American Control Conference*, vol. 1, pp. 429–434, 2001.

[69] S. M. Savaresi et al., "Identification of semi-physical and black-box non-linear models: the case of MR-dampers for vehicles control," *Automatica*, vol. 41, pp. 113–27, 2005.

[70] D. H. Wang and W. H. Liao, "Modeling and control of magnetorheological fluid dampers using neural networks," *Smart Materials and Structures*, vol. 14, pp. 111–126, 2005.

[71] N. M. Werely et al., "Idealized hysteresis modeling of electrorheological and magnetorheological dampers," *Journal of Intelligent Material Systems and Structures*, pp. 642-649, 1998.

[72] R. Stanway et al., "Application of electrorheological fluids in vibration control: A Survey, " *Smart Materials and Structures*, Vol. 5, pp. 464-482, 1996.

[73] E. R. Wang et al., "Modeling the hysteretic characteristics of a magnetorheological fluid damper," *Proc. Institution of Mechanical Engineers, Part D: Journal of Automobile Engineering*, vol. 217, pp. 537-550, 2003.

[74] X. Q. Ma et al., "Modeling hysteretic characteristics of MR-fluid damper and model validation," *Proc. 41st IEEE Conf. on Decision and Control,* vol. 2, pp.1675–1680, 2002.

[75] X. Q. Ma, "Relative assessments of current dependent models for magneto-rheological fluid dampers," *Proc. IEEE International Conference on Networking, Sensing and Control.*, Ft. Lauderdale, 2006, pp. 510–515.

[76] B. F. Spencer Jr. et al., "Phenomenological model of a magnetorheological damper," *Journal of Engineering Mechanics*, vol. 123, pp. 230-238, 1997.

[77] A. Dominguez et al., "A new dynamic hysteresis model for magnetorheological dampers," *Smart Materials and Structures*, vol. 15, pp. 1179–1189, 2006.

[78] A. Dominguez et al., "Semi-active vibration control of adaptive structures using magnetorheological dampers," *AIAA Journal*, vol. 44, pp. 1563–1571, 2006.

[79] X. Q. Ma et al., "Development and relative assessments of models for characterizing the current dependent hysteresis properties of magnetorheological

fluid dampers," *Journal of Intelligent Material Systems and Structures*, Vol. 18, pp. 487–502, 2007.

[80] X. Q. MA, "Dynamic characterization of a Magnetorheological fluid damper and synthesis of a semi-active suspension seat," Ph.D. dissertation, Dept. Mechanical and Industrial Engineering., Concordia University., Montreal, QC, Canada, 2005.

[81] F. Ikhouane and J. Rodelar, "On the hysteretic Bouc-wen model," *Nonlinear Dynamics*, vol. 42, pp. 63-78, 2005.

[82] W. H. Liao and C. Y. Lai, "Harmonic analysis of a magnetorheological damper for vibration control," *Smart Materials and Structures*, vol.11, pp.288–296, 2002.

[83] B. Sapinski, "Linearized characterization of a magnetorheological fluid damper," *Mechanics*, vol. 24, pp. 144-149, 2005.

[84] W. H. Li et al., "Testing and steady state modeling of a linear MR damper under sinusoidal loading," *Smart Materials and Structures*, vol. 9, pp. 95–102, 2000.

[85] L. Pang et al., "Analysis and testing of a linear stroke Magnetorheological damper," *Proc. The AIAA/ASME/AHS Adaptive Structures Forum*, vol. CP9803, pp. 2841-2856, 1998.

[86] G. Z. Yao, "MR damper and its application for semi-active control of vehicle suspension system," *Mechatronics*, vol. 12, pp. 963-973, 2002.

[87] G. Yang, et al., "Large-scale MR fluid dampers: modeling and dynamic performance considerations," *Engineering Structures*, vol. 24, pp. 309-323, 2002.

[88] R. C. Dorf and R. H. Bishop, *Modern control systems*. New Jersey: Prentice Hall, 2008.

[89] A. A. Stoorvogel, *The H∞ control problem: a state-space approach*. New Jersey: Prentice Hall, 1992.

[90] A. F. Jarhomi and A. Zabihollah, "Linear quadratic regulator and Fuzzy controller application in full-car model of suspension system with magnetorheological shock Absorber," *IEEE/ASME Conference on Mechatronics and Embedded Systems and Applications (MESA)*, Qingdao, 2010, pp. 522-528.

[91] M. S. Kumar and S. Vijayarangan, "Design of LQR controller for active suspension system," *Indian Journal of Engineering and Material Sciences*, vol. 13, pp. 173-179, 2006.

[92] A. H. Shirdel et al., "Comparison of H∞ and optimized-LQR controller in active suspension system," in *The Second International Conference on Computational Intelligence, Modeling and Simulation.*, Bali, 2010, pp. 241-246.

[93] H. Y. Son et al., "A robust controller design for performance improvement of a semi-active suspension systems," *Proc. The IEEE International Symposium on Industrial Electronics*, vol. 3, pp. 1458-1461, 2001.

[94] M. S. Fallah et al., "Robust model predictive control of shimmy vibration in aircraft landing gears," *AIAA Journal of Aircraft*, vol. 45, pp. 1872-1880, 2008.

[95] W. S. Levine, *The controls handbook (volume 1)*. Mumbai: Jaico Publishing House, 1999.

[96] R. S. Burns, *Advance controls engineering*. Oxford: Butterworth Heinemann, 2001.

[97] J. C. Doyle et al., "State-space solutions to standard H_2 and H∞ control problems," *IEEE Trans.on Automatic Control*, pp. 831-846, 1989.

[98] J. J. D' Azzo and C. H. Houpis, *Linear control system analysis and design: Conventional and modern*. New York: McGraw-Hill Book Company, 1981.

[99] A. F. Jahromi et al., "Ride control of passenger cars with semiactive suspension system using a linear quadratic regulator and hybrid optimization algorithm," *Proc. International Conference on Aerospace, Mechanical, Automotive and Materials Engineering (ICAMAME 2012)*, vol. 67, pp. 896-902, 2012.

[100] D. H. Perry, *Measurements of the moments of inertia of the Avro 707B aircraft*. London: Her Majesty's Stationery Office, 1963.

[101] H. H. Tsang et al., "Simplified inverse dynamic models for MR fluid dampers," *Engineering Structures*, vol. 28, pp. 327-341, 2006.

APPENDICES

Appendix A: State-space Approach for a Single Degree of freedom System

The state-space approach is a simplified method used in controls theory. In this thesis, a semi-active system is developed using two different control laws: (1) H_∞ and (2) LQR. The basic understanding of the state-space approach is necessary in order to deal with the complicated control laws used in mechanical systems.

The state-space method can be used for representing the complicated higher order system as a combination of the N first order differential equations. A state represents the condition of a physical system at time t. A state-space approach provides a complete description of the system at any given time. This method facilitates the design procedure of the control laws as well as the simulation procedures [95].

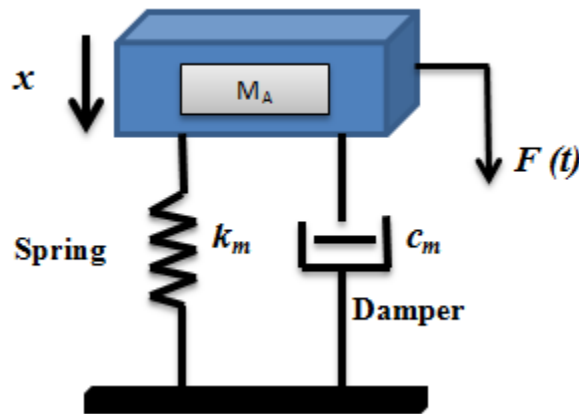The state-space methodology for a simple SDOF system can be explained as follows:

Figure A. SDOF system for state-space modeling

Figure A depicts the simplest SDOF system. The equation of motion for the system shown above can be derived using Newton's second law of motion. The equation of motion is as follows:

$$\sum F = M_A \ddot{x} \tag{A.1}$$

$$M_A \ddot{x} = -k_m x - c_m \dot{x} + F(t) \tag{A.2}$$
$$M_A \ddot{x} + k_m x + c_m \dot{x} - F(t) = 0$$

The above system can be represented in a state-space format as follows:

$$\dot{\vec{x}} = A\vec{x} + Bu \tag{A.3}$$
$$y = C\vec{x} + Du$$

In above equations, x represents the state vector and y represents the desired output of the system. For this case, the state of the system at any given time can be represented by its displacement (x) and velocity ($\dot{x}$). Therefore, a system has two states which can be represented using a state vector.

Assumptions: Let $\dot{x} = v$, be the velocity of mass M_A. Therefore, we can substitute the acceleration $\ddot{x}$, by $\dot{v}$.

Thus $\ddot{x} = \dot{v}$

Substituting the above variables in the equation of motion yield the following expression,

$$M_A \dot{v} + k_m x + c_m v - F(t) = 0 \tag{A.4}$$

The variable y represents the output of the system which is the displacement of the mass M_A for this case.

Therefore we have, $y = x$

Finally, to determine the elements of the matrices in the state-space plant, following equations can be used.

$$\dot{x} = v \tag{A.5}$$

$$\dot{v} = \left(\frac{-k_m}{M_A}\right)x + \left(\frac{-c_m}{M_A}\right)v + \frac{1}{M_A}F(t) \tag{A.6}$$

Referring to the state-space equation (A.3), the system in state-space can be represented as follows:

$$\begin{bmatrix} \dot{x} \\ \dot{v} \end{bmatrix} = A\begin{bmatrix} x \\ v \end{bmatrix} + BF(t)$$

$$y = C\begin{bmatrix} x \\ v \end{bmatrix} + DF(t) \tag{A.7}$$

In above equation, the matrices $[A]$, $[B]$ and $[C]$ represent the system matrix, the input matrix and the output matrix, respectively. The dimensions of these matrices can be determined from the number of states, the inputs and outputs of the system.

Let N represents the number of states, R represents the number of inputs and P represents the number of outputs of the system. The dimensions of the matrices can be defined as follows.

The system matrix $[A]$ is $N \times N$ matrix; the input matrix $[B]$ is $N \times R$ matrix and the output matrix $[C]$ is $P \times N$ matrix. Matrix $[D]$ represents the effect of the output on the input and it can be considered as zero for simple systems. The elements of these matrices can be determined using the equations A.5 and A.6.

Equation A.5 is the first state equation and its coefficients are the elements of the first rows of the matrices $[A]$ and $[B]$. Similarly, the elements in the second rows of these matrices can be determined by identifying the coefficients of the second state equation A.6. The elements of matrix $[C]$ are the coefficients of the output equation A.7 for y. Therefore, the matrices can be represented as follows,

$$A = \begin{bmatrix} 0 & 1 \\ -k_m / M_A & -c_m / M_A \end{bmatrix} \tag{A.8}$$

$$B = \begin{bmatrix} 0 \\ 1 / M_A \end{bmatrix} \tag{A.9}$$

$$C = \begin{bmatrix} 1 & 0 \end{bmatrix} \tag{A.10}$$

$$D = \begin{bmatrix} 0 \end{bmatrix} \tag{A.11}$$

The overall state-space model can be represented as shown in the following equation.

$$\begin{bmatrix} \dot{x} \\ \dot{v} \end{bmatrix} = \begin{bmatrix} 0 & 1 \\ -k_m / M_A & -c_m / M_A \end{bmatrix} \begin{bmatrix} x \\ v \end{bmatrix} + \begin{bmatrix} 0 \\ 1 / M_A \end{bmatrix} F(t)$$

$$y = \begin{bmatrix} 1 & 0 \end{bmatrix} \begin{bmatrix} x \\ v \end{bmatrix} + \begin{bmatrix} 0 \end{bmatrix} F(t) \tag{A.12}$$

A state-space model can be represented in MATLAB using the inbuilt function and the required response for a particular input signal can be achieved. A similar methodology is adopted for a 3 DOF model used in this study which simplified the simulation procedures.

Appendix B: Publications Revevant to Thesis work

In this section, the publications relevant to the study completed in this thesis are presented. Following are the abstracts of the two conference papers relevant to this thesis.

1.

Optimally Adaptive Oleo Strut Damping for Aircraft and UAV Using MR Fluid

Authors: Ajinkya A. Gharapurkar, Dr. Chandra B. Asthana and Dr. Rama B. Bhat

1st Annual International Conference on Industrial and Systems Engineering, 24-27 June 2013, Athens, Greece

ABSTRACT

It would be most desirable to have the same oleo strut perform optimally during widely different landing conditions of an aircraft and Unmanned Aerial Vehicle (UAV). These landing conditions may impose different requirements such as controlling vertical acceleration in a desired manner. As the atmospheric conditions change and the axial load on the strut changes during compression, the ability to control the damping force as function of time would be of great advantage. In this paper, it is shown that by using MR fluid in the oleo strut, it is possible to achieve optimal damping performance in every particular landing situation. Three different forces act along a conventional oleo strut which are: that due to the compression/expansion of gas, that due to the passing of fluid through the orifice and that due to the viscous force. The first is the spring force while the second and the third are the damping forces. The second is proportional to the square of compression/extension rate and the third is proportional to just the rate of compression/extension. Incorporating a metering pin that can change the orifice diameter in a prescribed fashion can change the damping force to some extent within limits. By using MR fluid in a conventional oleo strut the damping force can be altered in a desired

manner. A simulation model for a SDOF aircraft system is developed and a landing scenario at a particular sink velocity is simulated. The parameters controlling the behavior of MR fluid damper are tuned to get the optimal performance during landing.

2.

Semi-Active Control of Aircraft Landing Gear System Using H-infinity Control Approach

Authors: Ajinkya A. Gharapurkar, Ali Fellah Jahromi, Dr. Rama B. Bhat and Dr. Wen-Fang-Xie

The 2nd International Conference on Connected Vehicles & Expo (ICCVE 2013), 2013, Las Vegas, USA

ABSTARCT

The landing of an aircraft is one of the most critical operations because it directly affects the passenger safety and comfort. During landing, the aircraft fuselage undergoes excessive vibrations that cause the safety and the comfort problem and hence need to be suppressed quickly. A semi-active control system of a landing gear suspension by using Magnetorheological damper can solve the problem of excessive vibrations effectively. In this paper, a switching technique is developed in the simulation of the landing procedure which enables the system to switch from the single degree of freedom to three degrees of freedom system in order to simulate the sequential touching of the two wheels of the main landing gears and the nose landing gear wheels with the ground. A semi-active Magnetorheological damper is developed using two different control strategies namely, the Linear Quadratic Regulator and the H_∞. Spencer model is used to predict the dynamic behavior of the Magnetorheological damper. The results of the designed controllers are compared to study the performance of the controllers in reducing the overshoot of the bounce response as well as the bounce rate response. The simulation results validated the

improved performance of the robust controller compared to the optimal control strategy when the aircraft is subjected to the disturbances during landing.

Appendix C: Calculation of current relative to MR damper force

The output of the MR damper is the MR damper force, while the input of the MR damper model is a current signal function of time i (t). Therefore, a current signal corresponding to the damping force should be calculated. The inverse dynamic model of the MR damper using Spencer mathematical model is studied by Tsang et al. [101]. The mathematical relation between the force and the current is represented in equation.

$$i(t) = -\frac{1}{d_1} \ln\left(\frac{\left| F_{aj} \right| - \left| F_j \right|}{d_2} + e^{-b_1 i(t-\Delta t)} \right) \quad j = 1-3$$

where, F_{a1-3} represents the actual force which can be measured during each iteration (Δt). F_{1-3} presents the MR damper forces which are computed by the controller and defined by equation derived by Spencer for the hysteretic damping force F_D. The coefficients of the MR damper model d_1 and d_2 can be calculated by using the curve fitting approach based on the experimental results.